University of Plymouth

PEARL **https://pearl.plymouth.ac.uk**

04 University of Plymouth Research Theses 01 Research Theses Main Collection

2017

Calcification in Coccolithophores

Harper, Glenn Martin

http://hdl.handle.net/10026.1/8664

http://dx.doi.org/10.24382/666
University of Plymouth

All content in PEARL is protected by copyright law. Author manuscripts are made available in accordance with publisher policies. Please cite only the published version using the details provided on the item record or document. In the absence of an open licence (e.g. Creative Commons), permissions for further reuse of content should be sought from the publisher or author.

Calcification in Coccolithophores

By Glenn Martin Harper

A thesis submitted to Plymouth University

in partial fulfilment for the degree of

Master of Philosophy

School of Biological Sciences in collaboration with the Marine Biological Association

November 2015

This copy of the thesis has been supplied on condition that anyone who consults it is understood to recognise that its copyright rests with its author and that no quotation from the thesis and no information derived from it may be published without the author's prior consent.

Acknowledgements

The completion of this MPhil could not have possible without the overwhelming help and assistance from the following people. Thanks to my Supervisory team; Dr Roy Moate (director of studies), Professor Colin Brownlee, Dr Declan Schroeder and Dr El Mahdi Bendif. And also Dr Alison Taylor who was there at the beginning and whose contributions to chapter 3 were invaluable

Also Cecelia Bellestreli, Leela Chakravati. Matt Hall and Mags Davies.

Thanks also to the support of my colleagues Mr Peter Bond, Dr Paul Waines and Dr Natasha Stephen and anybody else who has listened.

Thanks to Andy Yarwood at Jeol and Stephen Murray at Leica for technical advice. To Peter Splatt at Exeter university.

To Debbie Petheric, Catherine McCoulough, Mandy MacDonald and Mick Fuller in the Graduate school for putting up with me

And of course my wife, Charlotte Harper and my children. You are my Rock.

Author's Declaration.

At no time during the registration for the degree of Master of Philosophy has the author been registered at another university.

Work submitted for this research degree at Plymouth University has not formed part of any other degree at Plymouth University or any other establishment.

The research has been conducted with the co-operation of the Marine Biological Association, Plymouth.

A programme of advanced study was undertaken which included modules in 'Skills' and 'Methods'.

Collaborative Publications can be found in Appendix 1.

External contacts: Professor C. Brownlee (cbr@mba.ac.uk)

Dr D. Schroeder (dsch@mba.ac.uk)

Dr E M Bendif (elmhid@gmail.com)

Word count of main body of thesis: 20, 329

Signed……..

Date……

Calcification in Coccolithophores

By Glenn Martin Harper

Abstract

Coccolithophores are uni-cellular phytoplankton and they form an exceedingly diverse group in the phylum Haptophyta. They produce highly complex structures known as coccoliths by a biomineralisation process known as calcification.

The first part of the work undertaken was to investigate the process of calcification in the coccolithophore *Coccolithus pelagicus using* a combination of Transmission Electron Microscopy (TEM), Scanning Electron Microscopy (SEM) and light microscopy techniques. This allowed better understanding of the formation, transit of the coccolith through the cell until its final placing in the coccosphere.

The second part of the work looked at the coccolithophore *Emiliania huxleyi* which is divided into several morphotypes with the two most widely recognised being A and B, it can be further subdivided into further groups according to genotype by Coccolithophore Morphology Motif (CMM). The CMMs lie in the 3′ untranslated region of the coccolith-

polysaccharide associated protein-GPA, which is associated with coccolith structure control and they are labelled I, II, III and IV.

The work undertaken used a Scanning Electron Microscope (SEM) to investigate the morphologies of homozygous CMM I and CMMIV cell's coccoliths. This information was used to establish a significant difference between the CMMI cells and CMMIV cells but only at certain locations. The cause for this is possibly as a result of several factors (temperature, salinity, pCO_2, Ca availability and light levels) and requires further investigation.

List of Contents

List of Abbreviations

ACC	Antarctic Circumpolar Current
af	actin filaments
ATP	Adenosine Tri Phosphate
BOC	British Oxygen Company
Bp	Base Plate
C	Chloroplast
Cb	cell body
CH	Chloroplast
Ci	Inorganic Carbon
cm	cell membrane
CMDS	Classic Multidirectional Scaling
CMM	Coccolithophore Molecular Motif
CP	Calcium binding Polysaccharides
cp	cuticular plate
CV	Coccolith vesicle
E	Enterocyte
ER	Endoplasmic reticulum
EM	Electron Microscopy
Fb	Flagellar base
Fr	Flagellar root

FS	Freeze Substitution
FSW	Filtered sea water
Ga	Golgi apparatus
Gg	Golgi body
GL	Gut Lumen
GPA	coccolith-polysaccharide associated protein
jc	junctional complex
JEOL	Japanese Electron Optical Laboratories
k	kino cilia
L	Lumen
lm	long microvilli
LM	Light microscopy
Lt	Coccolith
Mb	Microtubules
MDS	Multi-Dimensional Scaling
ml	millilitre
mRNA	Messenger Ribose Nucleic acid
Mt/M	Mitochondrion
Mv	Microvilli
N	Nucleus
nm	nanometre

NP	Nanoparticles
Nu	Nucleus
OHC	Outer Hair cells
PCR	Polymerise chain reaction
pH	power of hydrogen ions
pns	peripheral nerve
Pm	Plasma Membrane
PP	Phenotypic Plasticity
ps	phagosomes
Py	Pyrenoid
RB	Reticular Body
S	Scaly
sc	support cells
Sc	Organic Scale
Sd	Standard deviation
Se	Standard error
SDV	Silica Deposition Vesicle
SEM	Scanning Electron Microscopy
smv	short micro vili
TEM	Transmission Electron Microscopy
Tj	Tight junction
UTR	Untranslated Region
V	Vacuole

List of Figures

List of tables

Chapter one- Coccolithophores.

1.1 Introduction

Coccolithophores are uni-cellular phytoplankton and they form an exceedingly diverse group in the phylum Haptophyta. They can display high fecundity and under favourable conditions form blooms that are so large they can be seen from space (Winter *et al.,* 1994). They can produce highly complex structures known as coccoliths via a process known as calcification. These are made from predominantly calcite and can interlock to form elaborate coccospheres that can surround the individual cell (Westbroek *et al*., 1984).

Coccoliths can be produced externally and are known holococcoliths. Alternatively, they can be produced intracellularly. These are known as heterococcoliths. Coccolithophores can exhibit either no coccoliths (and are referred to as naked [Paashce 2002]), heterococcoliths, holococcoliths or a combination of both (Cros *et al*., 2000 and Cortes 2000). Some species can exhibit all of the above forms at various times and consequently result in a very complex area of study (Paasche 2002 and Cros 2000).

As previously mentioned, certain coccolithophores have both hetero and holococcolithic life stages. There is evidence to suggest that this is as a result of a response to changes in pelagic to coastal environments and changes in season (Noel *et al.,* 2003). However, some species (e.g. *Emiliania huxleyi* or

E. huxleyi) can exist in one of several forms. It can be either Calcified (C), Naked (N) or Scaly (S) (Paasche 2002). This way they maintain their heterococcolithic status.

It would appear that coccolithophores typically reproduce by binary fission and each of the above forms (C, N and S) is capable of reproducing thus.

Binary fusion is exceedingly advantageous in producing exponential growth in a population during bloom formation.

In *E. huxleyi*, the C and the N cells are non-motile whilst the S cells possess two flagella and are motile. In addition to this, studies have shown that the C and N cells are diploid whilst the S cells are haploid (Laguna 2001). As a result, the mobility and haploid nature of the S cells can act as gametes and fulfil that role allowing sexual reproduction (Schroeder *et al.*,2002 and Frada *et al.*, 2012).

This haplo-diploidy switching is also evident in coccolithophores that switch between hetero and holococcolith life stages (Houdan 2004).

Houdan (2004) also observed that haploid stages of these holo-heterococcolith switching species are also capable of fusion in a sexual way and also act as gametes as in *E. huxleyi.*

This ability to switch between life stages when (as suggested by Noel et al 2003) conditions dictate or directly as a result of normal life cycle changes

via mitosis and meiosis (Houdan 2004) or as a combination of both must result in an improved fitness. This has resulted in their placing as one of the dominant groups in global primary production.

Young (1994) commented that coccolith production must have an effect on the coccolithophore biochemistry. However, nothing is known for certain why coccolith production occurs. He stated that the function of the coccolith may include protection from predators and pathogens. It may provide protection from the outside environment (i.e. from osmotic, chemical or physical stress). Coccoliths may be involved in flotation regulation or they may be involved in the concentration of light or its reflection. Alternatively, it has been suggested that calcification is involved in facilitating photosynthesis (Brownlee and Taylor 2004. See the flow diagram on p10).

Understanding the role (or indeed roles) of coccoliths may help shed light on the method of their production. Coccolithogenesis shall be discussed later.

Coccolithophores account for half of the naturally produced $CaCO_3$ on the planet (Brownlee and Taylor 2002). They also provide a major sink for CO_2, with the oceans having absorbed about 1/3 of anthropogenic CO_2 and the coccolithophores a major part of that (Beaufort *et al.*, 2011). Given the current global concerns about the increased CO_2 emissions from the burning of fossil fuels, coccolithophores (as do all phytoplankton) have an important role to play. However, Riebesell., (2000) discussed that an increase in

atmospheric CO_2 would have a negative effect on coccolith production. This would ultimately affect the ability of coccolithophores and therefore the ocean's ability to act as a sink for CO_2. However, Barcelos e Ramos *et al.* (2010) speculated that this might not be the case.

In his 2010 paper, Barcelos e Ramos discussed that short term changes in sea water CO_2 concentrations resulted in cultures of *E. huxleyi* having the ability to change major metabolic pathways and acclimate to the changes. This suggests that any change in CO_2 in the oceans might not have a negative effect on coccolithophores as they have the ability to adapt.

Given this, it is clear that studying coccolithophores and calcification is significant.

1.2 Biomineralisation.

According to Nature.com: -

> 'Biomineralisation is the process by which living organisms produce minerals. Biomineralisation processes often lead to hardening or stiffening of the mineralised materials.'

There are many organisms that use Biomineralisation for this exact purpose. In human beings we use it to form complexes that contain calcium phosphates (bone and teeth) and it is the calcium that helps to give these

structures rigidity. In teeth, it forms crystals of apatite (a calcium phosphate) to result in enamel being formed one of the hardest substances in the human body (Ilijima *et al.*, 2012).

Many bacteria also biomeralise and the most well studied of these are the magnetosome or magnetotactic bacteria. These bacteria are capable of incorporating Iron oxide or Iron sulphide into them and it is believed that they use the magnetic biomierals for navigation. They

use the Earth's magnetic field to search for low-oxygen locations these cells prefer (Frankel and Basilinski, 2009). There are many other bacteria that mineralise many other metals and there has been some work into investigating the possibility of using bacteria as a method for extracting rare elements from the environment (Tanaka *et al*., 2010). Whilst this could be economically very useful, little is understood about the process and although it is assumed to be similar the way magnetotactic bacteria sequester Iron in that they import the iron via endocytosis (Rahn-Lee and Koneili, 2013).

Silica is also utilised for biomineralisation by organisms such as sponges and diatoms. In certain sponges the silica is sequestered by the cell and specialist cells known as *Sclerocytes* produce an enzyme known as silicatin and this then will form structures known as spicules. These long, rod like structures are excreted by the cells of the sponge to form part of a 'skeleton' made from

other spicules (Muller *et al.*, 2005. Wang *et al*., 2012). This process is similar to coccolith formation in coccolithophores as will be discussed in chapter 3.

Silica is used in a different way in diatoms in that rather than forming the long spicules they use silica to form a wide variety of structures know as *frustules* (Hildebrand, 2008). The frustules themselves are formed intra-cellularly in structures know as the silica deposition vesicle (SDV) after the silica has been transported through the cell via carrier-mediated transport (using silicic acid carrier proteins) or passive diffusion (Hildebrandt and Lerch. 2015). Once the frustule has been formed it is excreted and forms a 'shell' to surround the cell (Hildebrand and Lerch, 2015).

The function of the spicule in the sponge is structural and offers an element of rigidity it also provides a deterrent to some predators (Uziz *et al.*, 2003) whereas the functions of the frustules in diatoms are not clear. They are thought to have involvement in offering 'mechanical' protection against unfavourable conditions. They are also porous and so may have an active role in the uptake of nutrients by the diatom, the frustules also have an effect on the light coming onto the cells (essential for photosynthesis) offering either a protective shield to the light or focussing of the light (Hildebrand and Lerch, 2015).

Biomineralisation also occurs in coral. However, it isn't silica, it is calcium that is biomineralised. The calcium is formed into calcium carbonate ($CaCO_3$)

in the form of aragonite and is used primarily in the framework during the formation of coral reefs. The process that the corals use to biomineralised is not fully understood. However, it results in small structures known as polyps growing around a 'fibre' of aragonite and this process is repeated using a regulated organic matrix to result in the growing coral (Falini *et al.,* 2015).

$CaCO_3$ in the form of calcite is the result of biomineralisation in coccolithophores and that shall be the subject of the rest of this chapter.

1.3 History of coccolithophores

In 1836, whilst studying chalk from an island in the Baltic Sea, Christian Gottfried Ehrenburg described "elliptical flattened discs". He considered these structures to be wholly inorganic. And in 1857 samples of sea floor sediment were sent to Thomas H Huxley who described the same structures as Coccoliths as they reminded him of single cells from the plant protococcus [lith meaning stone] (Siesser 1994). Huxley also believed them to be inorganic.

However, work by G. C. Wallich (1861) and Henry Clifton Sorby (1861) (Both cited in Seisser 1994) concluded that coccoliths and the resultant coccospheres they'd observed were organic in origin when he saw the coccoliths forming coccospheres.

Thus was initialised the interest and study of the origins of these structures and this ultimately led to the study of coccolithophores.

Coccolithophores first came to prominence in the cretaceous period some 200-250 million years ago. They have been relatively well preserved in the fossil record and by studying the composition (namely the levels of alkenones-these are long chain molecules found in *Prymnesiophyceae* species that are known to change length depending on environmental conditions (Marlow *et al.* 1984), deductions can be made as to changes in global temperatures from prehistory until fairly recently (Brownlee and Taylor 2004).

As well as this chemical analysis coccolithophores have been and can be studied in many ways, this can include looking at deep sea sediment via multi-corers or drilling. Samples from the surface waters can be collected and living coccolithophores can be examined via neuston nets, filtration systems combined with pumps or simply water bottles and centrifugation (Winter *et al.,* 1994). Alternatively, specific strains can be cultured in the laboratory. Regardless of the source of the coccolithophores, all of the samples can be examined using light or electron microscopy. Alternatively, with samples in the controlled conditions of a laboratory, they can be exposed to elevated salinity levels (Paasche *et al*., 1996), different growth media and various chemicals (Fagerbaakke *et al*., 1994). They can have their cell membrane potentials studied via patch/clamp techniques (Taylor and

Brownlee 2003). Work has been undertaken undertaken to identify the genes involved in calcification (Billard and Inouye., 2004 and Mackinder *et al.*, 2010) and ultimately the mapping of the entire genome of *Emiliania huxleyi* (Read *et al.*, 2013).

All of these methods of study (and there are a great deal more that haven't been mentioned) attempt to answer the same sort of fundamental questions that include: Why do they have coccoliths? What is their function (or what are their functions)? How are they formed? And what is their importance globally?

1.4 Global implications of calcification.

Coccolithophores have a wide distribution globally and are found in high latitude regions to the tropics and from mid-ocean waters to coastal waters (Holligan *et al.*, 1993). They are at their most diverse when in warm low productivity areas and regions of limited circulation (Winter *et al.*, 1994). However, under certain conditions, coccolithophores can produce massive blooms. During this bloom formation reproduction rates can be as high as 2.6 divisions per day (Brand 1981). This level of fecundity can produce between 10^7-10^8 coccolithophores in a single litre of water (Berge 1962). This amount of coccolithophores and the resultant calcification that takes place can leave the top 60m in a bloom containing approximately 7.2 x 10^4 tonnes of $CaCO_3$ (Holligan *et al.*, 1993). When the bloom ends and the cells

die off all of the calcite in the dead cells becomes part of the oceanic sediment (Riebesell and Tortell, 2011)

This level of calcification must have an impact both locally and globally.

The basic formula for calcification is (from Balch 1992): -

$$2\ HCO_3^- + Ca^{2+} \longleftrightarrow CO_2 + H_2O + CaCO_3 \quad (1)$$

The HCO_3^- ions account for 90 % of the inorganic carbon (Ci) in sea water whilst CO_2 accounts for roughly less than 1 %. As a result of this imbalance in the Ci available in the seas, it has been suggested (and is generally accepted) that it is the substrate used during calcification (Paasche 2002). However, the use of it as the substrate (as in formula 1) results in the production of CO_2. Therefore, with the seas effectively removing 30% of anthropogenic CO_2 and calcification potentially having a net production of CO_2, calcification has the potential to affect the ocean's ability to remove CO_2 from the atmosphere (Berry *et al.*, 2002). However, the CO_2 produced during calcification may be utilised during photosynthesis (Young 1994). Given this, coccolithophores could represent a major sink for Ci. Alternatively, there is also evidence that suggests that HCO_3^- is the substrate utilised during photosynthesis in coccolithophores and that the production of the proton produced early in calcification is utilised in the production of CO_2 in the following way (from Brownlee and Taylor 2004):-

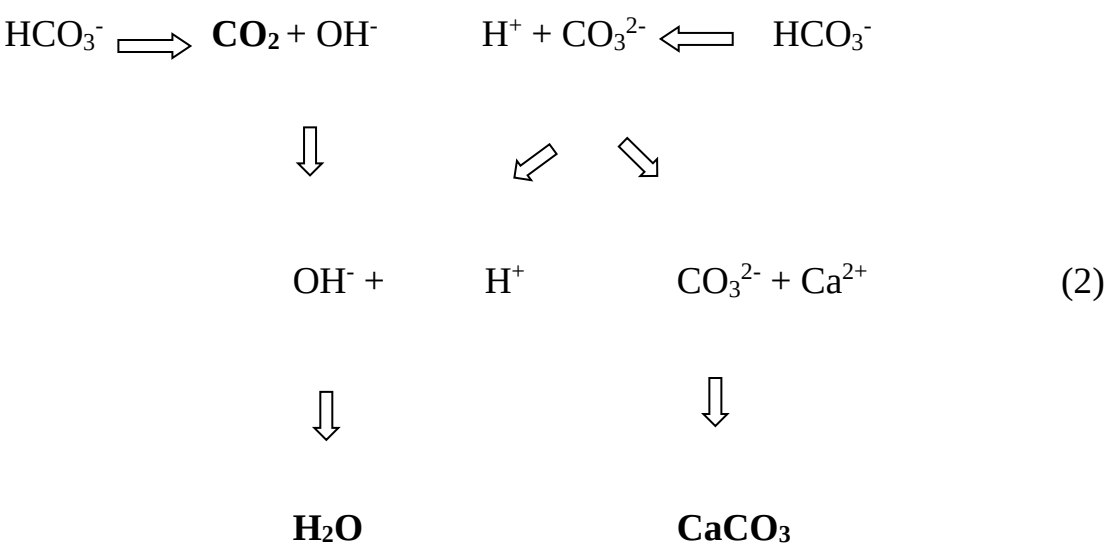

NB the items in bold are the end products.

There is other evidence that suggests that coccolithophores preferentially use CO_2 but when levels are limited they can utilise HCO_3^- as in the equation above (Berry *et al.*, 2002).

Lots of evidence suggests calcification does appear to have an important role in photosynthesis and as a result coccolithophores do represent a sink for Ci and consequently CO_2.

Chemistry, in particular carbonate chemistry of the oceans is extremely complex and the Ci levels are maintained by mechanisms know as pumps. The organic carbon pump draws down CO_2 from the atmosphere predominantly by organisms photosynthesising. A mechanism known as the carbonate counter pump acts antagonistically to the organic carbon pump. The removal of HCO_3^- from the oceans during calcification results in a net

decrease in pH and to maintain the equilibrium the transfer of CO_2 from the oceans to the atmosphere occurs (Rost and Reibesell 2004).

It is estimated that by the year 2100, the atmospheric CO_2 concentration (assuming that anthropogenic CO_2 production continues unabated) will have tripled when compared to pre-industrial revolution values (Barcelos e Ramos *et el.*, 2010). This will mean that there will be a net reduction in CO_3^{2-} concentration by approximately 50%. This will result in a reduction of 0.4 pH units at the surface of the oceans and a reduction in the availability of Ci.

This is often referred to as the "other CO_2 problem" (Doney *et al.*,2009). Ocean acidification has the potential to have dire consequences for all life in the oceans. Not just organisms that calcify such as sponges, coral and of course, coccolithophores, but all photosynthetic organisms.

To summarise, an increase in atmospheric CO_2, from anthropogenic sources, will decrease the pH of the oceans and ultimately affect the carbonate chemistry of the oceans. This could potentially have dire consequences for calcification. However, the effect it will have is not yet fully understood.

In addition to problems faced by coccolithophores by reduced Ci availability, increased ocean acidification can have an effect on coccolith production. It has been shown that this can result in deformed coccoliths and consequently a reduction in the formation of coccospheres (Reibesell *et al.*, 2000). However, other more recent work looking at *E. huxleyi* has shown it has the

ability to "acclimate" to changes in CO_2 concentrations and change its physiological state (Barcelos e Ramos *et el.,* 2009). Work by Feng *et al.* (2008) showed that there was no difference in coccolith morphology as a result of increased CO_2.

Potentially this could mean one of two things; either that the net result of the increase in atmospheric CO_2 will be a reduction in calcification (either from coccoliths being dissolved or fluctuations in carbonate chemistry) and ultimately, if this were the case, it will reduce the oceans ability to act as a sink for CO_2 via the organic carbon pump. Alternatively, if as Langer *et al.,* (2011) investigated that certain strains of *E. huxleyi* when exposed to a change in CO_2 remained unaffected (at least in as much as they continued to produce coccoliths). This could mean that changes in the carbonate chemistry and the effect on coccolithophores is strain specific and if this were the case, then it would result in different strains becoming dominant.

The implications of ocean acidification and the effect on calcification would have on coccolithophores, clearly are globally very significant and are deserving of more investigation.

1.5 General cell morphology and the site of calcification.

Figure 1.1 represents a typical heterococcolith. Crucial to the calcification process are two key structures: The coccolith vesicle (CV) and the reticular body (RB). The CV arises from conglomerating vesicles originating from

the Golgi body (Paasche 2002). The RB (which is comprised from anastomosing tubes near the CV) forms a very close association with the CV and forms the CV/RB complex.

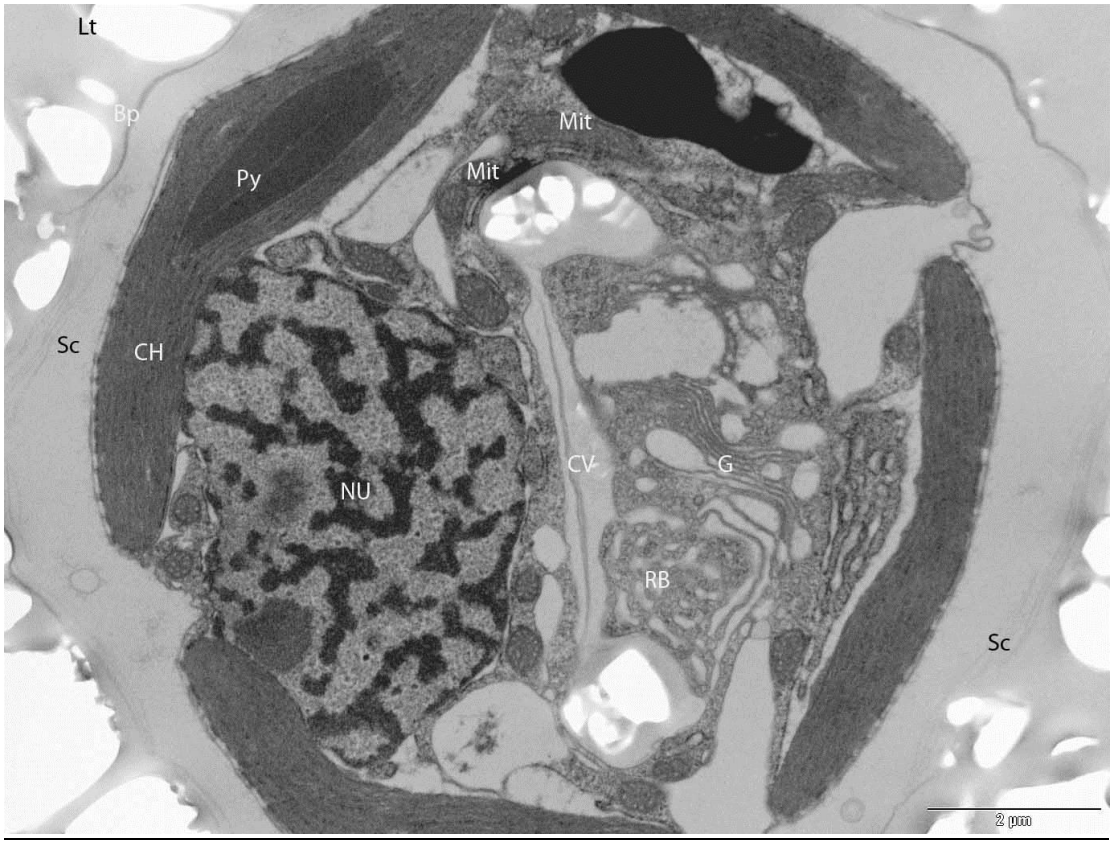

Figure 1.1 Transmission electron micrograph *Coccolithus pelagicus* (from Taylor et al 2007) showing impression left by Coccoliths (Lt). Also (NU) Nucleus, (Mit) Mitochondria, (Gg) Golgi apparatus, (RB) Reticular Body, (CV) Coccolith Vesicle, (CH) Chloroplast, (Py) Pyrenoid, (Bp) Base plate of coccolith and (SC) organic scales. Scale bar = 2um.

The CV/RB complex forms in very close proximity to the nucleus and as calcification occurs and the coccolith is formed the CV/RB complex moves to the edge of the cell where the coccolith is extruded. The time of this process is species specific, however Westbroek *et al.,* (1989) suggested a time of around two hours.

Once the coccolith is extruded through the plasma membrane of the cell it forms part of the coccosphere that surrounds the cell (Westbroek *et al.,* 1984 and Taylor *et al.,* 2007).

It has been postulated that the RB is recycled after the coccolith is extruded and returns to the nucleus for the next coccolith formation (Van Der Wal 1983).

1.6 Coccolith structure and formation (coccolithogenesis).

As previously discussed, there are two main types of coccolith: heterococcoliths that are produced internally and holococcoliths that are produced externally.

Holococcoliths are produced from simple crystals and are less complex than heterococcoliths. It is heterococcoliths that I am primarily concerned and in particular placoliths (a common type of heterococcolith) although it appears the mechanism applies to all coccolith types (Young *et al.,* 1992).

Coccolithogenesis occurs when the two precursors (acidic polysaccharides and an organic base plate) to the coccolith are in the Golgi and are subsequently transferred to a structure known as the proto-CV (Van Der Wal 1983 and Young *et al.,* 1999). Then, via the polysaccharides, mineralization of the organic base plate occurs. Initially a simple calcite ring is formed on the base plate. This is termed crystallisation. After this crystal growth occurs and the coccolith develops (Young *et al.,* 1992). Westbroek *et al.,* (1989) determined that it was the CV that determines the growth of the crystals and ultimately dictates the final complex coccolith morphology.

In placolith forming species (e.g. *E. huxleyi* and *Pleurochrysis carterea*) the calcium carbonate crystals come in two forms called R (radial) units and V (vertical) units. These two types of crystal interlock to form two discs that run parallel to each other and are known as the proximal shield elements. The two discs are linked vertically by tube elements (Marsh 2003). See figure 1.2 below.

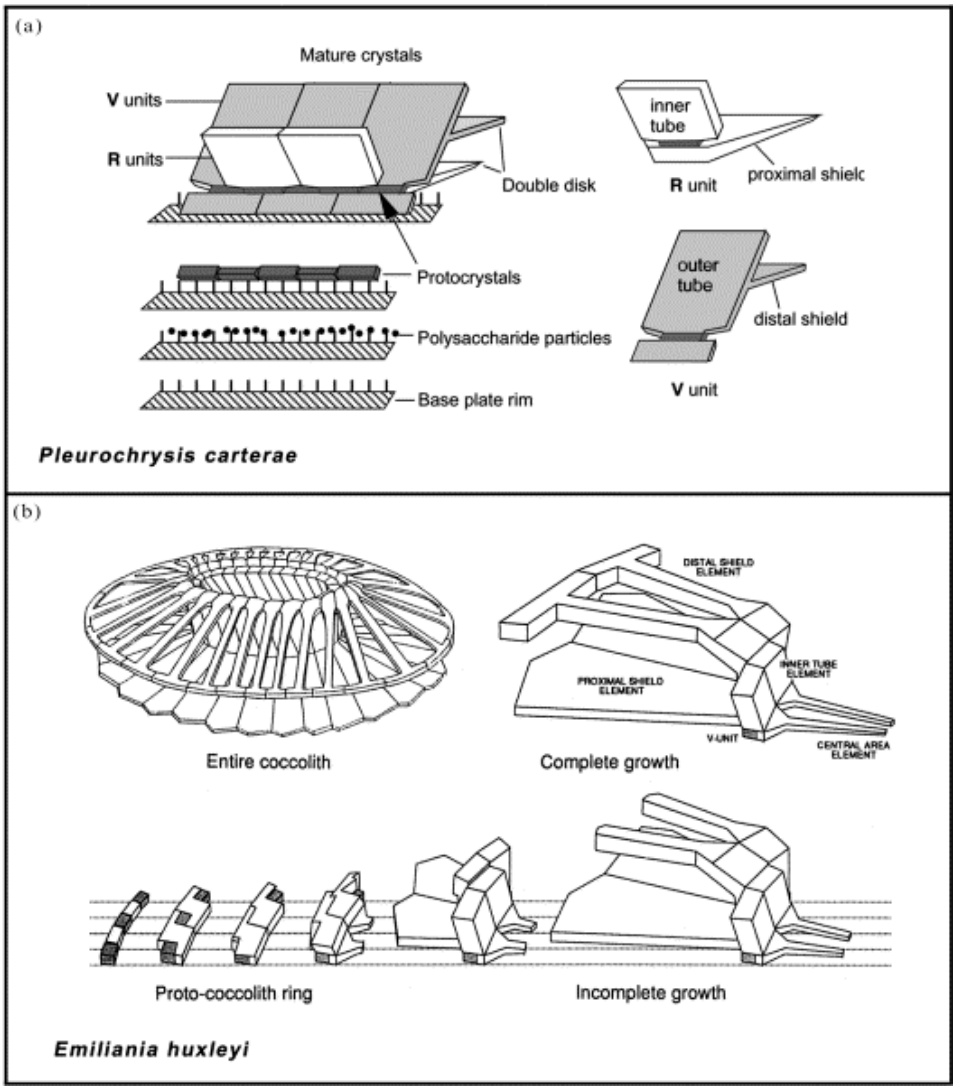

Figure 1.2 Diagrammatic representation of coccolith formation in *Pleurochrysis carterae* and *Emiliania huxleyi*. (Reproduced from Marsh *et al., 2002 –a. And* Young *et al*., 1992- b)

This structuring of the R and V units, results in the proximal shield and the distal proximal shield running parallel and allows the new coccoliths to lock together with existing ones in the coccosphere once they are extruded to the exterior of the cell.

The genetics controlling bio mineralisation have been studied at length (for example by Mackinder *et al.,* 2010 and Kreuger-Hadfield *et al.*,2014). Acquiring an understanding of its influence will help in the study of how coccolithophores can adjust and adapt to changes in ocean chemistry making the variations more predictable.

1.7 Calcium ion transportation.

Whilst there may be some question as to the source of inorganic carbon (although it is generally accepted that it is HCO_3^- [Berry *et al.*, 2002]) for calcification, there can be no doubt as to the requirement of Calcium.

In order for calcification to occur Anning *et al.*, (1996) discussed that Ca^{2+} concentration would need to be in the mM range. However, Brownlee *et al.*, (1995) measured the cystolic concentration in normal cells at around 100nM. Clearly, Ca^{2+} concentration is too low in the cytosol; therefore, the Ca^{2+} must enter the cell in another way.

Transporting Ca^{2+} from extra cellular sources to the CV/RB complex presents certain problems. Namely that transporting Ca^{2+} across the cytoplasm would be energetically constraining. Accompanying this is the

fact that Ca^{2+} is used in a great many cells as a signalling device (Sanders *et al.*, 2002 and Berridge, 2002).

Therefore, Berry *et al.*, (2002) proposed three ways of transporting Ca^{2+} which would overcome the energetic issues and the cell signalling issues that arise from having so much free-floating Ca^{2+} in the cytosol: -

If the Ca^{2+} was bound to chelators for transport across the cytosol it would avoid the signalling issues but it still would energetically be quite costly.

Alternatively, the Ca^{2+} could be endocytotically transported into and across the cell. This does overcome the flux and energetic problems but it does require high level of membrane recycling via the Golgi. However, Berry *et al.*, (2002) suggest that from their work this route doesn't account for a great deal of movement of Ca^{2+} into and across the cell.

The third route suggested was to transport the Ca^{2+} through channels in the plasma membrane via the Endoplasmic reticulum (ER) to the Golgi. And from there ultimately to the CV. This route overcomes the energetic and signalling constraints (Brownlee and Taylor 2004). In order for this to occur, then the ER needs to have a close proximity to the plasma membrane. This does in fact appear to be the case in many species as shown in electron micrographs (e.g. Outka and Williams 1971). Work by Brownlee and Taylor (2004) and Berry *et al.*, (2002) appear to support the ER/ Golgi route for transporting Ca^{2+} into the CV.

1.8 Functions of coccoliths.

There has been much work undertaken to establish coccolith structure and function. There has also been a great deal of work to establish their life-cycle and their impact globally. Alongside this work, studies have tried to elucidate the function(s) of coccoliths. Despite the best efforts of a great many people, their exact function(s) remains unexplained.

It has been suggested that there are the following function(s) for coccoliths (Young 1994).

There can be no doubt that the coccosphere separates the cell from the external environment. However, does this support the idea of the coccosphere bestowing protection on the cell? If so, protection from what?

Protection from predation has been suggested, but Harris (1994) has shown that faecal pellets from zooplankton contain the remains of coccolithophores. This therefore suggests that zooplankton don't select against eating coccolithophores and that possession of a coccosphere does not provide protection from predation (by zooplankton at least).

Protection from pathogens has also been suggested. But Wilson (2002) has shown that viral infections were just as high in cells with coccospheres as it was in cells of a non-calcifying strain from the same species.

Brownlee and Taylor (2004) in their review point out that various studies have suggested that calcification increases the sink rates of the cells allowing them to come into contract with more nutrients. The bestowing of this function arises out of the fact that coccoliths are twice as dense as the surrounding water (Paasche 2002). Despite this, to prevent the cells from falling out of the photic zone the cells can only rely on naturally occurring turbulence within the sea (Young 1994).

Young (1994) also suggested that light regulation was also a possible function of the coccosphere. However, there are two contradicting theories. Nielsen (1997) and Nanninga and Tyrell (1996) have both shown *E. huxleyi* (at least) has no inhibition of photosynthesis at high light levels (i.e. it can exist higher in the water column and gain more exclusive exposure to available nutrients). Therefore, the suggestion is that this is indicative of the coccosphere having a shading effect on the cells, i.e. a photo-protective role.

In direct contrast to this theory is that coccospheres enhance photosynthesis at lower light levels (i.e. deeper in the water column) by having a high refractive index and concentrating light into the cells (Gartner and Bukry 1969 in Young 1994).

It is clear that only further experimental work will establish whether coccospheres have a light regulatory role.

The final possible function for calcification is bio-chemical convenience. As has already been discussed, there may be a direct link between calcification and photosynthesis whereby calcification produces CO_2 which is utilised during photosynthesis where CO_2 levels would normally be prohibitive.

Further evidence to support this theory comes from Paasche (2002) who has shown (in *E. huxleyi* at least) that calcification and photosynthesis rates occur on a roughly similar scale and that cells will continue to produce coccoliths despite their coccospheres being complete, i.e. producing a surplus of coccoliths. Despite this, Young (1994) has suggested that this may not be true of all coccolithophores and also suggested that this may not be the original function for calcification.

Whatever the function or indeed functions of calcification they are likely to have had multi-evolutionary origins (Berry *et al.,* 2002) and it may transpire that some species rely on coccoliths and coccospheres for one function and another species require them for a wholly different reason.

1.9 Summary

Brownlee and Taylor (2004), Berry *et al.,* (2002) and Marsh (2003) amongst others all suggest that there is a great deal still to be learnt about coccolithophores.

It is the aim of this project to expand our understanding of calcification in coccolithophores.

Chapter 3 will look at coccolithogenesis specifically the formation and excretion of the coccoliths in the species *Coccolithus pelagicus (*ssp. *Braarudii*).

Chapter 4 will investigate the role genetics has in the morphology of the coccolithophore *Emiliania huxleyi* Hay and Mohler (prymnesiophyceae) in order to establish if the morphology of the cell can be directly linked to its genetics therefore allowing identification of the genotype rapidly and easily.

Chapter 2- General Materials and Methods

2.1 Introduction.

The following chapter discusses the basic techniques that were employed in order to produce the results found in chapter three and four. The techniques are tried and tested methods and are long established and are known to yield very few artefacts and to result in images which maintain as lifelike a quality as possible.

2.2 Cell culturing.

The cells were obtained from the Plymouth culture collection and they were used for the entirety of the experimentation. The cells used were calcifying, non-motile *Coccolithus pelagicus* Wallich (182g strain Plymouth culture collection) and *Emiliania huxleyi* (cmp 1516 Lohm, Hay and Mahler).

2.2.1 Producing growth media (Guillards f/2 medium)

The cells needed to be grown in a specific culture medium as described by Guillard and Ryther, 1962 and Davey et al, 2003. It is described below.

Initially sea water was collected from a location in the English Channel denoted by the location L4 (avoiding collection during the summer months as this is when algal blooms occur and these would contaminate the sea water) and it is first filtered through 30KD hollow fibre filters (Sartorius,

Gottingen, Germany). It was then Autoclaved (Autoclaving was achieved with a Priorclave 260 London UK) prior to addition of nutrients.

See Tables 2.1, 2.2 and 2.3 below.

Table 2.1 Basic ingredients to the growth media f/2.

Quantity per litre of Media	Compound	Stock Concentration	Molar Concentration in Final Medium
1.0 ml	NaNO3	75.0 g/L dH2O	8.83×10^{-4} M
1.0 ml	$NaH_2PO4-2H_2O$	5.0 g/L dH2O	3.63×10^{-5} M
1.0 ml	f/2 Trace Metal	See table 2.2	
0.5 ml	f/2 Vitamin	See table 2.3	

Table 2.2 f/2 Trace Metal Solution – to 950ml milliQ water add:

Quantity	Compound	Stock Solution	Molar concentration in Final Medium
3.15g	FeCl3.6H2O	-	1×10^{-5} M
4.36g	Na2EDTA.2H2O	-	1×10^{-5} M
1.0 ml	CuSO4.5H2O	980 mg / 100 ml dH20	4×10^{-8} M
1.0 ml	Na2MoO4.2H2O	630 mg / 100 ml dH20	3×10^{-8} M
1.0 ml	ZnSO4.7H2O	2.2 g / 100 ml dH20	8×10^{-8} M
1.0 ml	CoCl2.6H2O	1.0 g / 100 ml dH20	5×10^{-8} M
1.0 ml	MnCl2.4H2O	18.0 g 100 ml dH20	9×10^{-7} M

When initially made the solution will be cloudy. However, using 1M NaOH solution to reduce the pH to 4.5 will clear it. It is then made up to 1L with Milli-Q water.

Table 2.3 Ingredients for the Vitamin Solution - to 950ml milliQ water add

Quantity	Compound	1º Stock Solution	Molar Concentration in Final Medium
1.0 ml	Vitamin B12	10 mg / 10 ml dH2O	1×10^{-10} M
1.0 ml	Biotin	10 mg / 10 ml dH2O	2×10^{-9} M
200.0 mg	Thiamine HCl	-	3×10^{-7} M

Make final volume up to 1.0 L with milli-Q H_2O.
NB Milli-Q Water is made by filtration of fresh water using a Milli-Q filtration system (Millipore Corporation, Germany)

In summary to make 1L of media you add the 1ml of the two basic ingredients (table 2.1) and the 1ml of the f/2 solution and 0.5 ml of the vitamins.

With this complete the growth media is now ready for use.

All chemicals listed above came from Sigma Aldrich (Poole, UK).

2.2.2. Culture conditions.

20ml of cells from the culture collection were placed into an autoclaved Nalgene (Sigma Aldrich. Poole, UK) bottle containing 250ml of culture media.

The cultures were then incubated and allowed to grow at a temperature of 15ºC with an irradiance of 100umol photons m^{-2} s^{-1} with a 8 hour: 16 hour dark: light regime.

The cells were continuously sub-cultured by removing 20ml of the culture during the exponential log phase (see fig2.1) and placed into a new bottle of 250 ml of fresh culture media. This ensured a fast turnover of cells as the cells were at their highest rate of replication.

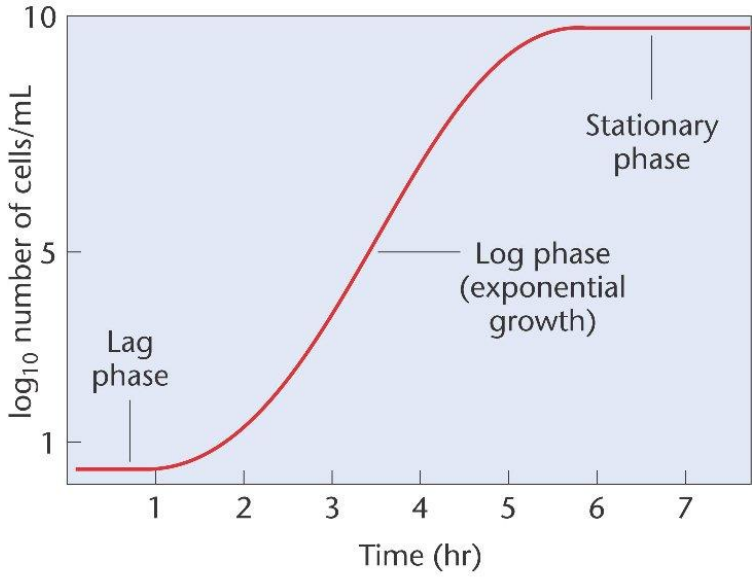

Figure 2.1 Example of an exponential growth curve

The exponential growth rate of the cells was established by cell counting. 10 ul drops of the culture were placed on a Neubauer Haemoctytometer (Agar Scientific, Stansted, UK). Over 200 cells were counted to ensure statistical accuracy.

All of the cells collected for the Electron Microscopy (EM) were collected from mid-log phase to ensure they were healthy.

2.3 Light microscopy.

Cells were removed from a mid-log phase culture and examined using a Leica DMIRB Leica, Wetzla, Germany) inverted microscope and images were captured using an Olympus E410 camera (Olympus, Japan). Images of a graduated graticule (Agar Scientific Stansted, UK) were also taken in order to obtain an accurate scale bar.

2.4 Conventional Scanning Electron Microscopy (SEM) preparation.

There were two approaches for the SEM preparation, one for *C. pelagicus* and one for *E. huxleyi*.

2.4.1 *Coccolithus pelagicus* SEM preparation.

The cultured cells in a volume of 90 ml of filtered Sea Water (FSW) and growth nutrients were fixed using glutaraldehyde (Agar scientific, Stansted, UK) (10ml of 25%) to achieve a concentration of glutaraldehyde of 2.5%.

The cultured cells were left and allowed to sink to the bottom of the bottle. This made collecting them easier as they were already starting to concentrate as they sank to the bottom.

They were then collected by sucking them up into a 10 ml syringe (Becton Dickinson, UK). The volume of liquid sucked up would range from between 2ml -10 ml dependant on the concentration of cells in the culture. A higher concentration (established via Light Microscopy) of cells meant less culture was sucked into the syringe and vice versa.

The culture media with the cells was then pushed through a Whatman track etched nucleopore filter (Agar scientific, Stansted, UK) measuring 13 mm in diameter and with a pore size of 1um (see figure 2.2). This removed the liquid and further concentrated the cells. The cells were then rinsed by sucking up 10 ml of distilled water into the syringe and pushing through the filter. This was repeated to ensure a thorough rinsing of the cells. This removed all of the glutaraldehyde and the FSW. By rinsing with distilled water rather than FSW it removed the salt from the cells which would obscure detail when it came to examining the cells.

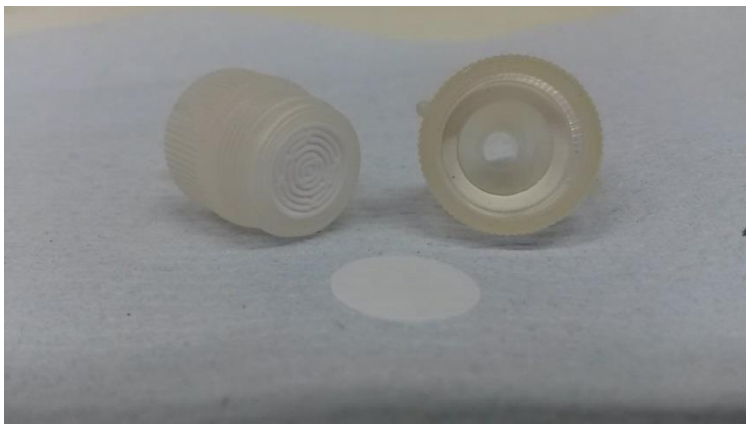

Figure 2.2 A Nucleopore filter (the white disc) and the filter holder (Agar Scientific, Stansted, UK).

Once this was done, the nucleopore filter was removed from the holder and placed cellulose nitrite filter paper (Agar scientific, Stansted, UK) and allowed to dry by placing it into a Taab oven at 40^{o}C (Taab, Aldermasten, UK) for at least one hour.

Once dry, the nucleopore filter was placed on an aluminium stub (Agar scientific, Stansted, UK) with a carbon infiltrated minitab (see figure 2.3). (Agar scientific, Stansted, UK)

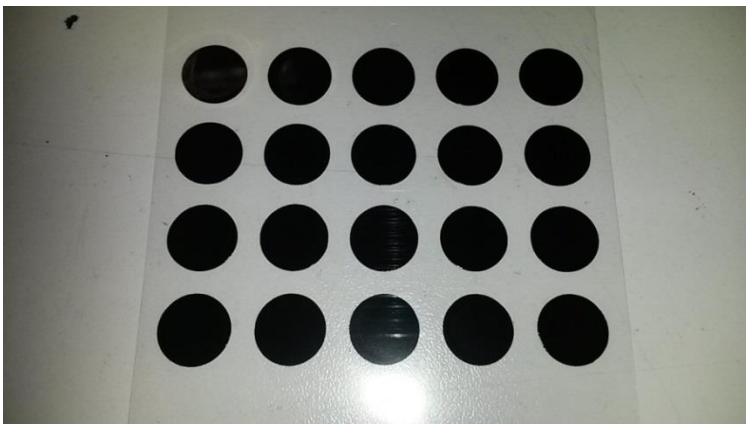

Figure 2.3 Carbon infiltrated minitabs, also known as ‘black spots’.

Once this was done, the stubs were then sputter coated with gold using an Emitech K550 (Quorum Technologies, Laughton, UK) gold sputter coating unit. (see figure 2.4).

Figure 2.4 Examples of gold sputter coated stubs.

The stubs were then examined using a JEOL JSM 5600 LV (Jeol UK, Welwyn garden city, UK) or JEOL JSM 6610 LV scanning electron microscope (SEM) using a variety of magnifications to produce the desired images.

It was found that in order to maximise resolution whilst minimising charging artefacts the samples were imaged at 15kV.

2.4.2 *Emiliania huxleyi* SEM preparation.

The SEM preparation of *E. huxleyi* was similar to that of *C. pelagicus*. The main difference was that the fixation stage (with the glutaraldehyde) was removed from the protocol and the cells were collected as they floated in the media after prior agitation.

Typically, 10 ml of media were required to ensure sufficient cells were collected for observation as without the fixation step the cells were floating in culture rather at a lower concentration than collecting at the bottom of the bottle.

The cells were again pushed through a 1um Nucleopore filter and rinsed with distilled water as before. However, this step was only to ensure the removal of the salt from the cells as it potentially would obscure the cells. They were mounted on stubs and gold sputter coated as before.

The use of the fixation step when imaging *C. pelagicus* was required as it promoted better structural detail which was lost due to shrinkage artefacts. This was not a problem when preparing and imaging *E. huxleyi* hence the requirement in the alteration of preparation protocols.

2.5 Conventional Transmission Electron Microscopy (TEM).

In order to prepare samples for conventional TEM, a sample of log phase cultured cells in a volume of 250 ml of FSW were fixed using glutaraldehyde (2.5% v/v).

This was then left for at least an hour to allow the fixed cells to sink to the bottom of the bottle thus allowing easier collection. These cells were then transferred to a tube (Eppendorf tube from Agar scientific, Stansted, UK) where they were centrifuged at approximately 3000 g for 2 minutes in a Sigma centrifuge (Sigma Aldrich, UK).

The supernatant was then removed and replaced with FSW and the pellet resuspended by shaking it. It was then left for 15 minutes to allow the removal of the glutaraldehyde. It was then centrifuged and supernatant

removed and replaced with fresh FSW allowing for complete rinsing of the cells.

This process was then repeated but with 30% ethanol instead of FSW. It was repeated again with 50%, then 70%, 90% and finally 100% ethanol. The rinse with 100% was repeated twice, each time using ‘dry’ ethanol (‘dry’ ethanol was achieved by placing molecular sieves (Agar scientific, Stansted, UK) in the bottle of 100% methanol).

Each rinse was left for 15 minutes to ensure adequate exchange of the liquids.

Once the alcohol dehydration was completed the 100% methanol was removed and replaced with a 30% Agar low viscosity resin (Agar scientific, Stansted, UK): 70% absolute methanol. The pellet was resuspended and left for 12 hours in order to allow the resin to mix with the cells and begin infiltration.

After 12 hours, the cells were centrifuged as before and the supernatant replaced with 50:50 resin: methanol. Again it was left for 12 hours.

This process was repeated again with 70:30 (resin: methanol) and finally with 100% resin. Again, it was left for 12 hours to allow the resin to fully infiltrate into the cells

The tube was then transferred to a Taab embedding oven were the resin was polymerised at 60^{o}C overnight (12 hours).

The resultant, hardened block was removed from the tube so it could be sectioned with a Leica Ultracut E ultramicrotome using a Diatome diamond knife (Agar scientific, Stansted, UK) (see figure 2.5). The resultant sections (80 nm thick) were supported on 200 mesh, thin bar copper grids (Agar scientific, Stansted, UK) (see figure 2.6).

Figure 2.5 Diatome diamond knife.

Figure 2.6 200 mesh thin bar copper grids used to support the section.

The copper grids with the sections on them were stained first with a saturated solution of uranyl acetate then with a solution of Reynold's lead citrate (Glauert, 1977).

Recipe for making a saturated solution of Uranyl acetate for staining sections prior to examination in a TEM is as follows: -

- Put 1-gram Uranyl acetate powder (Agar scientific, Stansted, UK) in an Eppendorf tube (Eppendorf, Agar scientific)
- Fill tube with 70% ethanol
- Shake vigorously until all of the powder is dissolved (see figure 2.7)
- Centrifuge at 3000 rpm in a Sigma micro centrifuge for 3 minutes until the powder has separated from the supernatant (see figure 2.8)
- Remove the supernatant and put in a 2 ml (Becton Dickinson, UK) syringe
- Put a Millipore, Millex syringe driven filter (Agar scientific, Stansted, UK) on the end of the syringe.
- Then place a Micro lance needle (Becton Dickinson, UK) on the end of the filter

  The saturated solution of uranyl acetate is now ready for use.

Figure 2.7 Uranyl acetate in tube having been shaken.

Figure 2.8 the same tube having been centrifuged. The desired supernatant is the clearer yellow on the left.

Once the Uranyl acetate stain was prepared then the grids were placed on drops of the stain. The drops themselves first being put onto a piece of stretched Parafilm (Agar scientific, Stansted, UK) which in turn was wrapped around a Perspex square. See figure 2.9.

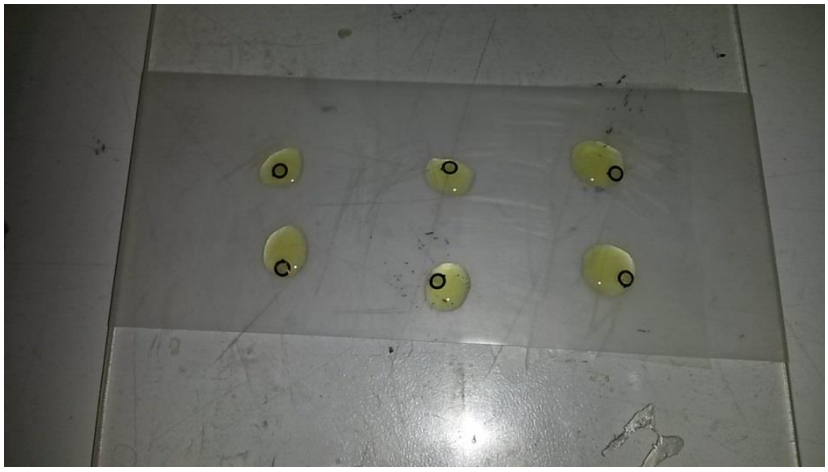

Figure 2.9 Copper grids being stained on drops of Uranyl acetate.

Once the grids had been on the stain for 15 minutes they were gently rinsed in distilled water as in figure 2.10.

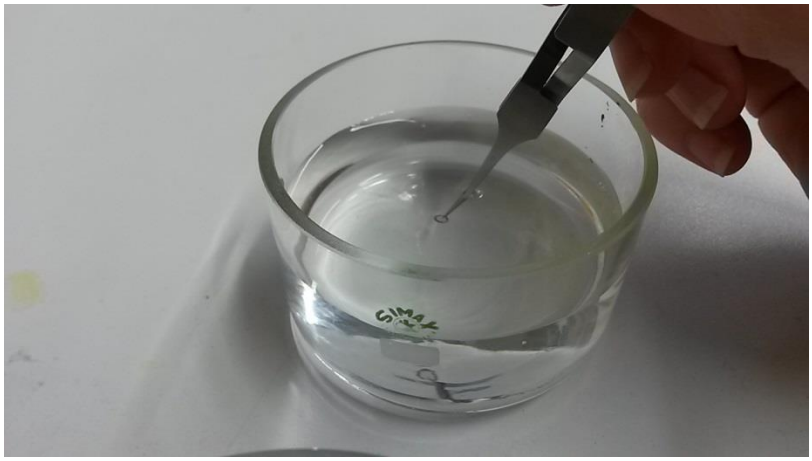

Figure 2.10 A copper grid being rinsed in distilled water.

Once rinsed the grids were then stained in Reynold's lead citrate.

Reynold's lead citrate was made in the following way: -

- Put 50ml of freshly distilled water into a 250ml conical flask (Agar scientific, Stansted, UK)
- Add 1 pellet (0.1-0.2 grams) of sodium hydroxide (Agar scientific, Stansted, UK)
- Add 0.25 grams of lead citrate powder (Agar scientific, Stansted, UK)
- Put in a stirring bean and seal with Parafilm to exclude excess CO_2

- Allow to mix on a Fisher Scientific heating, magnetic stirrer (Fisher scientific, Loughborough, UK) For 10 minutes until the lead citrate and the sodium hydroxide has been dissolved
- Remove the Parafilm and fill 3x 10 ml syringes.
- Place a Millipore, Millex syringe driven filter and a micro lance needle on the end of the syringe (see figure 2.11)

The Reynold's lead citrate is now ready for use.

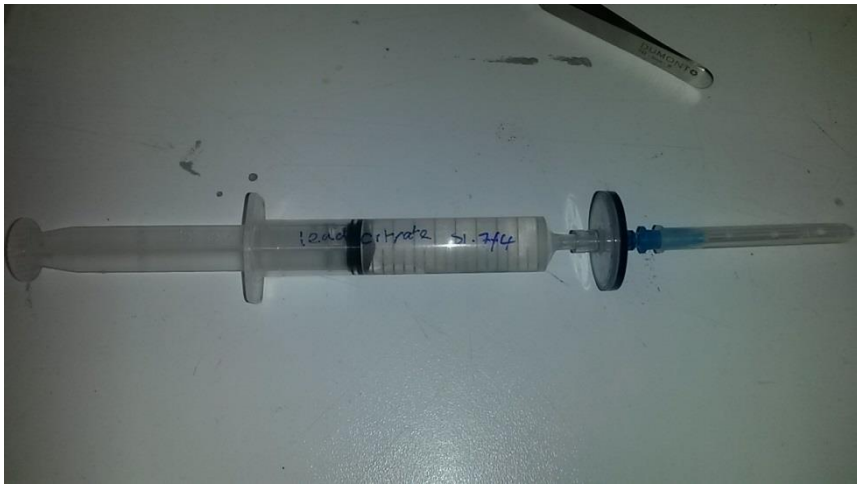

Figure 2.11 A syringe of Reynold's lead citrate with attached filter and needle ready for use.

Drops of Reynold's lead citrate were placed into a petri dish (Agar scientific, Stansted, UK) and surrounded with sodium hydroxide (Agar scientific, Stansted, UK) in order to eliminate unwanted CO_2 which would result crystals of lead forming on the sections potentially obscuring detail. See Figure 2.12.

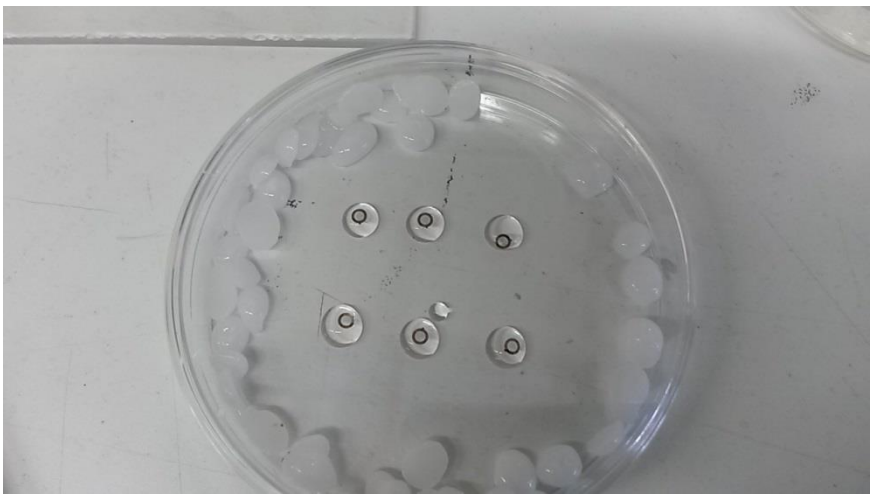

Figure 2.12 Grids being stained with Reynold's lead citrate in a Petri dish containing sodium hydroxide pellets.

Once the grids had been on the stain for a further 15 minutes they were rinsed as previously described (figure 2.10).

They were now ready for examination and imaging in a JEOL 1200 TEM using a variety of magnifications to yield the desired images. It was found that using an accelerating voltage of 120kV gave the best resolved images which were captured using an Olympus SIS Megaview III camera.

2.6 Cryo SEM.

A fresh sample of log phase cultured cells were centrifuged in a micro centrifuge (Fisher scientific, Loughborough, UK) at 2772 x g for 5 minutes. The supernatant was discarded in order to produce a highly concentrated solution of cells. A small aliquot of this solution was placed between two rivets (Quorum Technologies, Laughton,

UK) (see figure 2.13 and 2.14).

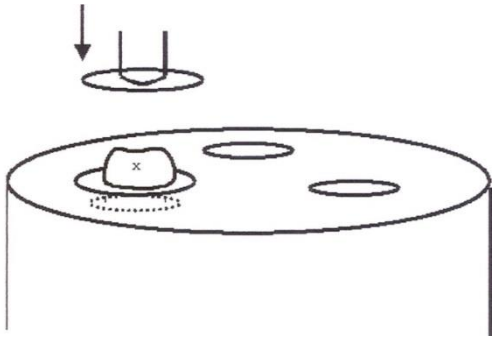

Figure 2.13 Diagrammatic representation of the initial freeze fracture step showing the aliquot, labelled x between the two rivets.

Figure 2.14 Rivets used in the Cryo SEM.

The rivets were then plunge frozen either in liquid ethane (obtained by cooling propane gas in a metal beaker (Agar scientific, Stansted, UK) in a

Liquid nitrogen bath) or in a nitrogen slush produced by Quorum PP3010T cryo SEM preparation system. (Nitrogen provided by BOC (Linde group, Germany).

The rivets were then mounted in the cryo chamber of a JEOL 6610 LV SEM under liquid nitrogen and subsequently fractured. It was found that a firm swing of the razor in the cryo chamber produced a better fracture rather than a gentle tap.

The cells were then transferred via a transfer rod to the microscope so initial imaging could be used to establish the integrity of the cells.

With this done, the cells were returned to the cryo chamber were they were etched by raising the temperature to -85^{o}C for 60 -120 seconds and then returning it to -135^{o}C.

The etching results from of raising the temperature so the ice can be sublimed and removed from the surface of the sample allowing detail to be revealed. The cells were then sputtered with gold prior to reinsertion to the SEM for imaging.

The results of this work can be found in the Taylor *et al.*, 2006, appendix 1.

2.7 Morphometric data acquisition.

For the acquisition of the morphometric data in chapter four *Emiliania huxleyi* isolates were collected from various locations in the Arctic and Southern Oceans and cultured as described in 2.2. They were then mounted on stubs as described in 2.4.2 with four filters per stub as illustrated in figure 2.15 below.

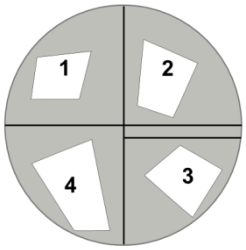

Figure 2.15 Illustration of how the four pieces of filter paper were arranged on a single 12mm diameter stub to reduce the number of stubs needed.

Over 50 stubs were prepared in this way ready for them to be imaged in a JEOL 6610 LV SEM (Jeol UK Welwyn garden city, UK) as described in 2.4. All of the images were taken at the same magnification to ensure correct measurement data acquisition.

Once the images were acquired they were analysed with Fiji-is just image J (National Institute of Health, Bethesda, Maryland USA) using a plug-in:

coccobiom2-SEM.ijm designed by Jeremy Young (University college, London, UK).

This was achieved as described below: -

- Open FIJI-is just image J and install the Biom macros
- Import the image sequence

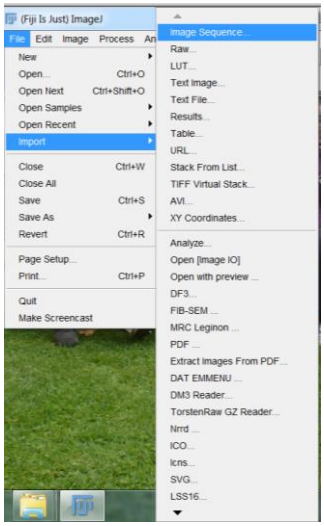

- Open the first image and draw a straight line below the scale bar.

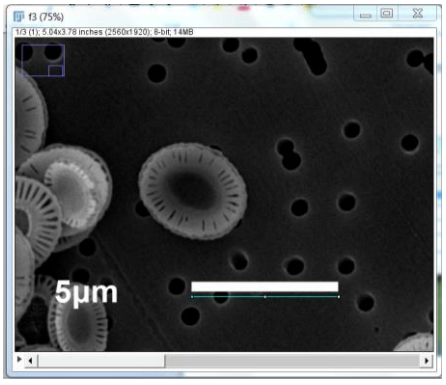

- Click on analyse, then set scale and change the known distance to whatever it was (in this case 5) set the units to um and the check the global box. This will ensure that the same scale will be applied to all subsequent images.

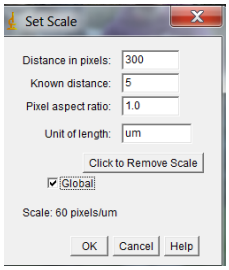

- Find a suitable coccolith (coccoliths were excluded from measurement if at least part of it wasn't touching the filter paper. Measuring these coccoliths could have introduced erroneous data resulting from issues with perspective. i.e. if the coccolith was higher up and therefore closer to the 'camera' it would have appeared larger than it was).

  Select the elliptical tool and draw an ellipse around the coccolith.

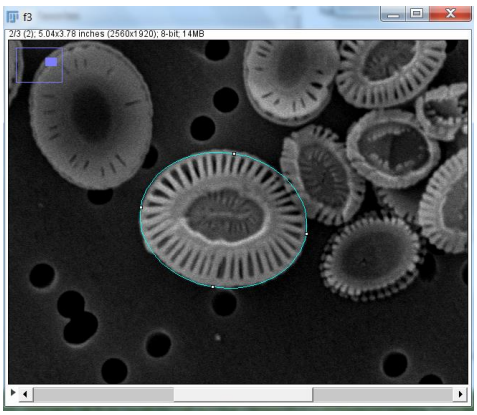

- With the mouse pointer in the ellipse, press 1. This measures the length and width (major and minor).

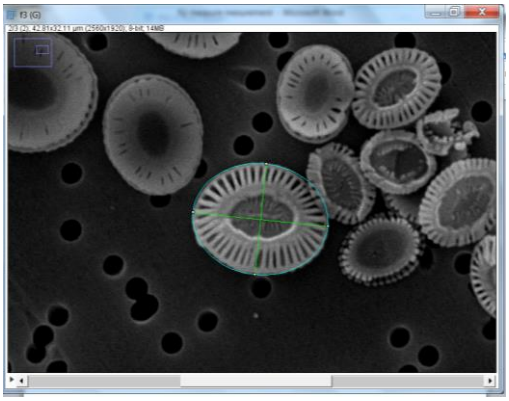

- With the mouse pointer on the inner edge of the tube (the red ellipse) press 2. This produces the ‘tube inside measurement and the

‘elements’ and ‘ray width’ data (thus counting the number and thickness of the rays-labelled with the small squares). These are also known as the ‘t’ elements.

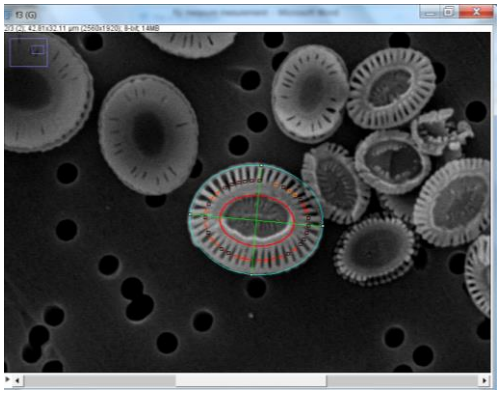

- With the mouse pointer on the outer edge of the tube press 3. This produces the ‘tube outside’ data. The tube being the elliptical region between the two red ellipses.

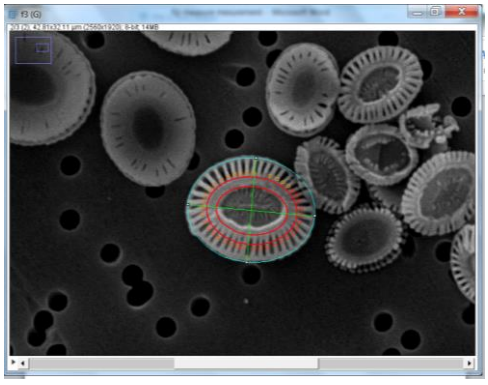

- Then label the coccolith and move on to the next one.

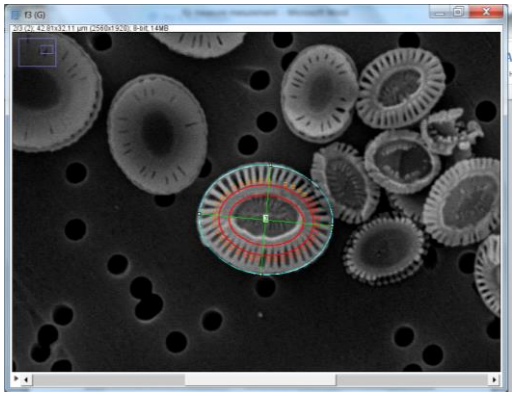

Using this method produced the following results: -

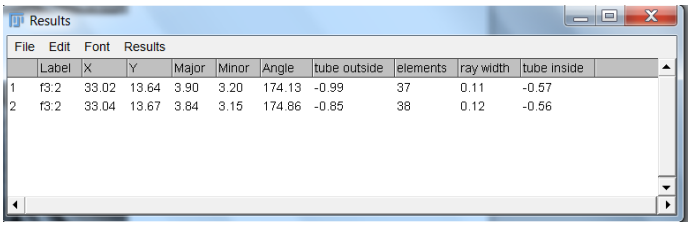

	Label	X	Y	Major	Minor	Angle	tube outside	elements	ray width	tube inside
1	f3:2	33.02	13.64	3.90	3.20	174.13	-0.99	37	0.11	-0.57
2	f3:2	33.04	13.67	3.84	3.15	174.86	-0.85	38	0.12	-0.56

The data used for the morphometric analysis was the major and minor (length and width of the coccolith). The size of the tube (acquired from the tube outside and inside data) and the number of elements and their width (ray width).

In order to provide statically relevant data, it was required to measure at least 60 coccoliths from each filter. To do this, two different approaches were employed. The first was to reduce the amount of time taking the

images by producing lower resolution images resulting from a faster scan (20 seconds). This allowed sufficient images to result in 60 coccoliths which produced the data for the tube measurements and the length and width.

In order for the 'plug-in' to measure the 't' elements, higher resolution images were required (produced by a slower 40 second scan). Fewer whole coccoliths were measured (10 instead of 60) however this still produced over 250't' element measurements for each filter.

The method described above was used for the higher resolution images. It was also used for the lower resolution images with the data acquired for the 't' elements simply being discarded.

All of this data was inserted into Microsoft Excel (Microsoft Redmond, Washington, USA) and using Excel, the Mean, Standard deviation and Standard error were calculated. This data was used to produce scatter plots and frequency distribution plots. All of these can be seen in chapter four.

Alongside this data in Excel are the geographical location, (Longitude and Latitude), the cell type and Coccolith Morphology Motif or CMM (for details see 4.2).

All of this was undertaken following the work of Young *et al.*, 2014.

2.8 Publications.

The skills developed during the course of the work were also used to contribute to the publications listed below. Indicated are the papers where my skills with the SEM contributed. Then is a list of where my skills in developing TEM technique. These publications can be found in Appendix A1 along with a more detailed description of my contribution.

Chapter 3.

Dynamics of formation and secretion of heterococcoliths by *Coccolithus pelagicus*.ssp. *braarudii*.

3.1 Abstract.

The non-motile life phase of the coccolithophore *Coccolithus pelagicus* is characterised by the formation and secretion of ornate calcified plates, heterococcoliths. The formation of these plates (coccoliths) was investigated by transmission electron microscopy (TEM).

Coccolithogenesis (the formation of these plates) in *C. pelagicus* exhibited a similar pattern to that seen in *Emiliania huxleyi* in that mineralization occurs in Golgi-derived and nuclear associated vesicles.

The TEM data acquired shows that only when the single coccolith is mature, does it begin to migrate away from the nucleus before secretion.

A structure known as the reticular body, distinct from the Golgi body, was also visible at the distal surface of the developing coccolith suggesting that it is a common feature of all placolith coccolith producing cells when only a single coccolith is produced and secreted at a time.

The TEM also revealed flagellar root apparatus at the anterior pole of the non-motile cell from which polarised secretion of coccoliths occurs. This may indicate a novel role for such cyto-skeletal structures.

3.2 Introduction.

Coccolithus pelagicus is similar to the extensively studied *Emiliania huxleyi* in that it too has a heteromorphic life cycle changing between haploid and diploid phases depending on conditions (Geisen *et al*., 2002; Houden *et al*., 2004). And as with *E. huxleyi*, *C. pelagicus* has an outer covering of ornate calcite plates: coccoliths. These are secreted by the non-motile, diploid cells to form an interlocking sphere surrounding the cell: the coccosphere.

Both *E. huxleyi* and *C. pelagicus* have a wide distribution (McIntyre and Be, 1967: Brand 1984) and are one of the most significant producers of calcite on earth and as such have a vital role in the marine carbon cycle and upper ocean carbonate chemistry (Rost and Reibsell, 2004). Despite their significance, the cellular mechanism and environmental regulation of coccolith production are not well understood.

Work in coccolithophore biology has resulted in considerable advances in the understanding of the biodiversity, ecology, life history and cell physiology of the important organisms (Paasche, 2002: Thierstein and

Young, 2004). Despite this, the function of the coccosphere and its production have not been fully demonstrated (Young, 1994).

The formation of coccoliths has been studied both biochemically (van der Wal *et al.*,1983) and ultrastructurally (Braarud and Nordli, 1952; Manton and Leedale, 1969; Klaveness, 1972 and 1976). It involves the formation of an organic scale or baseplate within a compartment derived from the Golgi to which calcite crystals nucleate. (For more specific information crystal nucleation and calcite deposition refer to chapter 1).

Despite all of the research and detailed studies of coccolith function and structure, little progress has been made in fully understanding the exact mechanism that results in the formation and extrusion of coccoliths through the plasma membrane of the cell to result in a continuous periplasmic coccosphere. The actual act of coccolith secretion remains un-described (Paasche, 2002).

The work discussed in the chapter is taken from the paper: Dynamics of formation and secretion of heterococcoliths by *Coccolithus pelagicus*.ssp. *braarudii*. Written by Alison R. Taylor, Mark A. Russell, Toby F. T. Collins, Colin Brownlee and myself. (See appendix 1)

The aim of the work undertaken was to use a combination of high resolution light microscopy and electron microscopy to ascertain the important structural features and characteristics that result in coccolith

formation and extrusion through the plasma membrane to result in a continuous coccosphere. The paper discusses the demonstration of how coccolith formation is as the result of light dependant coccolith formation (Coccolithogenesis) and secretion occurs rapidly as the result of a light independent phase.

The light microscopy also shows cellular contractile activity and the cells ability to rotate to orientate the secretion of the coccolith is fundamental in maintaining an intact coccosphere. Alongside this, a novel functional role of the layer of organic scales is proposed.

My significant contribution to this paper was the Transmission Electron Microscopy (TEM). Discussed in this chapter are the general ultrastructure, Coccolithogenesis and coccolith secretion as well as the role of the un-mineralised scales and the deposition of calcite.

The materials and methods used in acquiring the data in this chapter can be found in chapter 2.

3.3 General cell ultrastructure.

The ultrastructure and organelles observed with the TEM of the 182g strain of *C. pelagicus* are generally consistent with those observed in other coccolithophore species (Parke and Adams, 1960; Manton and Leedale, 1969; Klaveness, 1973; Inouye and Pienaar, 1984).

In figure 3.1 (below), it can be seen that the exterior of the cell is covered with a layer of coccoliths. The coccoliths themselves are not present in the images as a result of the inability of the resin to penetrate what is in essence a solid piece of calcite. The result of this is that only the impression of the coccolith remains in the imaged section. These are the areas of white on the periphery of the cell.

The coccosphere itself covers a layer of organic scales (as indicated by the arrows in Figure 3.1. These are visible as the feint lines and labelled Sc) and coccolith baseplates the role of which will be discussed later.

Within the cell there are two large lobed chloroplasts with internal pyrenoids just below the plasma membrane on opposite side of the cell. This arrangement was found in all observed cells. A large nucleus surrounded by endoplasmic reticulum was also observed. The endoplasmic reticulum was located towards the posterior end of the cell and most of the sections revealed a developing coccolith within a Golgi derived coccolith vesicle. There were mitochondria clearly located around the nucleus and

the rim of the coccolith vesicle suggesting that these are areas of high metabolic activity.

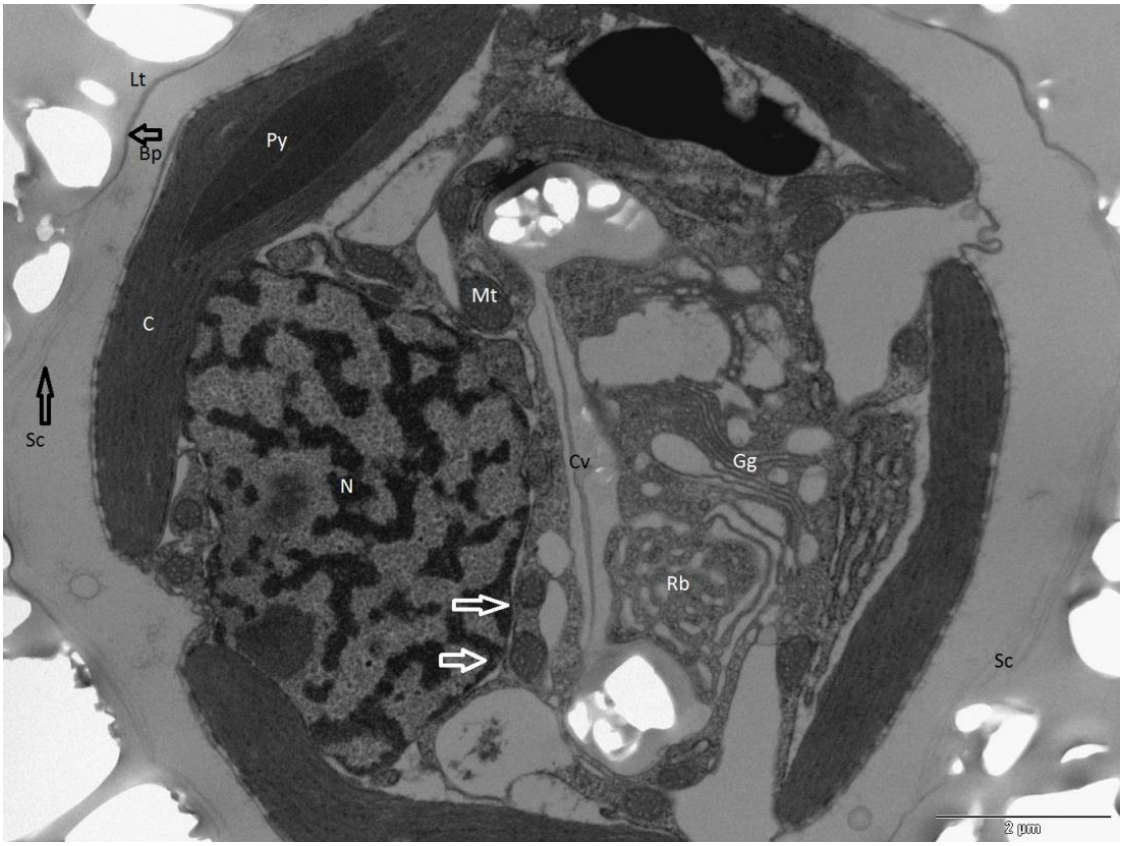

Figure 3.1 *C. pelagicus* ultrastructure as observed with a TEM. Clearly visible are the voids in the resin left by the external coccoliths (Lt) and their close association with the baseplate of the coccolith (Bp) and the layer of organic scales (Sc). Above the Nucleus (N) is one of the Chloroplasts (C) with a single thylakoid traversing Pyrenoid (Py). Also Reticular body (Rb) Golgi (Gg) Coccolith vesicle (Cv) Mitochondria (Mt)

The nucleus is surrounded by the Nucleoplastidial envelope (indicated by the two white arrows) and the mitochondria (Mt) are closely associated with the coccolith vesicle (Cv) which contains a newly forming coccolith.

The vesicle is in turn closely associated with the Golgi body (Gg) and the mass of anastomosing vesicles that resemble a reticular body (Rb). These are located in the distal pocket of the developing coccolith vesicle.

3.3.1 The Golgi and reticular body.

The image below (3.2) shows the details of the coccolith vesicle. It shows a single, large Golgi body. This was always present on the distal side of the developing coccolith vesicle. This is consistent with the placolith forming *Umbilicosphaera sibogae* Weber-van Bosse (Inouye and Pienaar, 1984) which is closely related to *C. pelagicus*. This is a marked contrast to *E. huxleyi* where the Golgi is found in a region peripheral to the margins of the coccolith vesicle (Klaveness, 1972; van der wal *et al*., 1983a).

Detailed inspection of the Golgi revealed dilated cisternae typical of coccolith forming prymnesiophytes (Pienaar, 1988; Klaveness and Lee 2001; Hawkins and lee 2001) and a Golgi vesicle containing a developing organic baseplate or organic scale.

In addition to the Golgi there is a large mass of anastomosing tubular structures that are remarkably similar to the reticular body found in *E. huxleyi* (Wilber and Watabe, 1963; van der Wal *et al*., 1983; westbroek *et al.,* 1984). This structure was always associated and localised with the

Golgi body in the distal pocket of the developing coccolith (see Figure 3.1). As a result of this similarity, the structure shall hereafter be referred to as the Reticular body or reticular mass.

This structure was not reported in *C. pelagicus (*Manton and Leedale, 1969). It was subsequently proposed (Paasche, 2002) that the missing reticular body was related to the fact that coccoliths formed in the Golgi cisternal comparments. The reticular body was thought to be unique to *E. huxleyi* and *Gephyrocapsa* Kamptner and was linked to the model whereby smaller Golgi vesicles would coalesce to form the coccolith vesicle (Paasche, 2002). Many coccolithophores do not have a reticular body. For example, the cricolith forming *Pleurochrysis carterae* Braarud And Fagerland (Pienaar, 1969; Outka and Williams, 1971) and the tremalith forming *Ochrosphaera neapolitana* Schussnig (Fresne and Probert, 2005). In species such as these, coccolith formation and mineralisation may occur in more than one compartment and coccolith maturation occurs in Golgi-derived vesicles that move towards the plasma membrane and are not associated directly with the nucleus (van Der Wal *et al.*, 1983).

In all of these species, the Golgi is always associated with coccolith formation and it is thought that the role of the Golgi is linked to the ability of the endomembrane system to sequester and transport high volumes of calcium to the site of mineralisation (Brownlee and Taylor, 2004).

An endoplasmic tubular reticular body may be a common feature of all placolith-forming species that produce coccoliths one at a time. However, *E. huxleyi* and *C. pelagicus* are both within the class Prymnesiophycae are only distantly related (Young *et al.*, 2005). In addition to this, *C. pelagicus* is a member of the order *Coccolithales* where there are species that produce either a single coccolith (Reticular body present) or multiple coccoliths (no reticular body). Therefore, a possible explanation for the reticular body is that it appeared early on in the evolution of placolith forming coccolithophores and has, subsequently be modified or lost in a number of groups.

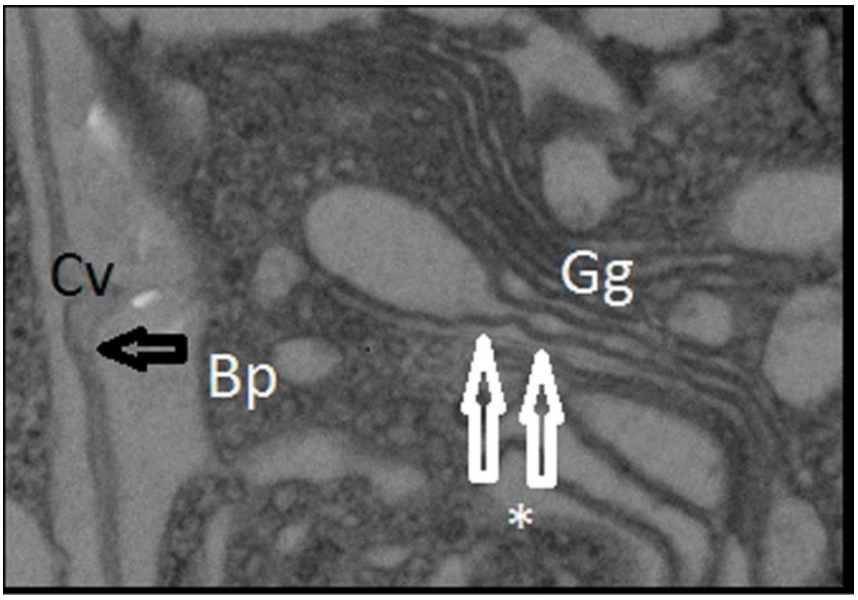

Figure3.2 Detail of the coccolith vesicle (Cv) from figure 3.1. The Golgi (Gg) can be seen closely associated with the central region of the Coccolith vesicle (Cv) containing a newly developing unmineralised section of the coccolith base plate (Bp). Just below the Golgi can be observed a newly

forming base plate or scale within the (indicated with the asterisk and arrows) within a distal Golgi cisterna.

3.3.2 Flagellar root and contractile microtubules.

Figures 3.3 to 3.5(below) show bundles of microtubules, commonly found in motile coccolithophores (Manton and Peterfi, 1969; Gayal and Fresnel, 1983; Inouye and Pienaar, 1988; Green and Hori, 1994; Fresnel and Probert, 2005). They are usually associated with the flagellar roots. These bundles were found in several ultrathin sections of *C. pelagicus.*

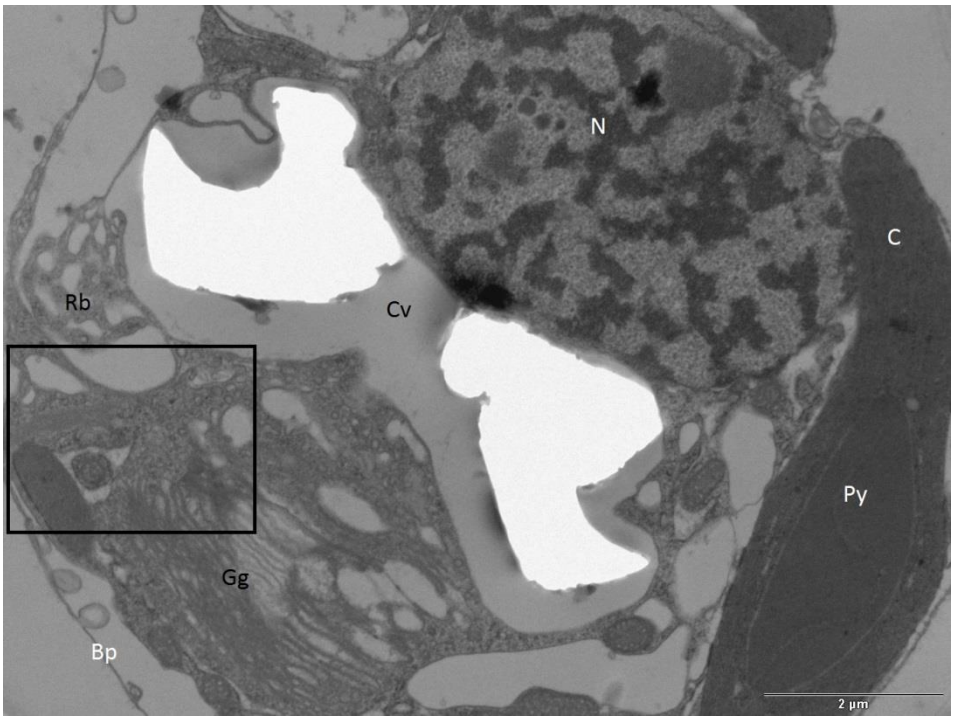

Figure 3.3. TEM section showing the typical location of microtubule bundles with respect to the coccolith vesicle and reticular body (reticular body, Rb; Base plate, Bp; Golgi, Gg; chloroplast, C; pyranoid, Py; nucleus, N ; Coccolith vesicle, CV).

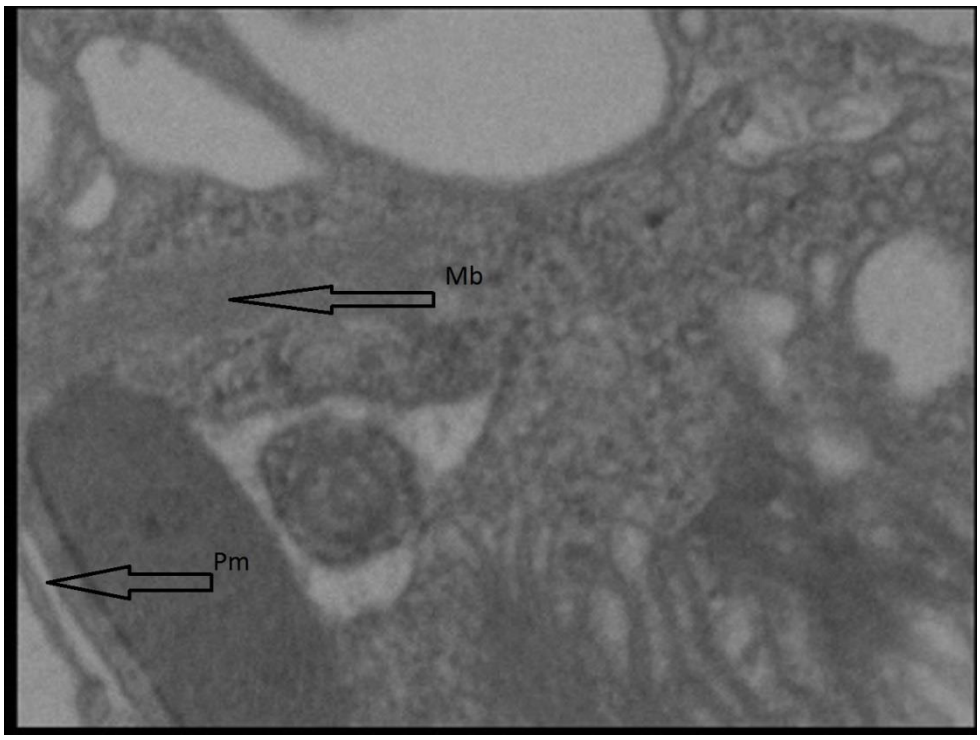

Figure 3.4 Detail from the box in figure 3.3 showing the bundle of microtubules (Mb) projecting from the Plasma membrane (Pm). This structure is similar to the flagellar apparatus root as described below.

The microtubular bundles seen in figures 3.3 and 3.4 were found in a gap between two chloroplasts and they extended quite a distance from the Plasma membrane into the interior of the cell.

The figure 3.5 (below) shows the detail of a compound flagellar root in close association to the reticular mass (body). Such compound flagellar roots have been described previously in the motile stage of *C. pelagicus* (Klaveness, 1973) but were not reported in a previous study of the ultrastructure of the non-motile cells where the flagellar bases were reported with no other comments (Manton and Leedale, 1969).

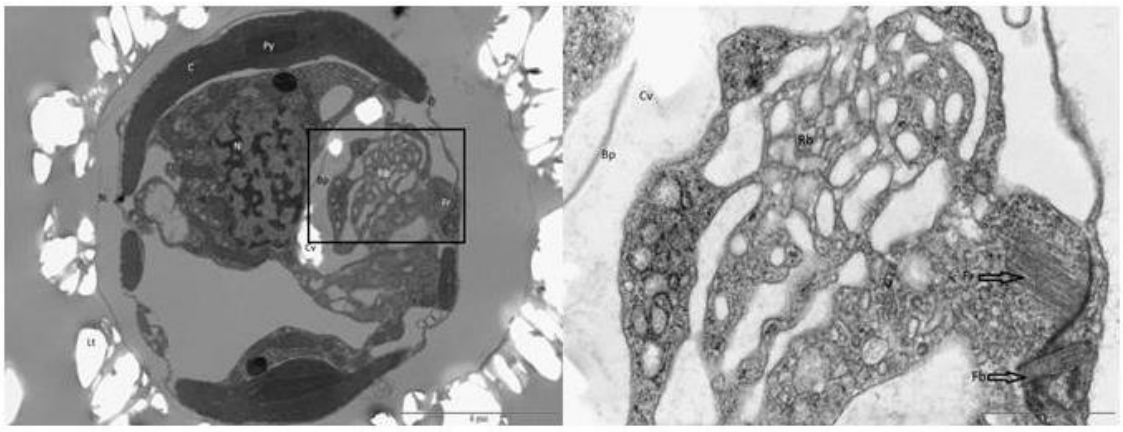

Figure 3.5. Cell (left) with insert (right)showing the detail of a compound Flagellar root (Fr) and its proximity to the Reticular mass (Rb). The Flagellar root (Fr) can be seen associated with the Flagellar base (Fb). For the other abbreviations see the legend for figure 3.3.

Interestingly, Inouye and Pienaar (1984) reported flagellar root bases in the non-motile placolith forming *U. sibogae*. The retention on the compound flagellar roots in non-motile placolith coccolithophores has a significant role in Coccolithogenesis as discussed below.

3.4 Coccolithogenesis.

Biomineralisation in *C. pelagicus* follows a similar pattern observed in *E. huxleyi* (de Vrind-de Jong *et al.*, 1994) and seen in light micrographs of *C. pelagicus* (Manton and Leedale, 1969). The TEM images below and the time lapse images seen in Taylor *et al.* 2007 (see appendix 1) confirm that as with the formation of coccoliths in *E. huxleyi*, a protococcolith ring of calcite forms at the peripheral edge of the organic base plate (Westbroek *et al.*, 1989;

Young *et al.*, 1999) and it extends in both directions as the coccolith matures. Once mature the coccolith is only connected to the peripheral edges of the base plate.

The coccolith vesicle maintains a close association with the nucleus until it is fully mature. Subsequent to its maturation, it migrates away from the nucleus prior to secretion. In in order for this occur; the coccolith vesicle migrates towards the plasma membrane whilst passing through the two chloroplasts at the anterior pole of the cell. The coccolith vesicle then fuses with the plasma membrane and the coccolith perforates the layer of organic scales before it 'slides' out and interlocks with the existing coccoliths in the coccosphere.

The layer of the organic scales as described by Manton and Leedale (1969), overlap by various degrees and in some cases they can be up to eight scales thick (See figure 3.6 below).

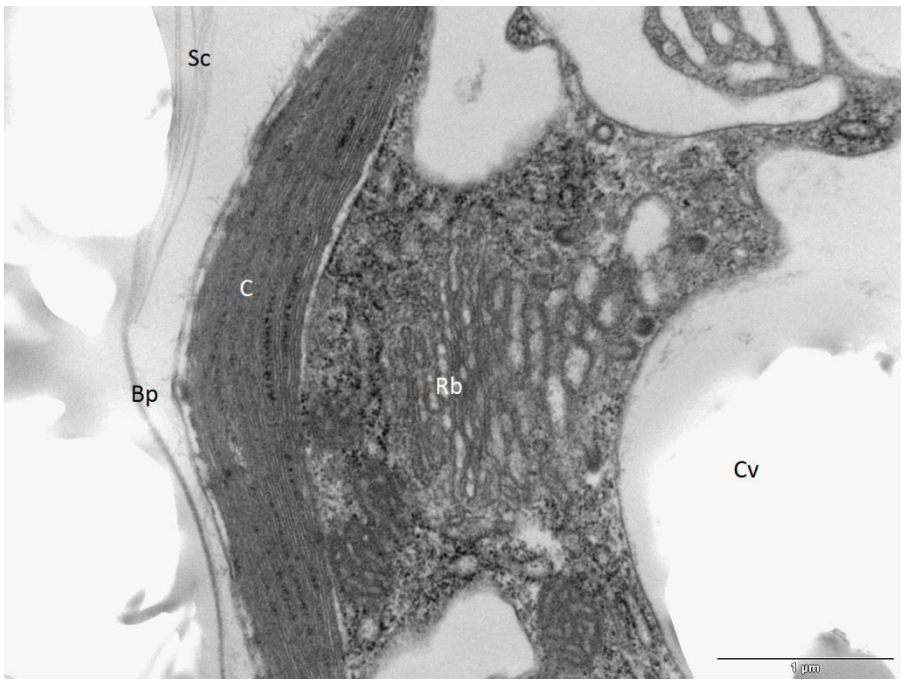

Figure 3.6 TEM showing the multiple organic scales (Sc) interspersed within organic base plate (Bp). (Other abbreviations as used previously).

The organic scales were always observed in the spaces between the interlocking coccoliths. This possibly arises due to the action of the newly emerging coccolith being pushed through the existing layer of organic scales and leaving the scales behind as it is extruded.

3.5 Coccolith extrusion.

Up until the publication of Taylor *et al.*, 2007 paper (see appendix 1) there had been no TEM data on the extrusion of coccoliths in *C. pelagicus.* The data published in the Taylor *et al.*, 2007 paper suggests that for the majority of Coccolithogenesis, the maturing coccolith stays closely associated to the nucleus and the reticular body. It would appear that it only moves away during the final stages of maturation prior to extrusion.

The events which lead to the final extrusion are fairly rapid as observed with the Light microscope and time lapse imaging in the Taylor *et al.*, 2007 paper. This meant that imaging the final extrusion event (typically taking around 77 seconds) remained elusive.

Below (3.7) are a range of images showing the transience of the coccolith from its initial site closely associated with the nucleus, up to the moment before its final extrusion.

They are a series of images of different cells. Due to the nature of specimen preparation for TEM which involves chemical fixation (see chapter 2.7) and consequently the cessation of all dynamic processes. It has been necessary to illustrate the coccolith extrusion on the TEM with a range of images from different cells that exhibited the desired features.

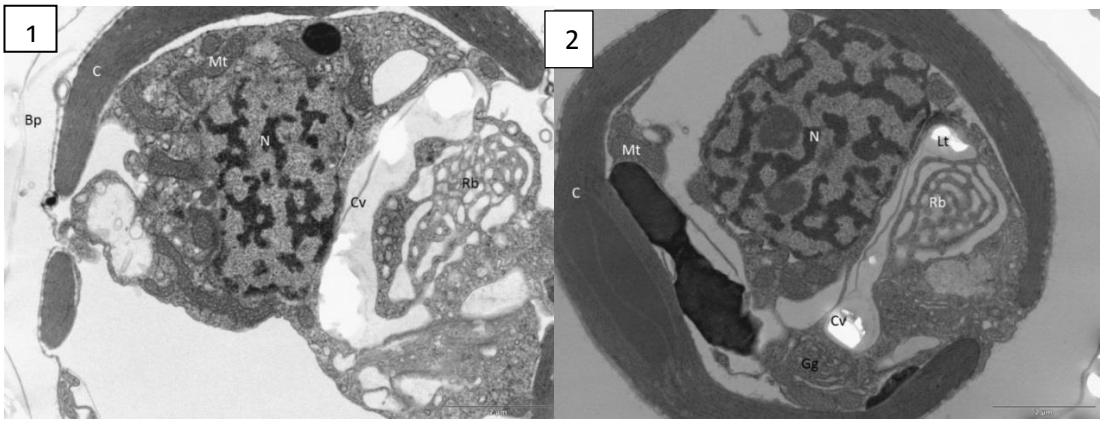
1
C
Mt
Bp
N
Cv
Rb
2
Mt
C
N
Lt
Rb
Cv
Gg

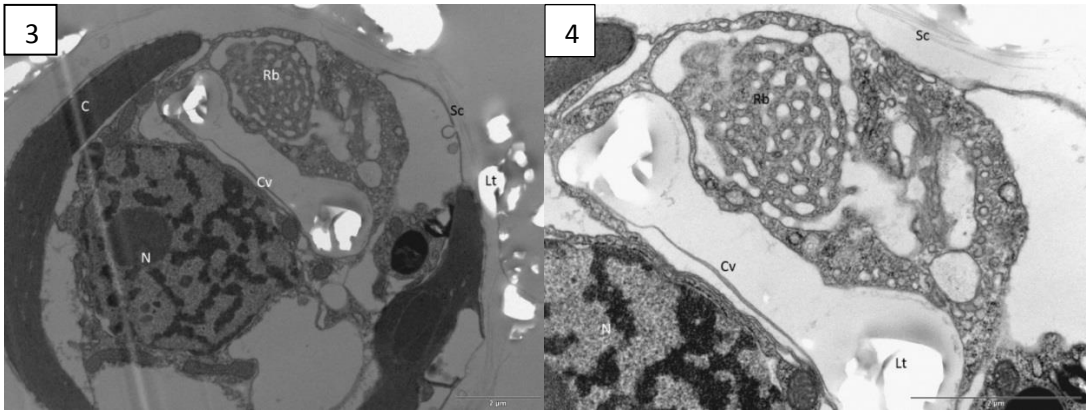
3
Rb
C
Sc
Cv
Lt
N
4
Sc
Rb
Cv
N
Lt

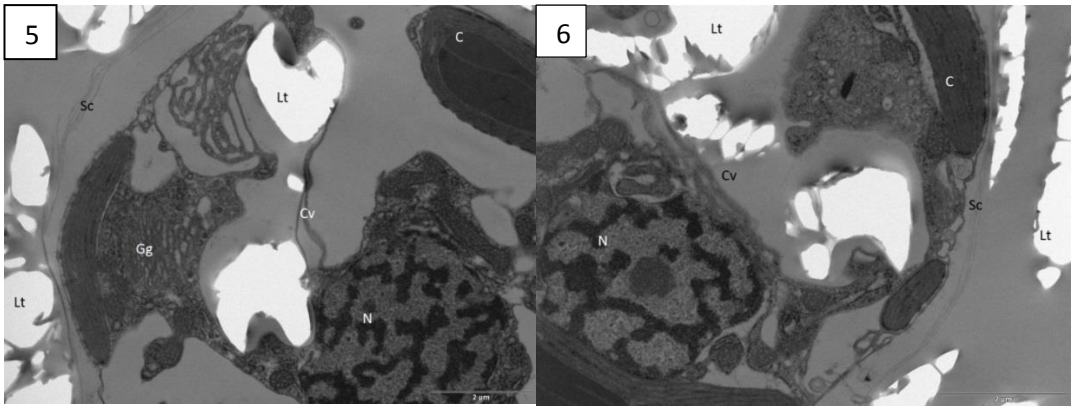
5
C
Sc
Lt
Cv
Gg
Lt
N
6
Lt
C
Cv
Sc
N
Lt

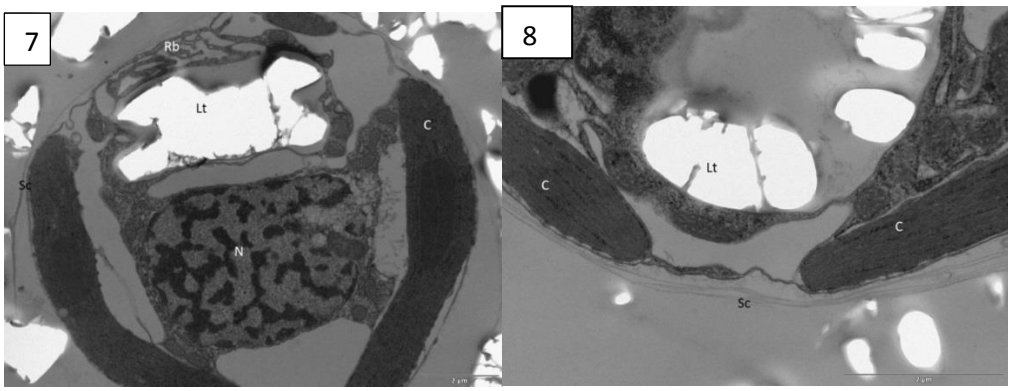

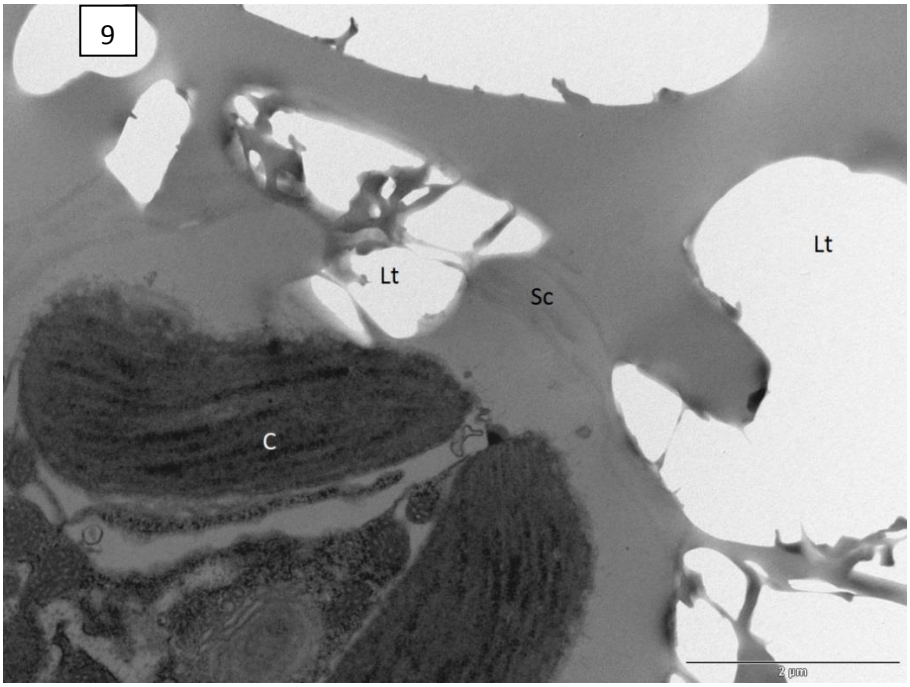

Figure 3.7 1. Image showing the coccolith vesicle (Cv) very close to the Nucleus (N) and the Reticular body (Rb). All other abbreviations as used previously.

2.Another image showing the coccolith vesicle (Cv) close to the Nucleus (N) and the reticular body. However, in this image, the Coccolith (Lt) appears to be growing in size.

3. Image showing the Coccolith vesicle (Cv) containing the coccolith further increasing in size.

4. The coccolith (Lt) and the coccolith vesicle (Cv) appear to be moving to the exterior of the cell in this image. Again the coccolith appears to be increasing in size.

5. The large, nearly fully formed Coccolith (Lt) begins to move away from the nucleus (N) and move further towards the exterior of the cell. It still remains closely associated to the Reticular body (Rb)

6. An image showing the coccolith moving towards the exterior of the cell through the gap in the Chloroplasts (C).

7. A large, fully formed Coccolith imaged between the two Chloroplasts (C) as it nears the completion of its journey prior to final extrusion through the layer of organic scales (Sc) and interlocking with the coccosphere.

8. A coccolith (Lt) about to push through the layer of organic scales.

9. Image of a coccolith (Lt) pushing through the layer of organic scales (Sc) immediately prior to the interlocking of the coccolith with the external coccoliths in the coccosphere.

3.6 Live cell imaging.

In the Taylor *et al.* paper (see appendix 1) there is a section devoted to the time lapse imaging of live cells with a light microscope. The images in the paper show how the coccolith is initially roughly perpendicular to the plasma membrane and then takes a roughly smooth trajectory during exocytosis until finally settling onto the exterior of the cell where it attains its position in the coccosphere. This process on average took 77 seconds.

In order for exocytosis of the coccolith, considerable contractile behaviour is undertaken by the cell. This contractile activity is co-ordinated using the cytoskeleton. The reason for the presence of the compound flagellar root and the microtubules (see figures 3.3-3.7) near the extrusion site at the anterior pole of the non-flagellated cell is not known.

However, flagellar movement, as observed in the prasinophycean *Tetraselmis* Stein (Salisbury *et al., 1984)* is dependent on calcium, ATP (Adenosine Tri Phosphate) and a contractile protein called centrin. It has also been observed in a range of dinoflagellates (Cachon *et al.,* 1994) and in *Chlamydomonas*. In *Chlamydomonas,* rapid nuclear movement occurs during deflagellation (Salisbury *et al.,* 1987) and in dinoflagellates, flagellar root contractions are responsible for excretion via contractile vesicles (Cachon *et al.*, 1983). The Taylor *et al.*, (2007) paper suggests that

whether or not the microtubule/flagellar apparatus have anything to do with coccolithogenesis in this non-motile strain of *C. pelagicus* remained to be determined.

The hypothesis that co-ordinated contractile activity occurs as a result of the inclusion of cytoskeletal involvement is supported by the observation that filamentous actin is specifically localised to the site of scale production in *Pleurochrysis* Pringsheim (Hawkins *et al.,* 2003) and its subsequent secretion.

The paper proposes that the microtubular structures associated with the flagellar apparatus in *Pleurochrysis pseudoroscoffensi* Gayral et Fresnel may be involved in the migration of the coccoliths (Gayral and Fresnel, 1983).

All of this, the paper suggests, that coccolith formation, cellular polarity and coccolith exocytosis is deserving of further investigation.

Since the publication of the initial paper work was undertaken by Langer *et al.* (2010). This work included the addition of a microtubule inhibitor to a culture of *Emiliania huxleyi.* The end result was that malformed and

incomplete coccoliths were formed. This further suggests that the microtubules are critical in the production of coccoliths as well as their secretion.

Drescher, Dillamen and Taylor produced work looking at coccolithogenesis in *Scyphosphaera apstenii* (Prynesiophyceae). They concluded, that despite the radical differences in coccoliths produced by *S. apstenii (*when comparing to coccoliths produced by *C. pelagicus)*, coccolithogenesis and especially the extrusion of the coccolith through the plasma membrane was intrinsically the same as in *C. pelagicus.* Certainly in as much as both cells undergo a series of contractions to achieve the final extrusion of the coccolith.

3.7 Discussion

Biomineralisation is not unique to Coccolithophores. Both sponges and Diatoms use silica instead of calcium as the mineral incorporated into the structure of the cell.

In the marine demosponge *Suberites domuncula* a siliceous skeleton is constructed of spicules (small needle like structures). These spicules contain an axial filament containing an enzyme, silicatein which is responsible for the formation of the spicules. This initially occurs intracellularly but ends extracellularly similar to the formation and exocytosis of coccoliths. The spicules themselves are surrounded by fibrils. It can be speculated that the fibrils have the same function as the cytoskeleton and the microtubule/flagellar apparatus in coccolithophores. (Muller *et al*., 2005).

In diatoms biomineralisation results in the formation of ornate structures known as scales. In diatoms these structures are formed after silica is transported across the cytosol as a result of the intervention of Silicic acid transporters into a structure known as the silica deposition vesicle (SDV) (Hildebrand, 2008). The structure must be analogous to the CV found in Coccolithophores and within the SDV is a structure known as the silicalemma. This appears to be intimately involved with scale formation in the same way the RB is intimately involved with coccolith production.

In diatoms, once the scale has been produced, it is moved within its vesicle which fuses with the cell membrane and the scale fuses with the cell wall. Again, mirroring the production of the coccosphere in calcifying coccolithophores.

There are many similarities in the life cycles of coccolithophores and Diatoms. Both are unicellular organisms that use biomineralisation to produces ‘plates’ that are incorporated into the periphery structure of the cell. One could speculate that there must have been a common progenitor to both types of cells. However, I suspect one would have to go back a long way to find it!

The work in this chapter (and the Taylor *et al.*, 2007 paper) shows that coccolith formation in *C. pelagicus* is reasonably similar to that shown in other placolith bearing species (such as *E. huxleyi*). In that the Coccolith is formed in a vesicle located to an anastomosing network of tubules (often called the reticular body) close to the nucleus. As the coccolith develops it gradually migrates away from the interior of the cell prior to its final

secretion in the coccosphere. (Inouye and Pienaar, 1984. Klaveness, 1972. Westbroek *et al.,* 1984)

The work undertaken showed that the rapid secretion of the coccoliths and accompanying contractile and rotary movements of the protoplasm which resulted in the positioning and final secretion of the coccolith. This was a novel finding and is deserving of further investigation.

Chapter Four – Intra specific variation within the *Emiliania huxleyi* (Prymnesiophyceae) morphotype A group.

4.1 Abstract.

Emiliania huxleyi (Prymnesiophyceae) is one of the most widely studied and best documented marine microalgae. It is covered with an elaborate covering of platelets called coccoliths and it is found in all of the world's oceans with the exception of the extreme polar oceans. It is divided into several morphotypes with the two most widely recognised being A and B. It can also be subdivided according to genotype by the Coccolithophore Morphology Motif (CMM). The CMMs lie in the 3′ untranslated region of the coccolith-polysaccharide associated protein-GPA mRNA, which is associated with coccolith structure control and they are labelled CMM I, II, III and IV. The CMMs have been shown to correlate with coccolithophore morphology with strains producing type B coccoliths always showing CMM II.

Scanning Electron Microscopy (SEM) was used to investigate whether any intraspecific variation could be detected within the coccolith morphologies of homozygous morphotype A CMM I and CMMIV genotyped isolates. Here we report for the first time that a significant morphometric difference

exists along the major axis of the coccolith between the CMMI and CMMIV isolates. Moreover, the origin of the isolates is an important factor in determining which CMM dominates and in one case, separates CMMI and IV into two distinct morphological subgroups.

4.2 Introduction.

*Emiliania huxleyi (*Lohmann.) Hay and Mohler (Prymnesiophyceae) is thought to be one of the main calcite producers on Earth (Westboek et al., 1993). It is an important species with respect to primary productivity in the marine environment and it is present in all of the Earth's oceans with the exception of the extreme polar oceans. It is the most abundant coccolithophore in our oceans and *Emiliania (*as well as *Gephyrocapsa* and *Reticulofenestra*) extant genera have been so for over 20 million years (Beaufort *et al.,* 2011) and it can often achieve such a high rate of fecundity that it produces massive blooms large enough to be are visible from space (Holligan et al., 1993). During and post bloom events, the coccoliths sink to the ocean floor taking large amounts of organic and inorganic carbon with it (Coxall et al., 2005). As a consequence, there is a net removal of CO_2 from the atmosphere (Robertson et al., 1994; Riebesell and Tortell, 2011). Coccolithophores have had this influence over the climate for over 200 million years (Read *et al.,* 2013) and with the increase of anthropogenic CO_2 it has become increasingly relevant (Donney *et al.,*

2009; Sabine *et al.*, 2004). Due to the role *E. huxleyi* has in the cycling of Carbon it has been studied extensively by groups ranging from oceanographers and ecologists to biostratigraphers and paleoceanographers (Young and Westbroek, 1991).

E. huxleyi exhibits a wide range of variation with regards to coccolith morphology, physiological properties and the immunological properties of the polysaccharides involved coccolith formation and as a consequence of this, it was separated into two main distinct morphotypes A and B, by van Bleijswijk *et al.* (1991) and Young *et al.* (1991). These were susbsequently formally described as varieties by Medlin *et al.* (1996) – type A as *E. huxleyi var huxleyi* and type B as *E.huxleyi var pujosae*. Additional morphotypes include type C (*E .huxleyi var. kleijniae*), type B/C (*E. huxleyi var aurorae*) and type O (Hagino *et al.*, 2011) which are all sub-variants of morphotype B. Sub-variants of type A include type R which is an over calcified sub-variant of morphotype A and *E. huxleyi* subspecies *corona* (Hagino *et a.*, 2011) have also been reported. (Nannotax3 website, Young, Bown and Lees (eds) viewed 21 May 2016, URL http://ina.tmsoc.org/Nannotax3)

Morphotypes A and B are the most widely recognised with morphotype A being the most prevalent in summer blooms (Hagino *et al.*, 2011 and Krueger-Hadfield *et al.,2014*) . Molecular genetic separation of groups with *E. Huleyi* has been problematic; however, work undertaken by

Schroeder *et al*. (2005) to identified an area in the 3′ Untranslated Regions (UTR) within the mRNA of the coccolith-polysaccharide-associated protein (GPA), which is associated with coccolith structure control. This region does appear to vary between morphotypes.

The identification of the GPA (so called due to its high glutamic acid, proline and alanine content) protein was achieved by using the solubility of calcium binding polysaccharides (CP) in a 7% trichloroacetic acid solution and its ability in precipitating proteins. Once these proteins were produced, work undertaken by Corstjens *et al.*, (1998), resulted in their isolation with gel electrophoresis and subsequently identification of the gene responsible (gpa) for their encoding led to further work looking at the GPA. This work identified its role, it is thought, to be involved in nucleating the calcium carbonate during coccolith development, or, alternatively, to having an involvement the calcium's delivery to the coccolith vesicle (Corstjens *et al.*,1998).

The exact role of the GPA protein still remains unclear; however, Schroeder *et al.*, - (2005) set out to determine whether GPA could be used as a molecular marker to support the separation of the main morphotypes, A and B, into distinct groups. The work resulted in the identification of a region in the UTR of mRNA of GPA which correlated with coccolith morphotype and this region was named the Coccolith Morphology Motif (CMM). Four discreet CMM groups were identified and

subsequently were characterised as CMM I, CMM II, CMM III and CMM IV (Schroeder *et al* 2005).

Morphotype A may show CMM I, III or IV or a combination of these, depending on whether the cells are homo or heterozygous (e.g. homozygous CMM I means two CMM I alleles where as CMM I/IV implies a heterozygous strain, with one CMM I allele and one CMM IV allele). However, CMM II is only associated with morphotype B strains (Schroeder et al 2005 and Krueger-Hadfield et al 2014).

This is summarised in figure 4.1, which shows SEM images of the homozygous forms of the main CMM morphotypes. Other variations within and near the CMM were since reported (Martinez-Martinez *et al*., 2012. and Krueger-Hadfield 2014) however their link to variations within the coccolith morphology have yet to be established.

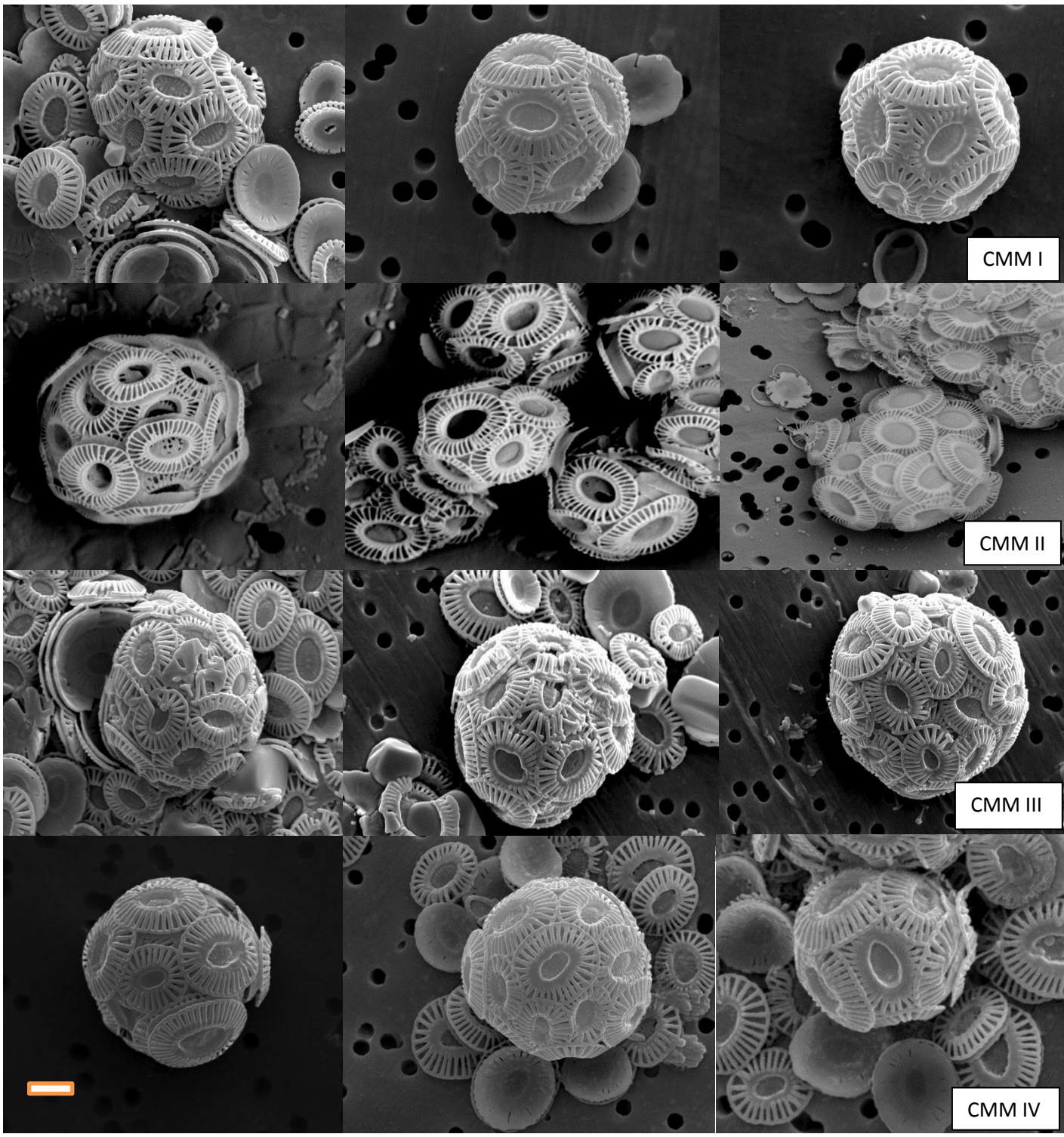

Figure 4.1 SEM images of *E. huxleyi* isolates representing the four CMM genotypes. First row, morphotype A, CMM I. Second row, morphotype B, CMM II. Third row, morphotype A CMM III. Forth row morphotype A, CMM IV. Acknowledge Dr E M Bendif for the images in the second row. Scale bar=1um.

Krueger-Hadfield *et al* (2014) looked at the CMM genotypes from 91 clonal isolates from various locations around the world. They found a predominance of CMM I and CMM IV in these strains.

It would appear from the work of Schroeder *et al.* (2005) and Krueger-Hadfield *et al.* (2014) that the CMM is the only genetic marker that has a significant correlation with the different morphotypes (see figure 4.1) and from that list only morphotype A isolates were used and of those CMM I and CMM IV.

Schroeder *et al*. (2005) suggested that as the CMM may be associated with either the initiation of coccolithogenesis and therefore control the morphology of the coccolith or the CMM may be involved in the regulation of proteins which control the development of the coccolith in the coccolith vesicle. Whatever the role of the CMM, it was suggested the different CMM types would have an effect on the shape and size of the coccolith. Therefore, the work undertaken in this chapter was to use the SEM to take images of the coccoliths and then use image analysis to measure various features of the coccoliths of dominant *E. huxleyi* morphotype genotypes. The aim was therefore to see is the Difference in CMMs correlated with differences in the morphology of CMM I and IV. This data was then further analysed in order to see if the different CMMs resulted in an identifiable change in the morphology of the coccolith, ultimately enabling

for the positive discrimination of *E. huxleyi* genotypes in crude environmental samples using electron microscopy.

4.3 Materials and methods.

Refer to 2.4 for the acquisition of the images and 2.7 for the image analysis.

4.3.1 Locations of the different CMMs isolates.

Table 4.1 lists 88 isolates and their geographical location. They were collected during two cruises by Cecilia Balestreri:-

- **RR1202** (18th February 2012, Durban-South Africa - 23rd March 2012, Fremantle-Australia) on board the R/V Roger Revelle (USA).
- **JR271** (1st June 2012, Immingham-UK - 3rd July 2012, Reykjavik) on board the RRS James Clark Ross (UK).

Only strains with homozygous CMMI and CMMIV were included in this study.

Table 4.1 Isolates used in the study.

Strain	Location	Date Collected	Latitude	Longitude	CMM
SO 1-3	Above ACC-Indian Ocean	Feb-12	-38.32	40.96	IV
SO 1-4	Above ACC-Indian Ocean	Feb-12	-38.32	40.96	IV
SO 1-6	Above ACC-Indian Ocean	Feb-12	-38.32	40.96	IV
SO 1-8	Above ACC-Indian Ocean	Feb-12	-38.32	40.96	IV
SO 5-1	Above ACC-Indian Ocean	Feb-12	-35.50	37.50	IV
SO 5-3	Above ACC-Indian Ocean	Feb-12	-35.50	37.50	IV
SO 7-1	Above ACC-Indian Ocean	Feb-12	-35.50	37.50	IV
SO 7-2	Above ACC-Indian Ocean	Feb-12	-35.50	37.50	IV
SO 19-1	Above ACC-Indian Ocean	Feb-12	-38.31	40.96	IV
SO 19-4	Above ACC-Indian Ocean	Feb-12	-38.31	40.96	IV
SO 21-2	Above ACC-Indian Ocean	Feb-12	-38.31	40.96	IV
SO 21-3	Above ACC-Indian Ocean	Feb-12	-38.31	40.96	IV
SO 21-4	Above ACC-Indian Ocean	Feb-12	-38.31	40.96	IV
SO 21-5	Above ACC-Indian Ocean	Feb-12	-38.31	40.96	IV
SO 23-2	Above ACC-Indian Ocean	Feb-12	-37.92	40.44	IV
SO 23-3	Above ACC-Indian Ocean	Feb-12	-37.92	40.44	IV
SO 30-1	Below ACC-Indian Ocean	Feb-12	-43.14	102.19	IV
SO 30-2	Below ACC-Indian Ocean	Feb-12	-43.14	102.19	IV
SO 30-4	Below ACC-Indian Ocean	Feb-12	-43.14	102.19	IV
SO 40-1	Above ACC-Indian Ocean	Feb-12	-38.32	40.96	IV
SO 40-2	Above ACC-Indian Ocean	Feb-12	-38.32	40.96	IV
SO 40-3	Above ACC-Indian Ocean	Feb-12	-38.32	40.96	IV
SO 40-4	Above ACC-Indian Ocean	Feb-12	-38.32	40.96	IV
SO 40-5	Above ACC-Indian Ocean	Feb-12	-38.32	40.96	IV
SO 42-1	Above ACC-Indian Ocean	Feb-12	-35.50	37.50	IV
SO 42-2	Above ACC-Indian Ocean	Feb-12	-35.50	37.50	IV
SO 42-3	Above ACC-Indian Ocean	Feb-12	-35.50	37.50	IV
SO 42-4	Above ACC-Indian Ocean	Feb-12	-35.50	37.50	IV
SO 52-5	Below ACC-Indian Ocean	Feb-12	-42.08	113.40	IV
SO 52B-1	Below ACC-Indian Ocean	Feb-12	-42.08	113.40	IV
SO 52B-2	Below ACC-Indian Ocean	Feb-12	-42.08	113.40	IV
SO 55-1	Below ACC-Indian Ocean	Feb-12	-42.08	113.40	IV
SO 55-2	Below ACC-Indian Ocean	Feb-12	-42.08	113.40	IV

SO 55-3	Below ACC-Indian Ocean	Feb-12	-42.08	113.40	IV
SO 63-5	Above ACC-Indian Ocean	Feb-12	-38.32	40.96	IV
SO 69-1	Above ACC-Indian Ocean	Feb-12	-38.32	40.96	I
SO 69-2	Above ACC-Indian Ocean	Feb-12	-38.32	40.96	I
SO 69-5	Above ACC-Indian Ocean	Feb-12	-38.32	40.96	IV
SO 69B-1	Above ACC-Indian Ocean	Feb-12	-38.32	40.96	IV
SO 69B-5	Above ACC-Indian Ocean	Feb-12	-38.32	40.96	IV
ARC 13-2	Southern Icelandic Sea	Jul-12	61.00	-19.43	I
ARC 13-5	Southern Icelandic Sea	Jul-12	61.00	-19.43	I
ARC 15B-1	Southern Icelandic Sea	Jul-12	61.00	-19.43	IV
ARC 15B-3	Southern Icelandic Sea	Jul-12	61.00	-19.43	IV
ARC 15B-4	Southern Icelandic Sea	Jul-12	61.00	-19.43	IV
ARC 15B-5	Southern Icelandic Sea	Jul-12	61.00	-19.43	IV
ARC 16-2	Southern Icelandic Sea	Jul-12	61.00	-19.43	I
ARC 17-3	Southern Icelandic Sea	Jul-12	61.00	-19.43	I
ARC 23-2	Southern Icelandic Sea	Jul-12	61.00	-19.43	I
ARC 23-3	Southern Icelandic Sea	Jul-12	61.00	-19.43	I
ARC 23-4	Southern Icelandic Sea	Jul-12	61.00	-19.43	I
ARC 23-5	Southern Icelandic Sea	Jul-12	61.00	-19.43	I
ARC 27-1	Greenland Sea	Jul-12	78.51	-6.14	I
ARC 27-4	Greenland Sea	Jul-12	78.51	-6.14	I
ARC 28-3	Greenland Sea	Jul-12	78.41	-1.49	I
ARC 28-4	Greenland Sea	Jul-12	78.41	-1.49	I
ARC 28-5	Greenland Sea	Jul-12	78.41	-1.49	I
ARC 28B-1	Greenland Sea	Jul-12	78.41	-1.49	I
ARC 28B-2	Greenland Sea	Jul-12	78.41	-1.49	I
ARC 28B-4	Greenland Sea	Jul-12	78.41	-1.49	I
ARC 28C-4	Greenland Sea	Jul-12	78.41	-1.49	I
ARC 28C-5	Greenland Sea	Jul-12	78.41	-1.49	I
ARC 29-1	Greenland Sea	Jul-12	78.70	3.28	I
ARC 29-2	Greenland Sea	Jul-12	78.70	3.28	I
ARC 29-3	Greenland Sea	Jul-12	78.70	3.28	I
ARC 31-1	Western Coast of Svalbard	Jul-12	77.90	9.14	I
ARC 31-3	Western Coast of Svalbard	Jul-12	77.90	9.14	I
ARC 31-4	Western Coast of Svalbard	Jul-12	77.90	9.14	I
ARC 37-1	Greenland Sea	Jul-12	76.30	-2.92	IV
ARC 38B-1	Greenland Sea	Jul-12	76.30	-2.92	IV
ARC 38B-4	Greenland Sea	Jul-12	76.30	-2.92	IV
ARC 50-3	Barents Sea	Jul-12	72.90	26.00	I
ARC 51-3	Barents Sea	Jul-12	72.90	26.00	I
ARC 51-4	Barents Sea	Jul-12	72.90	26.00	I
ARC 51-5	Barents Sea	Jul-12	72.90	26.00	I
ARC 52-1	Barents Sea	Jul-12	72.90	26.00	I
ARC 52-2	Barents Sea	Jul-12	72.90	26.00	I

ARC 52B-1	Barents Sea	Jul-12	72.90	26.00	I
ARC 52B-4	Barents Sea	Jul-12	72.90	26.00	I
ARC 52B-5	Barents Sea	Jul-12	72.90	26.00	I
ARC 55B-7	Barents Sea	Jul-12	72.90	26.00	I
ARC 55B-9	Barents Sea	Jul-12	72.90	26.00	I
ARC 63-2	Norwegian Sea	Jul-12	71.75	8.44	IV
ARC 63-3	Norwegian Sea	Jul-12	71.75	8.44	IV
ARC 63-4	Norwegian Sea	Jul-12	71.75	8.44	IV
ARC 63-5	Norwegian Sea	Jul-12	71.75	8.44	IV

(NB ACC= Antarctic Circumpolar Current)

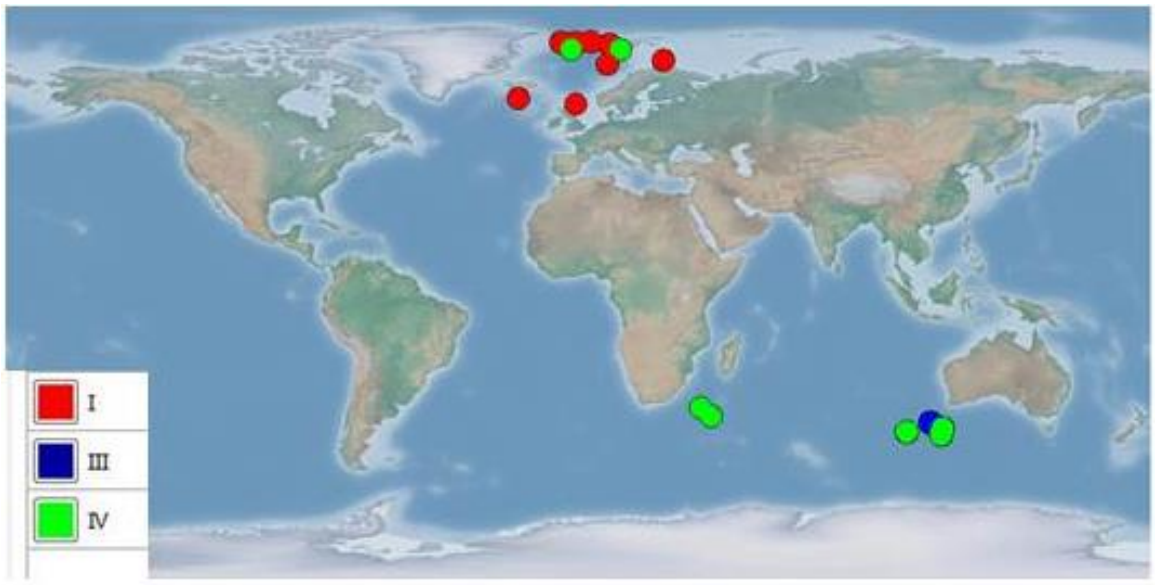

Figure 4.1a Geographical locations of the isolates

The Map above (4.1a) shows the geographical location of the isolates used in this study. It includes the location CMM III cells were found. However, there were insufficient cells of this type to use in this study.

The map was produced using GenGIS. It is a bioformatics application that allows you to combine geographical data and biological data to produce a map. (Parks DH, Mankowski T, Zangooei S, Porter MS, Armanini DG,

Baird DJ, Langille MGI, Beiko RG. 2013. **GenGIS 2: Geospatial analysis of traditional and genetic biodiversity, with new gradient algorithms and an extensible plugin framework**).

4.3.2. Measuring the cells

The techniques used to measure the coccoliths from the isolates were developed by Young *et al* (2014).

The cells were measured as described in Figure 4.2 and scatter plots (figures 4.3, below) were compiled using data from the SEM images and Excel (Microsoft Redmond, Washington, USA) (see chapter 2.7) The data can be seen below in table 4.2 and it was used to produce the following plots: -

- Mean minor against mean minor
- Mean EW against mean major
- Mean tube against mean major
- Mean EW against mean minor
- Mean tube against mean minor
- Mean EW against mean tube

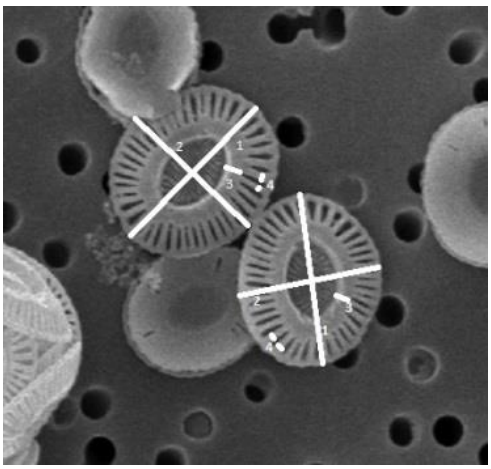

Figure 4.2 SEM image illustrating the dimensions measured. **1** is the length or Major. **2** is the width or minor. **3** is the tube. **4** Element Width or EW.

4.3.3 Multidimensional scaling

A Classic Multidimensional Scaling (CMDS) has been generated (Gower J C. Some distance properties of latent root and vector methods used in multivariate analysis. Biometrika 53:325-38, 1966), using Euclidian distance to create the similarity matrix. The analysis was carried out using R statistic cmd scale function (R Core Team (2015). R: A language and environment for statistical computing. R Foundation for Statistical Computing, Vienna, Austria. URL http://www.R-project.org) and the results were plotted in order to highlight different locations and cell types.

4.4 Results

Table 4.2 contains the means of the major, minor, tube and EW measurements.

Table 4.2 Data acquired from the SEM images showing means, standard error (se) and standard deviation (sd).

Strain	CMM	mean major	sd major	se major	mean minor	sd minor	se minor	mean tube	sd tube	se tube	mean EW	sd EW	se EW
SO 1-3	IV	3.031	0.324	0.042	2.562	0.284	0.037	0.427	0.077	0.010	0.117	0.0100	0.0006
SO 1-4	IV	2.832	0.265	0.034	2.315	0.238	0.031	0.389	0.074	0.010	0.122	0.0098	0.0006
SO 1-6	IV	3.166	0.322	0.042	2.664	0.285	0.037	0.405	0.078	0.010	0.118	0.0098	0.0006
SO 1-8	IV	3.008	0.323	0.042	2.503	0.283	0.036	0.449	0.083	0.011	0.123	0.0142	0.0008
SO 5-1	IV	3.063	0.337	0.044	2.625	0.305	0.039	0.420	0.070	0.009	0.118	0.0108	0.0006
SO 5-3	IV	3.078	0.284	0.037	2.571	0.274	0.035	0.457	0.062	0.008	0.120	0.0126	0.0007
SO 7-1	IV	3.340	0.327	0.042	2.816	0.302	0.039	0.424	0.081	0.010	0.119	0.0083	0.0005
SO 7-2	IV	3.503	0.355	0.046	2.946	0.317	0.041	0.481	0.086	0.011	0.127	0.0078	0.0004
SO 19-1	IV	3.119	0.369	0.048	2.597	0.319	0.041	0.354	0.071	0.009	0.109	0.0070	0.0004
SO 19-4	IV	3.333	0.413	0.053	2.836	0.370	0.048	0.392	0.071	0.009	0.119	0.0054	0.0003
SO 21-2	IV	3.587	0.286	0.037	2.606	0.275	0.036	0.434	0.077	0.010	0.118	0.0108	0.0007
SO 21-3	IV	3.237	0.359	0.046	2.736	0.308	0.040	0.455	0.077	0.010	0.123	0.0100	0.0006
SO 21-4	IV	3.237	0.351	0.045	2.701	0.291	0.038	0.467	0.083	0.011	0.120	0.0077	0.0004
SO 21-5	IV	3.106	0.391	0.050	2.596	0.379	0.049	0.418	0.090	0.012	0.114	0.0111	0.0006
SO 23-2	IV	3.247	0.378	0.049	2.755	0.331	0.043	0.400	0.091	0.012	0.120	0.0077	0.0004
SO 23-3	IV	3.338	0.368	0.047	2.831	0.313	0.040	0.428	0.105	0.014	0.118	0.0098	0.0006
SO 30-1	IV	3.426	0.418	0.054	2.860	0.386	0.050	0.319	0.066	0.008	0.122	0.0125	0.0007
SO 30-2	IV	3.509	0.392	0.051	2.896	0.348	0.045	0.354	0.080	0.010	0.117	0.0064	0.0003
SO 30-4	IV	3.210	0.329	0.043	2.647	0.268	0.035	0.300	0.044	0.006	0.111	0.0122	0.0007
SO 40-1	IV	3.412	0.401	0.052	2.880	0.362	0.047	0.410	0.086	0.011	0.115	0.0112	0.0007
SO 40-2	IV	3.212	0.368	0.047	2.642	0.316	0.041	0.368	0.082	0.011	0.115	0.0112	0.0007

SO 40-3	IV	2.933	0.287	0.037	2.473	0.260	0.034	0.349	0.080	0.010	0.115	0.0112	0.0007
SO 40-4	IV	2.924	0.305	0.039	2.401	0.290	0.037	0.406	0.093	0.012	0.115	0.0112	0.0007
SO 40-5	IV	2.993	0.311	0.040	2.527	0.297	0.038	0.368	0.079	0.010	0.115	0.0112	0.0006
SO 42-1	IV	3.363	0.245	0.032	2.817	0.224	0.029	0.443	0.080	0.010	0.115	0.0112	0.0006
SO 42-2	IV	3.376	0.283	0.036	2.802	0.242	0.031	0.397	0.086	0.011	0.115	0.0112	0.0006
SO 42-3	IV	3.200	0.389	0.050	2.720	0.345	0.045	0.380	0.076	0.010	0.115	0.0112	0.0007
SO 42-4	IV	3.360	0.362	0.047	2.877	0.315	0.041	0.379	0.077	0.010	0.115	0.0112	0.0006
SO 52-5	IV	3.029	0.239	0.031	2.572	0.219	0.028	0.344	0.064	0.008	0.115	0.0112	0.0006
SO 52B-1	IV	3.128	0.325	0.042	2.580	0.266	0.034	0.333	0.057	0.007	0.121	0.0130	0.0130
SO 52B-2	IV	3.262	0.348	0.045	2.742	0.285	0.037	0.388	0.063	0.008	0.112	0.0108	0.0006
SO 55-1	IV	3.393	0.304	0.039	2.815	0.251	0.032	0.440	0.251	0.032	0.121	0.0114	0.0006
SO 55-2	IV	3.326	0.321	0.041	2.694	0.271	0.035	0.414	0.083	0.011	0.121	0.0083	0.0004
SO 55-3	IV	3.470	0.378	0.049	2.866	0.324	0.042	0.397	0.094	0.012	0.116	0.0092	0.0005
SO 63-5	IV	3.340	0.426	0.055	2.824	0.367	0.047	0.378	0.087	0.011	0.112	0.0087	0.0005
SO 69-1	I	2.946	0.296	0.038	2.398	0.238	0.031	0.320	0.066	0.008	0.096	0.0066	0.0004
SO 69-2	I	3.063	0.294	0.038	2.620	0.248	0.032	0.383	0.063	0.008	0.101	0.0094	0.0005
SO 69-5	IV	2.890	0.230	0.030	2.438	0.190	0.025	0.407	0.065	0.008	0.104	0.0049	0.0003
SO 69B-1	IV	3.630	0.405	0.052	3.111	0.373	0.048	0.460	0.070	0.009	0.119	0.0130	0.0007
SO 69B-5	IV	3.137	0.259	0.033	2.655	0.235	0.030	0.412	0.062	0.008	0.108	0.0087	0.0005
ARC 13-2	I	3.687	0.336	0.043	3.088	0.291	0.038	0.556	0.091	0.012	0.120	0.0134	0.0007
ARC 13-5	I	3.404	0.395	0.051	2.809	0.332	0.043	0.477	0.085	0.011	0.107	0.0119	0.0007
ARC 15B-1	IV	3.313	0.381	0.049	2.712	0.325	0.042	0.381	0.063	0.008	0.105	0.0157	0.0009
ARC 15B-3	IV	3.345	0.291	0.038	2.768	0.265	0.034	0.523	0.073	0.009	0.123	0.0119	0.0007
ARC 15B-4	IV	3.313	0.236	0.030	2.754	0.200	0.026	0.547	0.083	0.011	0.118	0.0125	0.0007
ARC 15B-5	IV	3.586	0.359	0.046	2.963	0.317	0.041	0.587	0.286	0.037	0.111	0.0170	0.0009
ARC 16-2	I	3.532	0.324	0.042	3.003	0.305	0.039	0.401	0.087	0.011	0.114	0.0128	0.0007
ARC 17-3	I	3.686	0.333	0.043	3.117	0.290	0.037	0.396	0.077	0.010	0.111	0.0094	0.0005

ARC 23-2	I	3.257	0.349	0.045	2.727	0.286	0.037	0.421	0.066	0.009	0.120	0.0110	0.0006
ARC 23-3	I	3.437	0.396	0.051	2.896	0.325	0.042	0.413	0.066	0.008	0.123	0.0078	0.0004
ARC 23-4	I	3.245	0.406	0.052	2.676	0.334	0.043	0.426	0.071	0.009	0.123	0.0110	0.0006
ARC 23-5	I	3.362	0.398	0.051	2.775	0.327	0.042	0.453	0.081	0.010	0.111	0.0083	0.0005
ARC 27-1	I	3.531	0.302	0.039	2.968	0.246	0.032	0.488	0.061	0.008	0.125	0.0112	0.0006
ARC 27-4	I	3.650	0.427	0.055	3.113	0.380	0.049	0.433	0.071	0.009	0.105	0.0157	0.0009
ARC 28-3	I	3.954	0.429	0.055	3.334	0.409	0.053	0.471	0.055	0.007	0.120	0.0077	0.0004
ARC 28-4	I	3.710	0.358	0.046	3.009	0.327	0.042	0.433	0.068	0.009	0.124	0.0136	0.0007
ARC 28-5	I	3.736	0.358	0.046	3.187	0.332	0.043	0.450	0.062	0.008	0.111	0.0137	0.0007
ARC 28B-1	I	3.731	0.293	0.038	3.118	0.279	0.036	0.388	0.056	0.007	0.109	0.0094	0.0005
ARC 28B-2	I	3.591	0.319	0.041	2.948	0.300	0.039	0.400	0.055	0.007	0.126	0.0120	0.0006
ARC 28B-4	I	3.770	0.362	0.047	3.127	0.332	0.043	0.371	0.042	0.005	0.113	0.0078	0.0004
ARC 28C-4	I	3.841	0.331	0.043	3.223	0.298	0.039	0.391	0.062	0.008	0.117	0.0119	0.0006
ARC 28C-5	I	3.638	0.313	0.040	3.029	0.286	0.037	0.387	0.044	0.006	0.112	0.0087	0.0005
ARC 29-1	I	3.749	0.336	0.043	3.158	0.328	0.042	0.411	0.051	0.007	0.135	0.0092	0.0005
ARC 29-2	I	3.614	0.292	0.038	2.988	0.278	0.036	0.399	0.053	0.007	0.118	0.0098	0.0005
ARC 29-3	I	3.613	0.339	0.044	3.022	0.308	0.040	0.369	0.055	0.007	0.113	0.0100	0.0005
ARC 31-1	I	3.257	0.339	0.044	3.587	0.286	0.037	0.320	0.053	0.007	0.104	0.0049	0.0003
ARC 31-3	I	3.040	0.293	0.038	2.531	0.260	0.034	0.326	0.042	0.005	0.103	0.0064	0.0004
ARC 31-4	I	3.027	0.290	0.037	2.505	0.252	0.033	0.321	0.047	0.006	0.101	0.0137	0.0008
ARC 37-1	IV	3.051	0.305	0.039	2.511	0.243	0.031	0.351	0.051	0.007	0.112	0.0060	0.0003
ARC 38B-1	IV	2.981	0.260	0.034	2.480	0.225	0.029	0.359	0.070	0.009	0.114	0.0102	0.0006
ARC 38B-4	IV	3.165	0.294	0.038	2.600	0.257	0.033	0.381	0.050	0.006	0.119	0.0083	0.0005
ARC 50-3	I	3.336	0.451	0.058	2.745	0.395	0.051	0.353	0.068	0.009	0.116	0.0080	0.0004
ARC 51-3	I	3.227	0.366	0.047	2.619	0.299	0.039	0.382	0.047	0.006	0.117	0.0090	0.0005
ARC 51-4	I	3.160	0.335	0.043	2.518	0.265	0.034	0.347	0.049	0.006	0.103	0.0090	0.0005
ARC 51-5	I	3.216	0.321	0.042	2.415	0.309	0.040	0.357	0.046	0.006	0.114	0.0066	0.0004

ARC 52-1	I	3.385	0.341	0.044	2.868	0.311	0.040	0.355	0.059	0.008	0.107	0.0110	0.0006
ARC 52-2	I	3.434	0.329	0.043	2.830	0.315	0.041	0.350	0.053	0.007	0.109	0.0104	0.0005
ARC 52B-1	I	3.696	0.520	0.067	3.101	0.448	0.058	0.374	0.049	0.006	0.114	0.0080	0.0004
ARC 52B-4	I	4.008	0.439	0.057	3.358	0.401	0.052	0.370	0.047	0.006	0.115	0.0067	0.0004
ARC 52B-5	I	3.437	0.355	0.046	2.844	0.304	0.039	0.374	0.049	0.006	0.113	0.0110	0.0006
ARC 55B-7	I	3.423	0.362	0.047	2.859	0.328	0.042	0.357	0.048	0.006	0.115	0.0112	0.0006
ARC 55B-9	I	3.361	0.351	0.045	2.801	0.337	0.044	0.439	0.050	0.006	0.119	0.0114	0.0006
ARC 63-2	IV	3.497	0.360	0.047	2.906	0.320	0.041	0.442	0.080	0.010	0.118	0.0108	0.0006
ARC 63-3	IV	3.196	0.340	0.044	2.643	0.291	0.038	0.407	0.057	0.007	0.126	0.0066	0.0004
ARC 63-4	IV	3.325	0.373	0.048	2.763	0.343	0.044	0.445	0.065	0.008	0.118	0.1180	0.0006
ARC 63-5	IV	3.364	0.261	0.034	2.784	0.228	0.029	0.424	0.052	0.007	0.126	0.0102	0.0005

Figure 4.3 are the scatter plots produced with the data from Table 4.2.

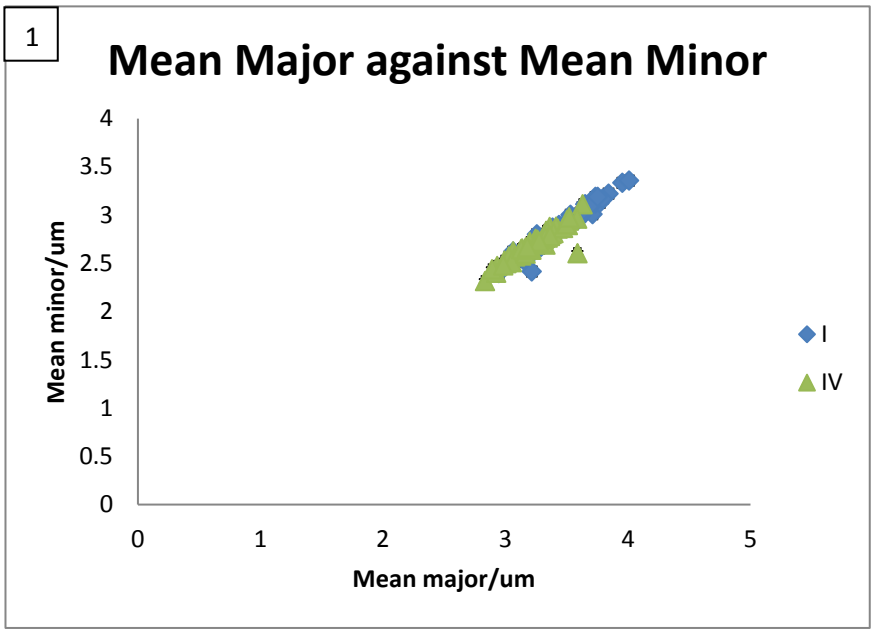

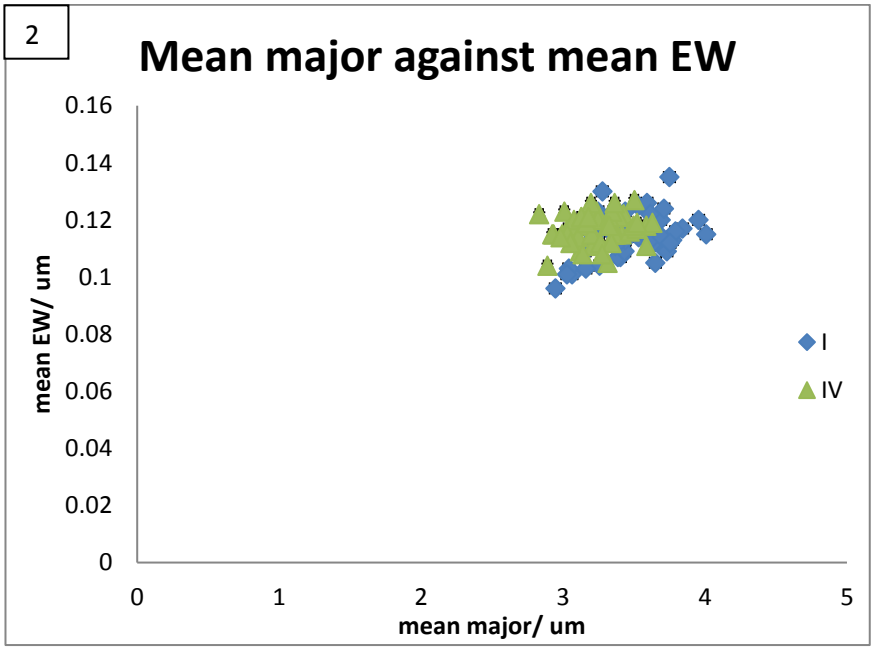

3

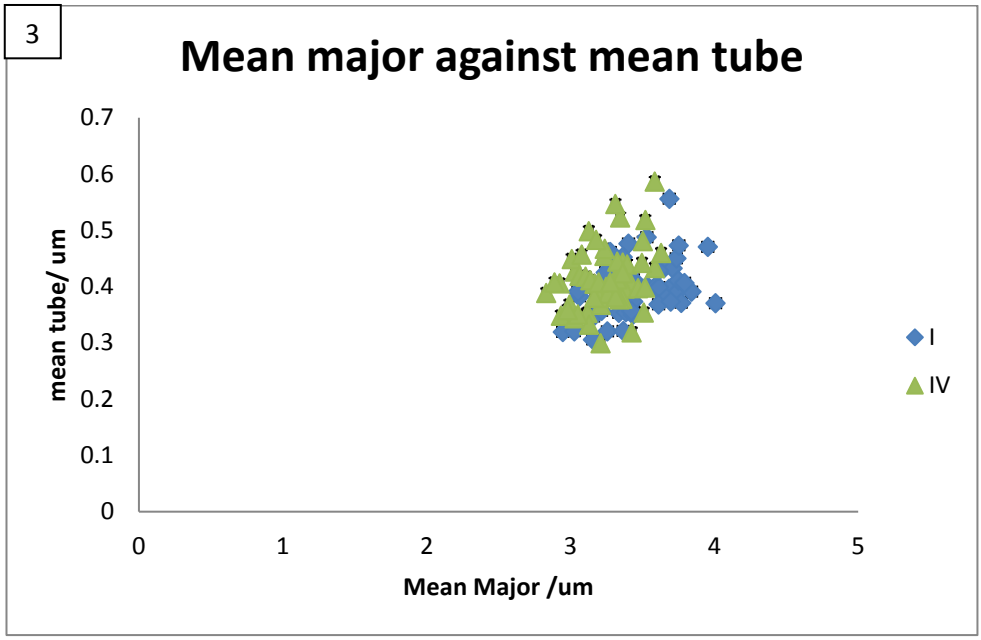
Mean major against mean tube
mean tube/ um
0.7
0.6
0.5
0.4
0.3
0.2
0.1
0
0
1
2
3
4
5
Mean Major /um
I
IV

4

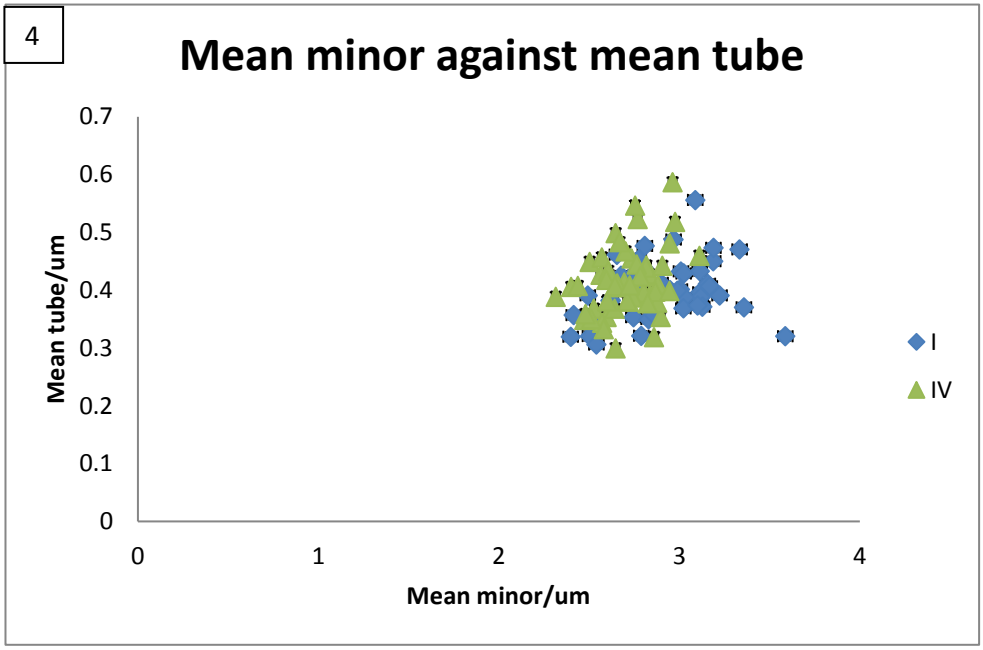
Mean minor against mean tube
Mean tube/um
0.7
0.6
0.5
0.4
0.3
0.2
0.1
0
0
1
2
3
4
Mean minor/um
I
IV

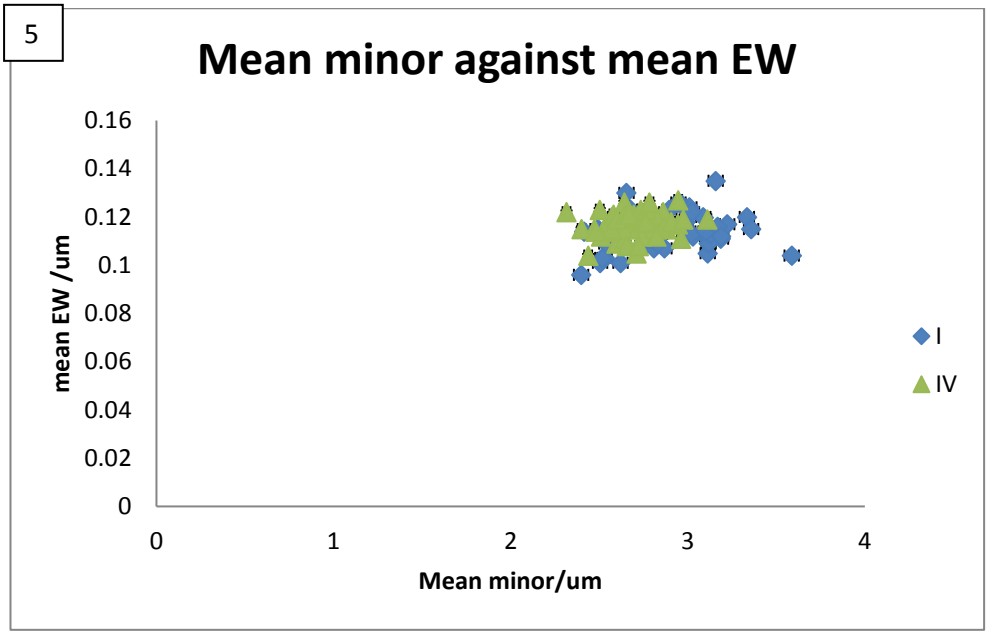

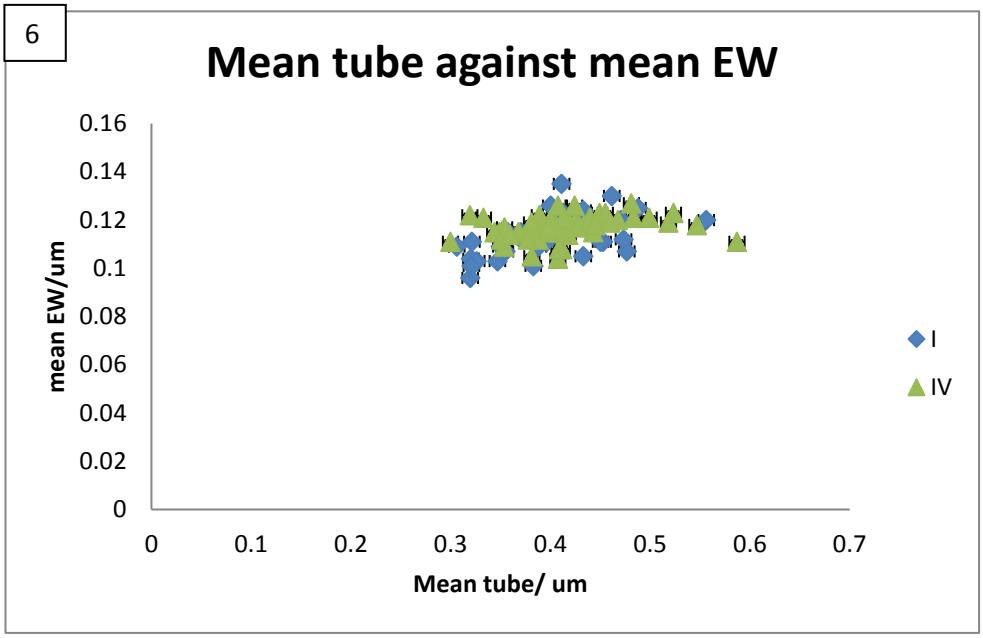

Figure 4.3 Above Scatter plots of the data acquired from the homozygous CMMI and CMMIV samples: **1**. Mean Major against Mean Minor. **2.** Mean 'Major against MeanEW. **3.** Mean Major against mean tube. **4.** Mean Minor against Mean EW. **5.** Mean Minor against Mean Tube. **6.** Mean tube against Mean EW.

The scatter plots (Figure 4.3, 1) shows that the CMM I and IV morphotypes show variation along the major axis suggesting that CMM I coccoliths are larger than CMM IV

In Figure 4.3,2 (EW vs Major), it looks like the range of sizes for EW is spread between CMM I and IV but again with the Major exhibiting that CMM I is larger than IV.

This is also true for Figures 4.3, 3 (Tube vs Major), 4.3, 4 (EW vs Minor) and 4.3, 5 (Tube vs Minor) where the only difference is in the size with CMM I being larger than IV and the other parameters being evenly spread.

With Figure 4.3, 6 (EW vs Tube) there is no obvious difference between the two morphotypes with the CMMI and CMMIV data points being mixed.

Table 4.3 Mean of means data produced from the data for the homozygous samples in table 4.2 for CMM I and CMM IV

CMM		mean major	mean minor	mean tube	mean EW
I	mean	3.469617651	2.901169897	0.39652653	0.114156
	stdev	0.264337095	0.271501005	0.05239939	0.007957
	st er	0.039405048	0.04047298	0.00781124	0.001186
IV	mean	3.250109747	2.710069272	0.41482592	0.116944
	stdev	0.192571964	0.162137151	0.05597217	0.00495
	st er	0.026451794	0.022271251	0.00768837	0.00068

Figure 4.4 (below) uses the data in a column chart to allow direct comparison with the different lengths measured for the homozygous CMM I and IV. Error bars are the Standard deviation.

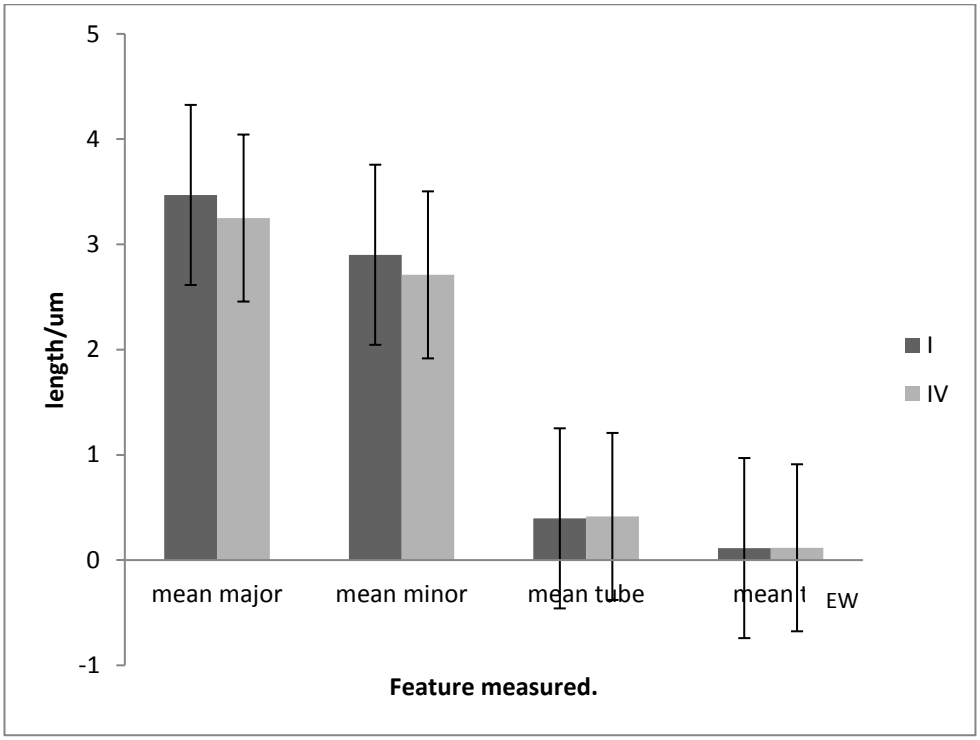

Figure 4.4. The mean of means for the four parameters measured.

The data from table 4.3 has also been plotted onto a single scatter plot (figure 4.5, below) comparing the major against minor; major against tube; major against EW; minor against tube; minor against EW and tube against EW. The error bars are the standard error. In this figure it can be seen that all of the standard error of the points overlap. This indicates that whilst there are differences between I and IV the range of measurement means that it is not possible to accurately identify morphotypes within the two CMMs using the means of all of the data.

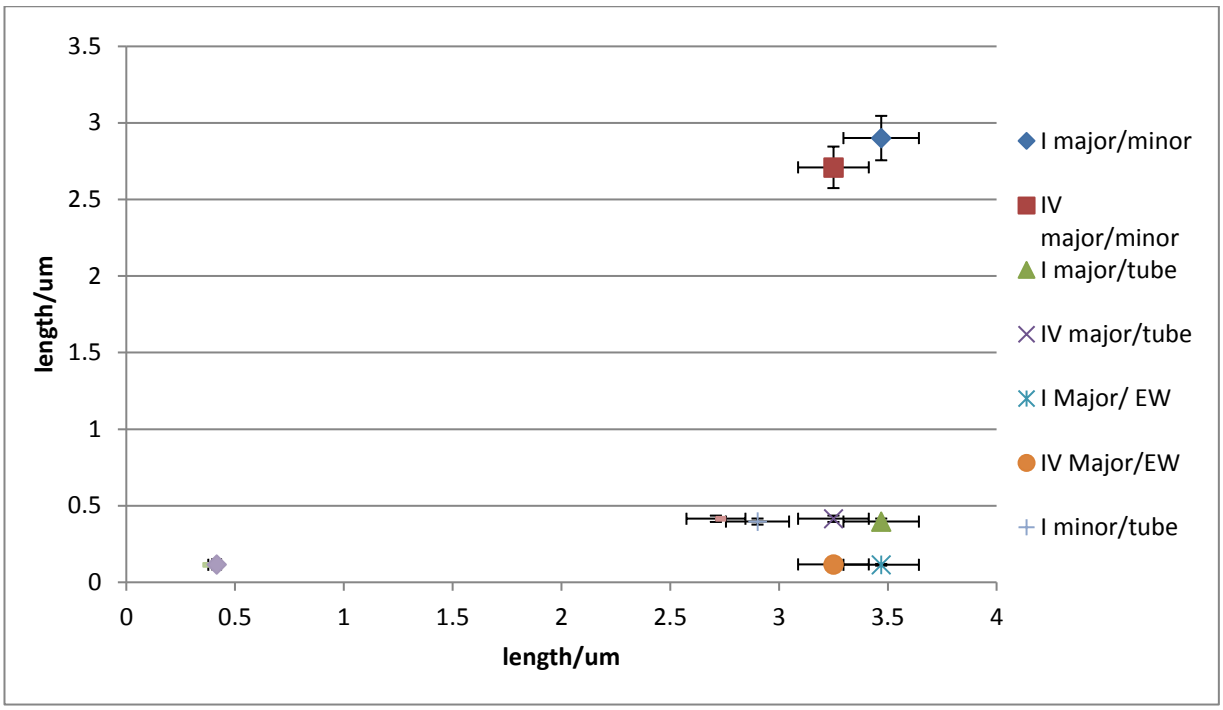

Figure 4.5. Scatter plot comparing the mean measurements for the morphotype CMM I and CMM IV isolates.

In order to investigate this more thoroughly I used a T test and the data in table 4.3 where I calculated the mean of all of the mean measurements and the means of the Standard deviation and Standard Error. The mean Major of CMM I was tested against the mean Major of CMM IV, as with Minor, Tube and EW.

The results are in Table 4.4, below.

Table 4.4 Summary of the T testing looking at major, minor, tube and EW means.

		Confidence interval		
Parameter	P value	mean of I - IV	95% inter. of this diff	RESULT
Major	0.0001	0.2195	0.12811 to 0.3108	Extremely significant
Minor	0.0001	0.1911	0.10389 to 0.2878	Extremely significant
Tube	0.1024	-0.01829	0.04033 to 0.003736	NOT significant
EW	0.0353	-0.002788	0.00538 to 0.00019	significant

As can be seen from the results of the T test in table 4.4, the difference in the Major and Minor of I and IV is 'extremely significant' with I being lager than IV as seen in figures 4.3, 1-5. The difference in EW in I and IV is significant with the EW of IV being larger than I (as seen in the means in table 4.3).

However, despite this, the conclusion that the morphotype CMM I *is* bigger than CMM IV cannot be drawn. The reason for this is that the T test looked at the means of all of the data. Looking at figure 4.4 and especially 4.5, the error bars overlap considerably and likewise in figure 4.3, the overlap in data is significant. As a result of this overlap it is impossible to look at a cell from one of the location listed in table 4.1 and establish its CMM. The cell could be a large IV falling into the spread of the I data or a small I falling into the spread of the IV data.

On average the coccoliths from CMM I strains are bigger than those from CMM IV strains, but only on average.

Analysis using Classic Multidimensional scaling (CMDS)

Figures 4.6 to 4.11 are plots of the data using Classic Multidimensional Scaling (CMDS). The sets of data included in the plots correspond to those of the scatter plots in Figure 4.3: - Figure 4.6; Major vs Minor. Figure 4.7; Major vs EW. Figure 4.8; Major vs Tube. Figure 4.9; Minor vs EW. Figure 4.10; Minor vs Tube. Figure 4.11; Tube vs EW.

In addition, on the MDS plots (Figures 4.6 – 4.11) the data points have been colour- coded according to the location the isolate was collected from and different shape symbols are used for the two CMM types (circles for CMM I and triangles for CMM IV).

In figure 4.6, Major vs Minor, it can be seen that most of the data points are spread out indicating that there is a wide range of data, especially on the Major (x axis) with less range on the Minor (y axis). A point to note is the obvious clustering for the Greenland Sea, with the CMMI plots on the right and the three CMMIV on the left.

Figure 4.6, EW vs Major, the points show much more variety on both axis indicating that the data is widely spread. Again, there is the obvious split in the Greenland Sea data points. It is also possible to see two data points for

CMMI for the ‘above ACC’ below the spread of CMMIV and one CMMI above those points. It is also more obvious in this plot that there are only CMMIV isolates at the Norwegian Sea and the ‘below ACC’ sites. There are also only CMMI isolates at the Western coast of Svalbard, and Barents Sea sites.

Figure 4.7, Major against Tube shows a similar pattern to Figure 4.8. However, whilst the data points for the CMMIV are spread as in figure 4.8, the three CMMI points are spread one above 0 (on the y axis) one on 0 and one below.

Figure 4.8 shows us that there is less variety in the Minor when compared to the variety on the EW. Again we can see the 3 CMMI data point for ‘above ACC’ one above all of the rest of the data and two below.

Figure 4.9 again shows that there is less variation in Minor when it is plotted against Tube.

Figure 4.10 Tube vs EW shows a similar range of data with the data points for ‘above ACC’ showing the same pattern they did in the previous plots.

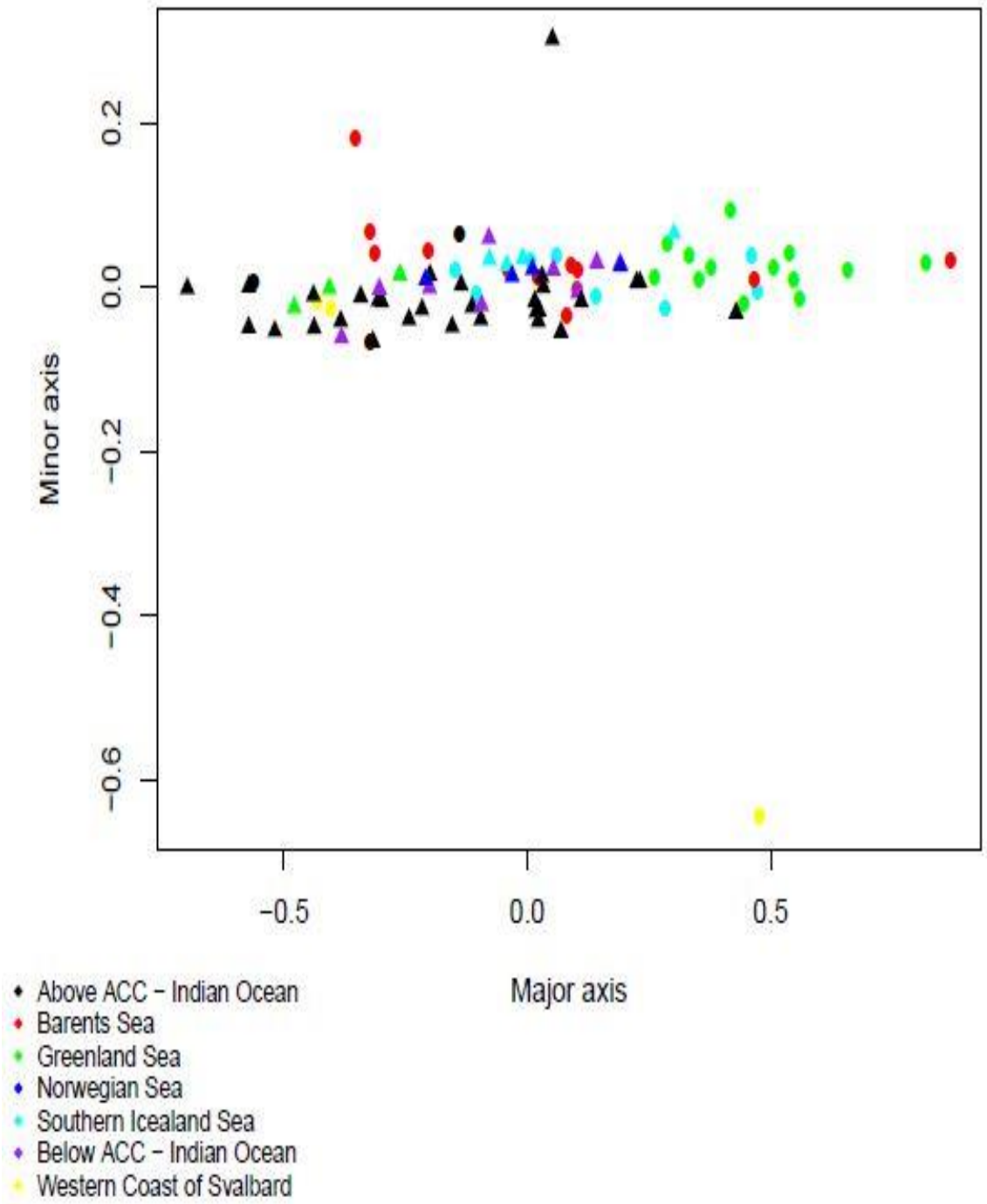

Figure 4.6 CMDS plot of Major against Minor. ▲ =CCM IV ● =CMMI

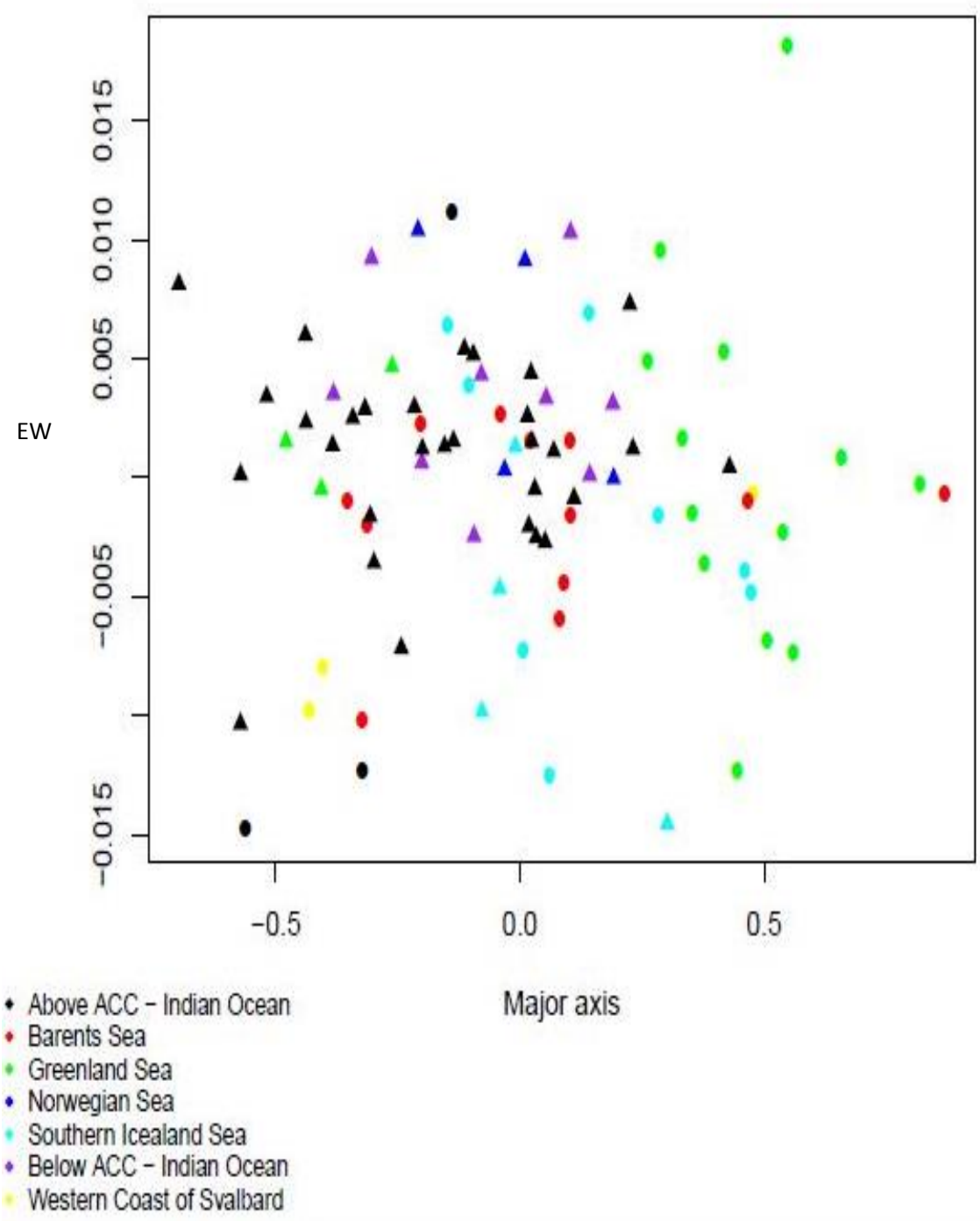

Figure 4.7 CMDS plot Major against EW ▲ =CCM IV ● =CMMI

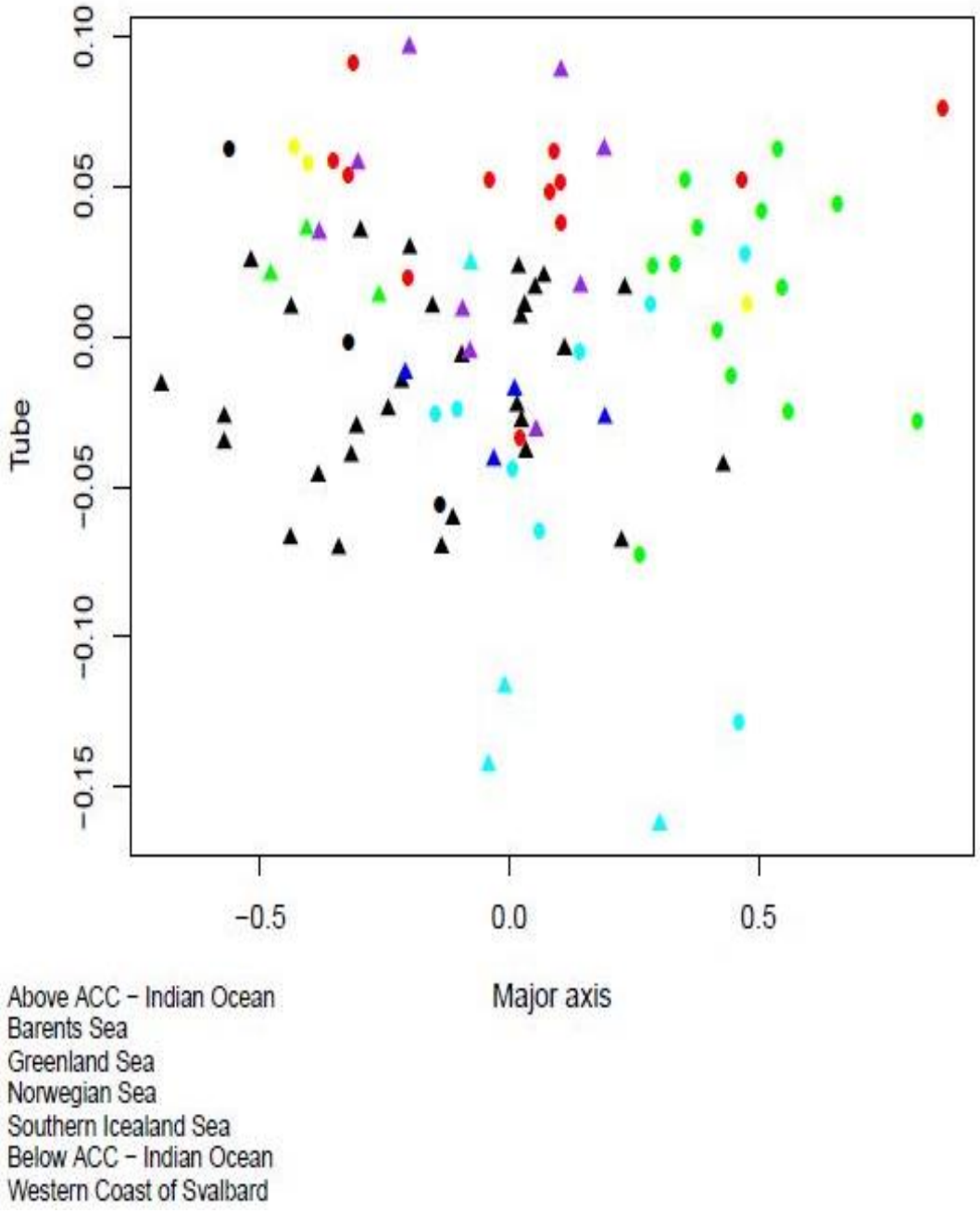

Figure 4.8 CMDS plot of Major against Tube. ▲ =CCM IV ● =CMMI

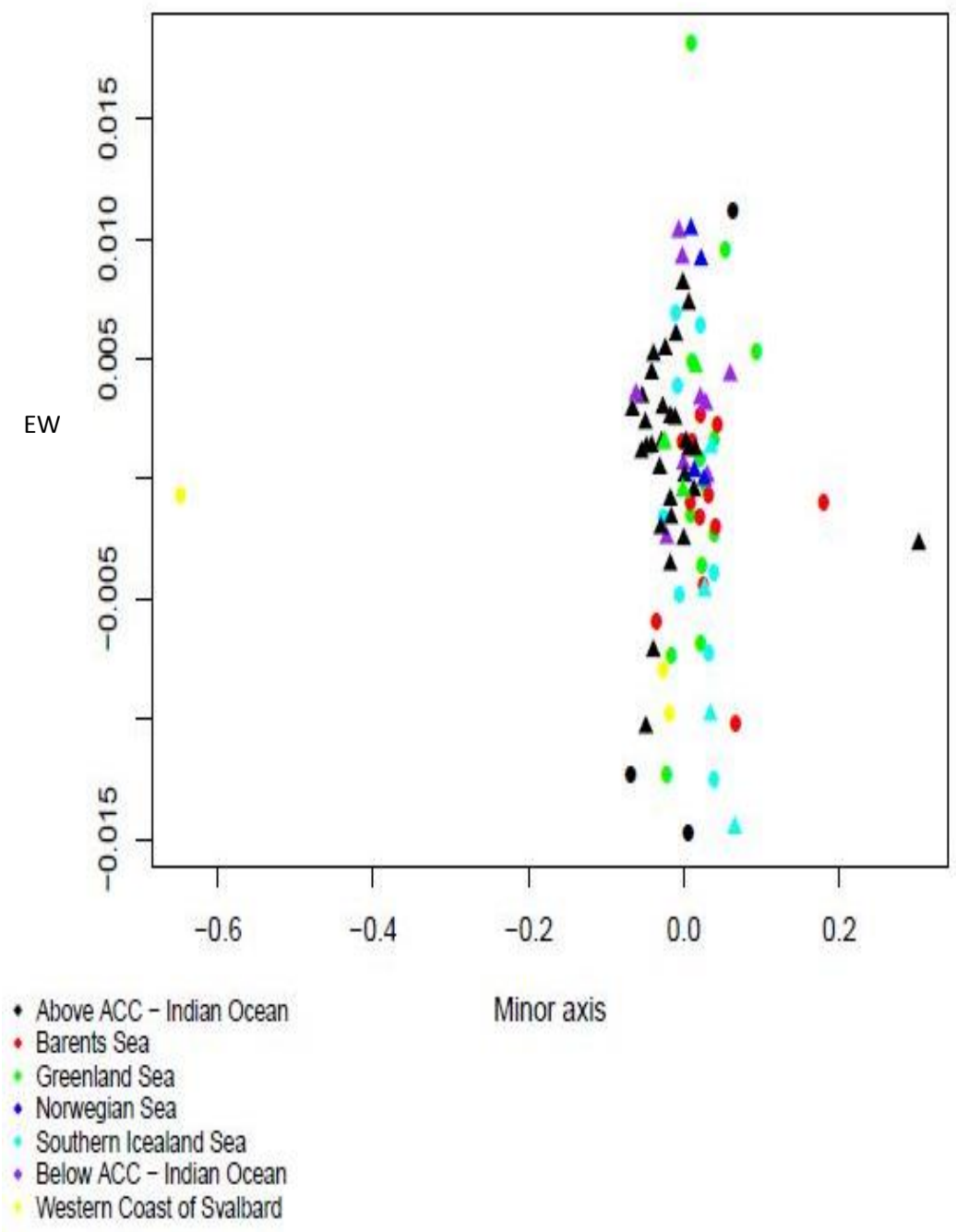

Figure 4.9 CMDS plot of Minor against EW. ▲ =CCM IV ● =CMMI

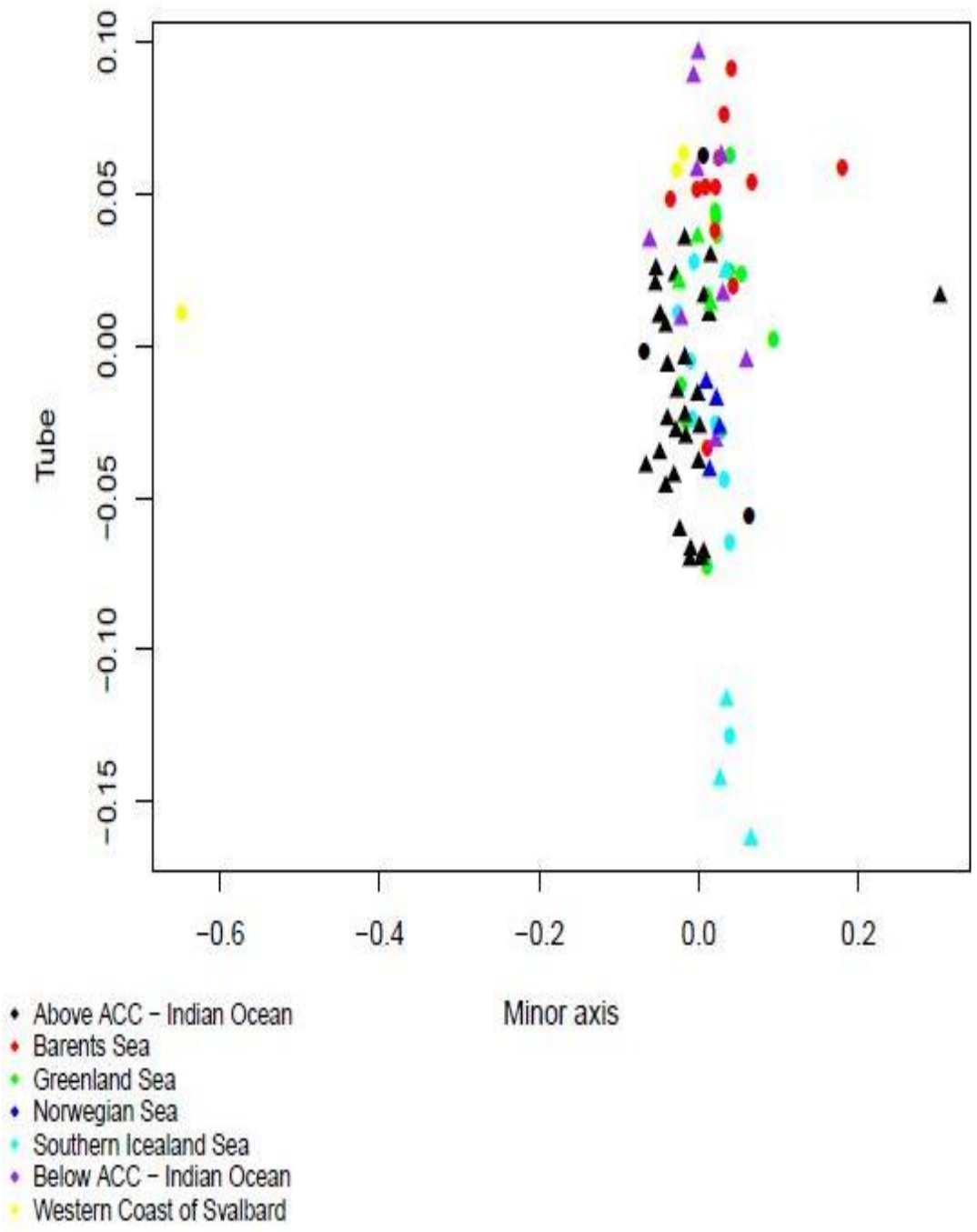

Figure 4.10 CMDS plot of Minor against Tube. ▲ =CCM IV ● =CMMI

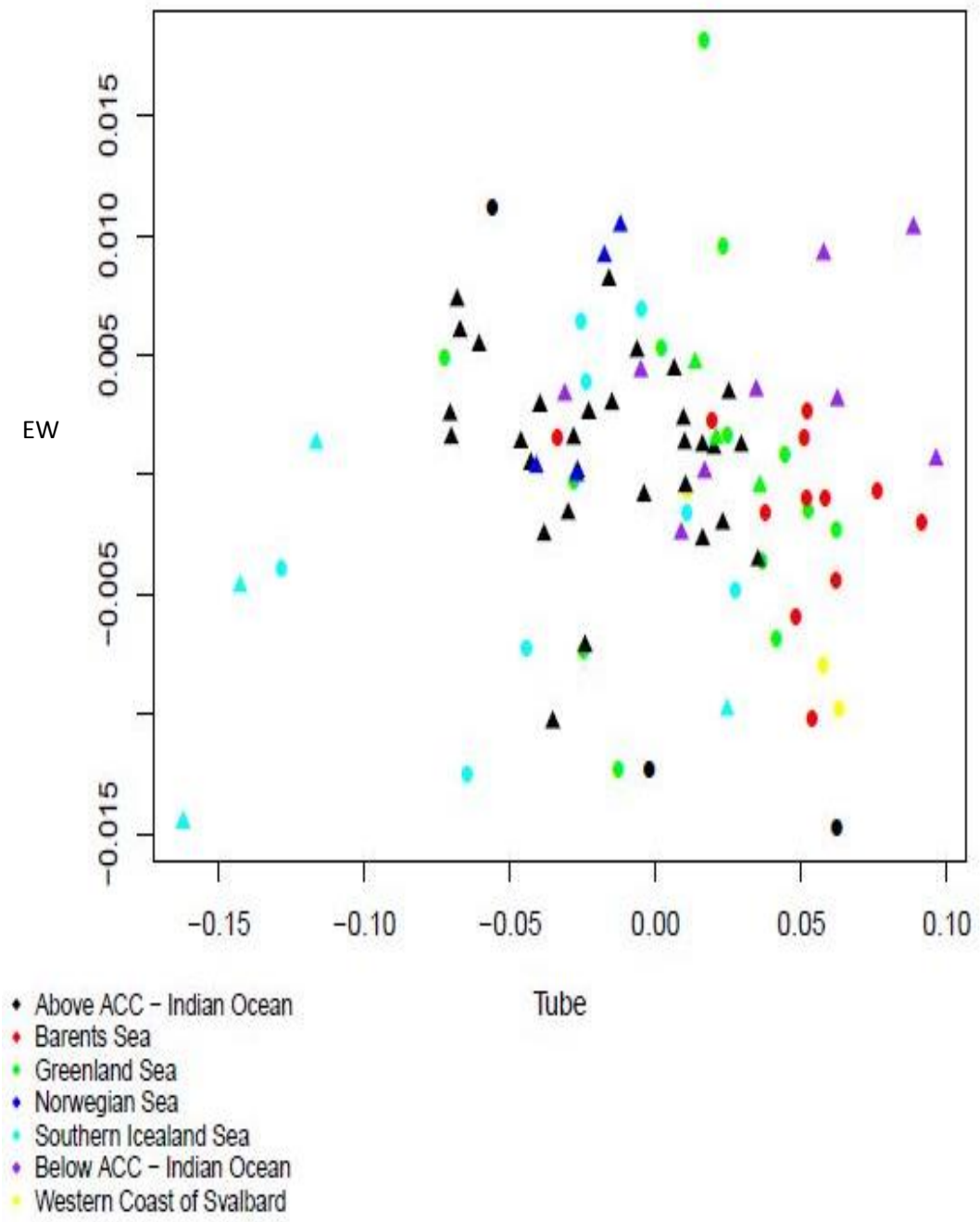

Figure 4.11 CMDS plot of Tube against EW▲ =CCM IV ● =CMMI

In Figure 4.8 (Tube vs Major), most of the points are mixed suggesting, as with the plots in figure 4.3; 3, that there is ‘overlap’ in the data suggesting as was previously stated, that identifying CMM from phenotype is impossible. However, if the samples from the Greenland Sea are looked at, then there is a clear difference with I being on the right of the plot (i.e they are larger) and the 3 IV on the left (i.e they are smaller) in this location. This correlates with the data in figure 4.5. This difference is also visible when looking at the samples from the Greenland Sea in figure 4.6(Major vs Minor) and 4.7 (EW against Major). In Figure 4.6, the difference in the plots is on the Major axis not the Minor indicating less variation with the Minor but again the difference in the Greenland Sea CMM samples is clear. In Figure 4.7 again the difference on the Major axis but there is a much greater spread on the EW axis. Despite this the CMM I and CMM IV are mixed on the EW axis indicating ‘overlapping’ of the points. This indicates that this location (Greenland Sea) has an impact on Major.

However, with figure 4.7 (EW vs Major) there is another clear difference if the points for the ‘Above ACC-Indian ocean’ are looked at. There are 3 CMM I points. There is one above the cluster of CMM IV points and two below indicating a difference in the size of the EW elements at this location.

This difference is also visible in Figures 4.9 and 4.11. The MDS is EW vs Minor or Tube. This would indicate that this location (above ACC-Indian ocean) has some effect on the EW elements.

In Figure 4.12 and 4.13 (below) are SEM images of the coccoliths from the Greenland Sea. 4.12 are of the CMMI coccoliths and 4.13 of the CMMIV. Each of the numbered images (1, 2 and 3) is from a different location within the Greenland Sea.

According to the data in the MDS plots, these cells should be a different size (I being larger than IV). Examination of these images does indeed show this. It is particularly apparent with image 1 in both figures with image 1 in Figure 4.13 being smaller than the coccoliths in image 1 in Figure 4.12.

Figures 4.14 and 4.15 are of coccoliths from Above the ACC-Indian Ocean. Again 1, 2 and 3 are from different locations. In Figure 4.14, images 1and 2 are of coccoliths that, according to the MDS plot are points below the CMMIV and image 3, is above the IV points. The images in Figure 4.15 are of coccoliths from the CMMIV and according to the MDS plots, these are points that lie between the CMMI coccoliths in figure 4.14.

In Figure 4.14, the coccolith images 1 and 2 look different. The coccoliths in image 4.14/3 shows thicker tubes than those images 4.14/ 1 and 2 and the EW elements appear to be more numerous in image 3 compared to 1

and 2. The EW elements in 1 and 2 also appear to be distinct elements as opposed to the EW elements in image 3 where they appear to be fusing with less defined gaps between each element.

If images 1 and 2 from figure 4.14 are compared to 1 and 2 from Figure 4.15 it can be seen that the EW elements in 4.15 are more in number and comparing 1and 2 from 4.14 to all of the images in 4.15 the EW elements appear longer.

These differences in the images support the data from the MDS plots.

The next question, is why?

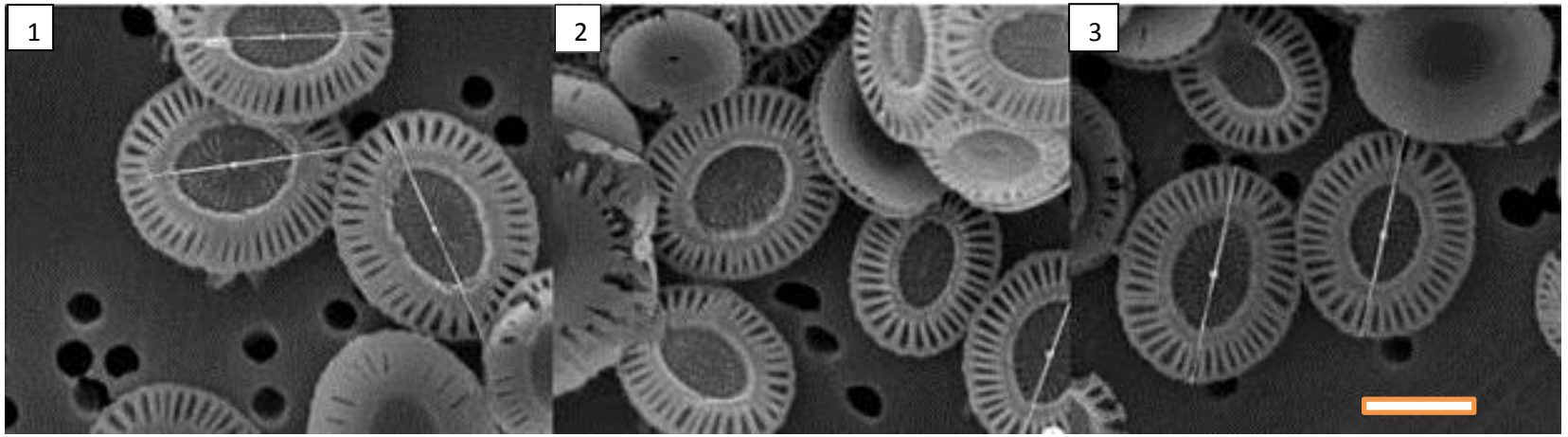

Figure 4.12 Coccoliths of CMMI cells from the Greenland Sea. Scale bar = 5um

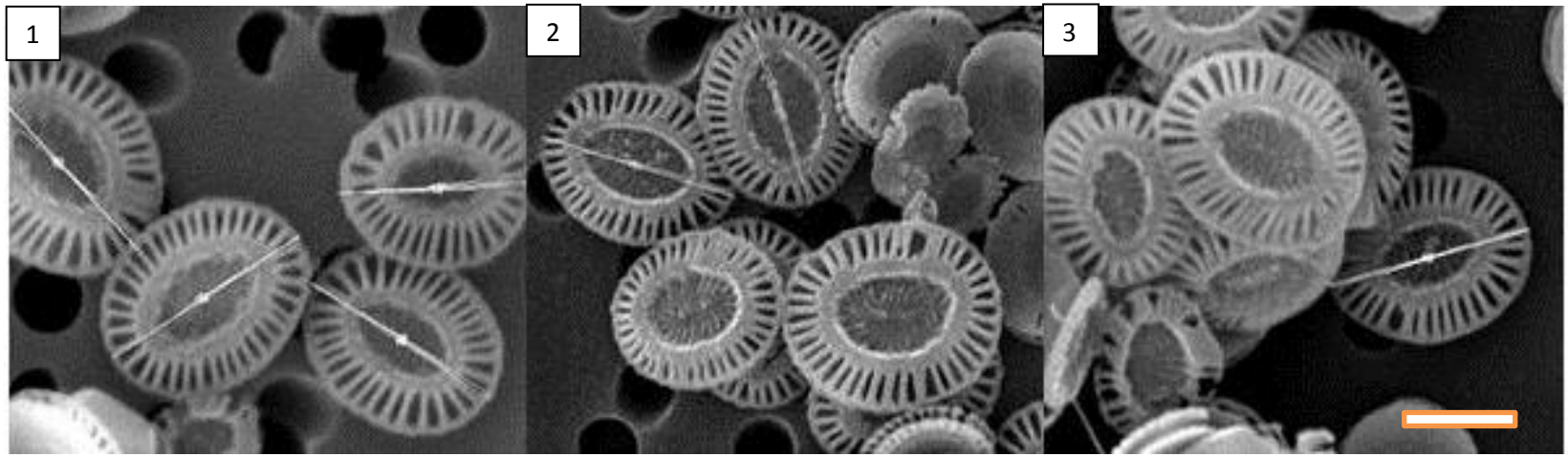

Figure 4.13 Coccoliths of CMMIV cells from the Greenland Sea. Scale bar = 5um

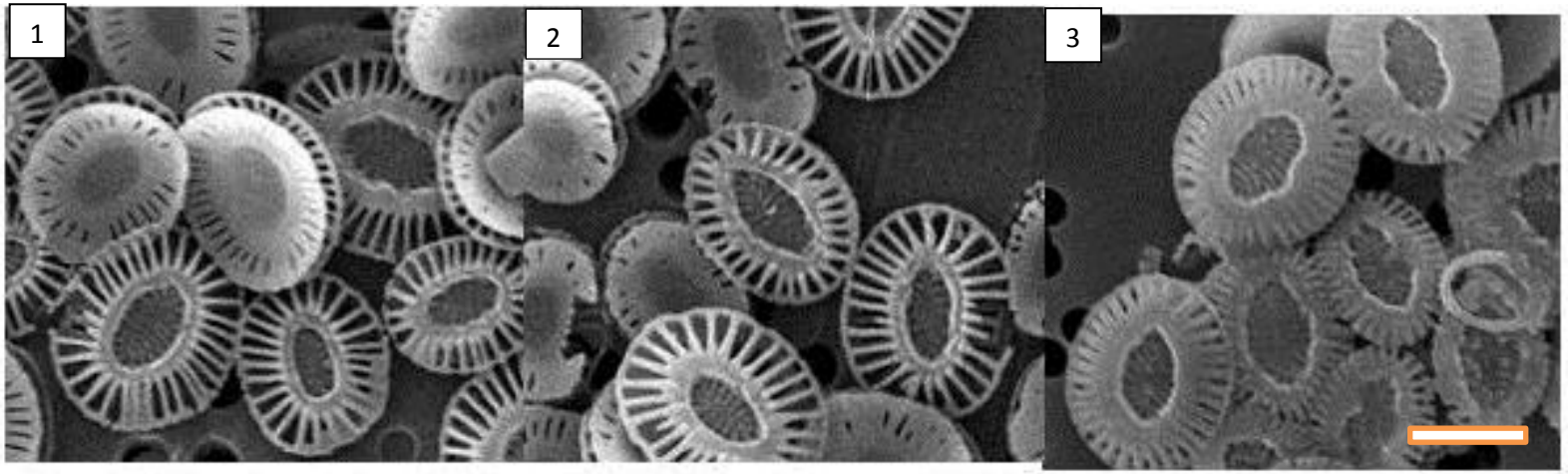

Figure 4.14 Coccoliths from CMMI cells from Above ACC. Scale bar = 5um.

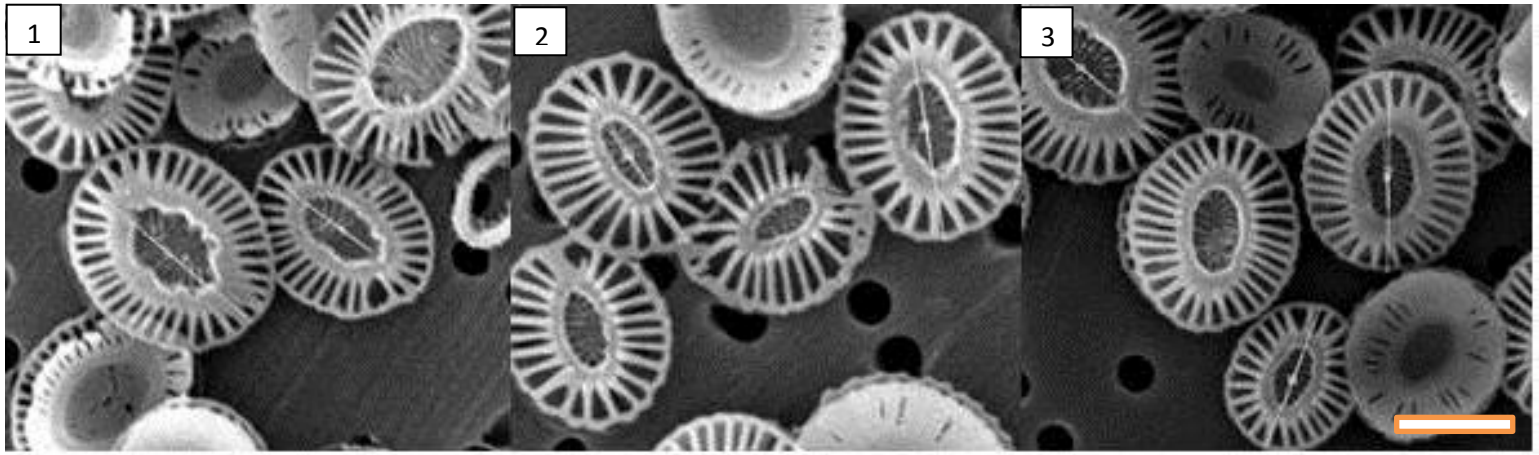

Figure 4.15 Coccoliths from CMMIV cells from above ACC. Scale bar = 5um,

4.5 Discussion

The results of the T test showed that on average, I and IV were different in Major, Minor, Tube and the EW elements as previously discussed, this difference is based on the averages and as such it was not possible to identify any intraspecific variation within the morphologies when looking at all of the cells from all of the locations. Looking at the T test, it showed a significant difference between the isolates, however the T test used the average to produce a result and with significant 'overlaps' in the data it was impossible to separate the morphotype CMM I from the CMM IV.

However, when the data is plotted using MDS and the locations that the isolates were collected from are identified, there are two locations where it is possible to identify CMM from phenotype: The Greenland Sea and 'Above the ACC'-Indian Ocean.

In the Greenland Sea, with the MDS plots, the difference was most obvious when looking at the Major plots, coccoliths from CMMI cells being larger than those from CMM IV cells and according to Saruwatari *et al* (2015), larger coccoliths implies larger cells.

The cells possess different genetic motifs-labelled CMMI and CMMIV. We know that the CMM is from an UTR in the mRNA of the coccolith-polysaccharide-associated protein (GPA), which is associated with coccolith structure control and in most locations (apart from the Greenland

Sea when considering coccolith size) there is no difference in phenotype as shown in the MDS plots with the changing morphotype. CMMI and CMMIV points are spread out indicating no pattern.

We also know that the EW elements differ in CMMI and CMMIV cells collected from the 'Above ACC-Indian Ocean' Location as described using figures 4.14 and 4.15.

What is causing this?

Phenotypic plasticity (PP) is the ability of the cells to adjust its phenotype in response to changes in the environment (Relyea, 2001).

Phenotypic plasticity has been observed in *E. huxleyi* as a result of changes in CO_2 concentrations (Barcelos e Ramos *et al.*, 2010). These changes occurred in a very short space of time and the resultant changes in the cells occurred within a matter of hours. Read *et al.* (2013) reported plasticity in *E. huxleyi* as a result of changes in, amongst other things light levels and virus susceptibility. Changes were also observed in *E. huxleyi* by Saruwatari *et al.* (2015) where they exposed cultured cells of the same strain to different levels of salinity and different temperatures. They reported that an increase in temperature produced smaller cells with smaller coccoliths. This is an indication of a reduction in calcification. They also reported that a change in salinity produced larger cells at lower salinity and larger coccolith at higher salinity.

All of these factors can affect the phenotype of the cells irrespective of CMM. However, what causes the cells collected at the Greenland Sea and 'Above ACC' to react so markedly. In the Greenland Sea, the morphotype CMMI cells are *all* larger and the CMMIV *all* smaller. This means at this location it would be possible to ascertain morphotype from phenotype.

It would also be possible (but potentially more difficult as the differences are less obvious) the ascertain CMM looking at the EW elements in cells from 'Above ACC'. With CMMI having longer and thinner EW element. Again, what is special about these locations that result in phenotypic plasticity being so active? Or what's stopping the CMMs from being active in the other locations.

This warrants further investigation initially looking at the various parameters of the 7 locations (Above ACC, Barents Sea, Greenland Sea, Norwegian Sea, South Icelandic Sea, below ACC and the Western Coast of Svalbard) the temperature, salinity, pCO_2, Ca availability and light levels all need to be investigated in order to ascertain whether there is an observable factor that results in significant and observable differences in the different isolates. With this information it might be possible to identify the factor that results in the genotype correlating with morphology.

It is these parameters that may have an influence on the fact the only CMMI cell were found at the Western coast of Svalbard and Barents Sea sites and only CMMIV cells were found at the Norwegian Sea and the

'above ACC' sites. It may also be these parameters that affect the CMMI and CMMIV cells in the Greenland Sea and 'above the ACC' but not the cells in the Southern Icelandic Sea where there are a mix of both I and IV but there is no pattern obvious. What is the difference in the locations? Again, looking at the variations in the collection sites (temperature, salinity, pCO_2 and light levels) might hold the key to answering this question.

It would also be interesting to take the cells collected from each of the locations and vary the conditions in which they grew. This would make it possible to see if, for example some smaller CMMIV cells from the Greenland Sea were exposed to the conditions of the Southern Icelandic Sea site (where there was no observed difference in the different CMMs). Would the morphotype of the CMMIV cells from the Greenland Sea change resulting in a wider, undifferentiated range of coccolith sizes as was observed in cells from the Southern Icelandic Sea?

Further work could also involve the collection of more cells from more sites. This could result in other CMM morphotypes being collected (including heterozygous) cells to see if there are any correlations with what has been observed here.

4.5 Conclusions.

The initial question of this chapter was, is it possible to identify morphotype from phenotype. If one looks at all of the samples as a whole (ignoring the location they were acquired from) then, despite the results of a T test stating the results were significantly different, it was clear from the results that the morphology of a small CMMI can be confused with a large CMMIV. Therefore, you cannot ascertain morphotype from phenotype. This is as a result of the T test looking at the averages of all of the data.

However, in certain locations, the CMM affects the phenotype and it is possible to ascertain morphotype. There *is* a significant morphometric difference between the two genotypic isolates. It results in, dependant on the origin of the isolates, a significant size difference in the isolates which results in the separation of the morphometric sub-groups of CMM I and CMM IV. The factors that cause this warrant further investigation.

GPA is responsible, it is thought, for nucleating the calcium carbonate during coccolith development, or, alternatively, to having an involvement the calcium's delivery to the coccolith vesicle (Cortsjens *et al.*,1998). Therefore, the significant correlation between CMM and the protein GPA (Schroeder *et al.*, 2005.) appears to be resulting in a clear link between CMM and morphotype.

I quote directly from Schroeder *et al* (2005): -

"The relationship between CMM and *E. huxleyi* may prove to be purely coincidental…"

However, the evidence from this work suggests that this is not the case.

Chapter 5 Summary

5.1 Introduction

The mechanism and function of calcification is significant in that it has produced one of the most successful organisms in the ocean (Monteiro *et al.* 2016). Several suggestions have been made as to the function of calcification (Young 1994) including protection from predation, virus infection or an ability to exist higher or lower in the water column as a result of light regulation. Alternatively, an ability to sink faster in the water column to introduce the cells to more nutrients or there may be a direct link between calcification and photosynthesis whereby calcification produces CO_2 which is utilised during photosynthesis where CO_2 levels would normally be prohibitive. Whatever the function or indeed functions of calcification they are likely to have had multi-evolutionary origins (Berry *et al.*, 2002) and it may transpire that some species rely on coccoliths and coccospheres for one function and another species require them for a wholly different reason.

The mechanism of calcification has been studied at length by many people and the fundamental of coccolith formation is well understood (Young *et al.*, 1992 and Marsh *et al., 2002)* and the work in chapter 3 investigated coccolithogenesis-the production of the coccoliths in the non-motile stage of the heterococcolith producing *Coccolithus pelagicus*. Using a combination

of Transmission Electron Microscopy (TEM), Scanning Electron Microscopy (SEM) and light microscopy (LM) to investigate the production development and the final extrusion of the coccolith to the exterior of the cell in order to form part of the coccosphere surrounding the cell. The use of the TEM was necessary as it was the only technique available that had sufficient resolution to image the ultrastructural details of the production of the heterococcolith.

Emeliania huxleyi is one of the most abundant coccoliths in our oceans (Beaufort *et al.*, 2011) and as a consequence of its role in the net removal of CO_2 from the atmosphere (Coxall et al., 2005) it has been studied by groups ranging from oceanographers and ecologists to biostratigraphers and paleoceanographers (Young and Westbroek, 1991).

The genetics involved in coccolithogenesis has been studied extensively (for example by Mackinder *et al.*, 2010 and Kreuger-Hadfield *et al.*, 2014).

E. huxleyi exhibits a wide range of variation with regards to coccolith morphology, physiological properties and the immunological properties of the polysaccharides involved coccolith formation and as a consequence of this, it was separated into two main distinct morphotypes A and B, by van Bleijswijk *et al.* (1991) and Young *et al.* (1991). These were subsequently formally described as varieties by Medlin *et al.* (1996) – type A to *E.*

Morphotypes A and B are the most widely recognised with morphotype A being the most prevalent in summer blooms (Hagino *et al.*, 2011 and Krueger-Hadfield *et al., 2014*).

Molecular genetic separation of groups with *E. huxleyi* has been problematic; however, work undertaken by Schroeder *et al*. (2005) identified a region in the 3′ Untranslated Regions (UTR) within the mRNA of the coccolith-polysaccharide-associated protein (GPA), which is associated with coccolith structure control. This region does appear to vary between morphotypes. This region was named the Coccolith Morphology Motif (CMM). Four discreet CMM groups were identified and subsequently were characterised as CMM I, CMM II, CMM III and CMM IV (Schroeder *et al* 2005).

The work in chapter 4 concerned the study of two different morphotypes of *Emiliania huxleyi* (specifically CMMI and CMM IV) and the impact it had on their genetics, more specifically whether it was possible to identify genotype from the phenotype. The cells were imaged with an SEM and different dimensions were measured (including the length and the width) using image analysis software and from this data, various scatter plots and Multi-Dimensional Scaling (MDS) plots were produced and from these conclusions were drawn about the ability to identify genotype from phenotype.

5.2 Summary of chapter 3- Dynamics of formation and secretion of heterococcoliths by *Coccolithus pelagicus*.ssp. *braarudii.*

Coccolithus pelagicus is characterised by the formation and secretion of ornate calcified plates, heterococcoliths and the formation of these plates (coccoliths) was investigated by transmission electron microscopy (TEM).

This work and investigation of the cells via SEM and LM from the paper: Dynamics of formation and secretion of heterococcoliths by *Coccolithus pelagicus*.ssp. *braarudii*. (Taylor *et al., 2007).* The goal of the research was to investigate the major structures involved in heterococcolith production and how the coccoliths were finally extruded to form the coccosphere.

Live cell imaging was used to identify that the cells use highly dynamic behaviour to move the maturing coccolith (a process that takes around 2 hrs) to the edge of the cell and once there, to secrete the mature coccolith rapidly in a dynamic exocytotic event that lasted around 1-2 minutes.

The TEM work not only investigated the gross morphology of the cell but also produced a series of images that showed how the coccolith was produced in a distinct vesicle (Coccolith Vesicle, CV) that was closely associated with a series of anastomosing tubes that form a Reticular Body (RB). The CV/RB complex was closely associated with the nucleus of the cell and as the coccolith matured it moved to the edge of the cell and it was this work that led to the formation of a hypothesis that the layer of organic

scales that surrounded the outside of the cell played a critical role in the positioning and rotating of the mature coccolith to form a continual, complete coccosphere. The work in this paper showed the formation of the coccoliths showed that the production of coccoliths in *C. pelagicus* was consistent with production of coccoliths in the widely studied *Emiliania huxleyi*.

5.3 Summary of chapter 4: Intraspecific variation within the *Emiliania huxleyi (*Prymnesiophyceae) morphotype A group.

Work by Schroeder *et al.* (2005) identified a genetic marker in the 3/ Untranslated Regions (UTR) within the mRNA of the coccolith-polysaccharide-associated protein (GPA), which is associated with coccolith structure control. The differences were labelled as Coccolith Morphology Motif (CMM) and the four were grouped into CMM I, CMM II, CMM III and CMM IV. These genotypes correlated significantly with morphotype.

E. huxleyi cells were collected during various cruises from various sites during two cruises by Cecilia Balestreri in 2012 and from these sites various isolates were cultured. Two different types of genetic isolates were (specifically CMM I and CMM IV) cultured (as described in chapter 2). The cells were processed (as described in chapter 2.7) and examined in the

SEM at the same magnification in order to make image analysis easier. The image analysis measured length, width, the tube and the ‘t’ elements and then this data was compiled using an Excel spread sheet. From this data, various scatter plots were produced and alongside this a T-test was done which stated that the data for length, width and ‘t’ elements were significantly different with CMM I being larger than CMM IV. However, when this data was plotted in a scatter plot and a bar chart with the error bars it was clear that there were significant problems with trying to use the average of all of this data to identify CMM from phenotype, the error bars overlapped greatly meaning that a large CMM IV could be mistaken for a small CMM I. Using the average of all of the data was not applicable. On average I is bigger than IV but only on average.

When the data was plotted in a Multi-Dimensional Scaler (MDS) plot with the locations it became clear that at certain locations there was only one morphotype: CMMIV cells at the Norwegian Sea and the ‘below Arctic Circular Current (ACC)’ sites and there were only CMMI cells at the Western coast of Svalbard and Barents Sea sites. It also became clear that at the Greenland Sea, ‘Above ACC’ and Norwegian Sea sites there was a mix of both morphotypes and at the Greenland Sea and ‘Above ACC’ sites there was a pattern in the distribution of the data points, this pattern was not seen at the Norwegian Sea site (where there a mix of both CMM I and IV morphotypes). This would suggest that some factor, possibly temperature,

salinity, pCO_2 or calcium availability was causing this to happen. However, further work, in particular looking at the conditions that the cells were growing in (in particular temperature, salinity, pCO_2 and calcium availability), in order to see if there is an obvious difference in the locations and from this, it would then be possible to identify genotype from phenotype providing that the cells were collected from a location that matched the conditions found in the Greenland Sea and 'Above ACC' locations.

This work proved that CMM does have in influence on morphotype, at least in certain specific locations.

We report for the first time that a significant morphometric difference exists along the major axis of the coccolith between the CMMI and CMMIV isolates. Moreover, the origin of the isolates is an important factor in determining which CMM dominates

5.4 Further work.

Drescher *et al.* (2012) investigated Coccolithogenesis in *Scyphosphaera apsteinii* (Prymnesiophyceae). This paper described how coccolithogenesis in this species bore a similar pattern to many other heterococcolith bearing species including *E. huxleyi* and *C. pelagicus.*

The work in chapter 3 and the techniques used in Chapter 3 and Drescher *et al.* (2012) can be extended and used to investigate coccolithogenesis in

other coccolith producing species. Given that there are 168 different species in the North-western Mediterranean Sea (Cros and Fortuno, 2002) alone from different genera and taxa it would be a source of a great deal of information looking at how different species undergo calcification.

Further work looking at the morphotyping of *E. huxleyi* should predominantly involve establishing why in certain locations, the CMM has a greater influence on the morphotype. This would then enable the genotyping of *E. huxleyi* from the phenotype without the need for more involved sequencing and genotyping.

An expansion of the work could involve looking at other homozygous CMMs (e.g. CMMIII and CMM IVb) and heterozygous CMMs (e.g. CMMI/IVb or CMMI/IV) and investigating if any of these display differences similar to those observed in the MDS plots in the Greenland Sea and 'Above ACC' locations. Further work could also involve collecting more samples from other locations to see if there were any more sites with only one CMM in evidence as with Barents and Norwegian Sea locations or sites like the Southern Icelandic Sea where there are two CMMs present but (according to the MDS plots) no obvious pattern in the data.

All of this work would result in more data being used to identify genotype from phenotype thus allowing genotyping from simply observing the cells.

Both chapters used Electron Microscopy (EM) (chapter 3 both TEM and SEM and chapter 2 just SEM) to produce the data and it is development of the use of EM that could help further our understanding of other aspects of Coccolithophores. One of these aspects is to establish the route of calcium sequestration in coccolithophores, something that I attempted during the initial phase of this research. The technique involved the use of an SEM with x-ray microanalysis capability (this uses the energy of x-rays produced by the sample as a result of specimen beam interaction that are characteristic to the element that emits them) and it is the x-rays that can identify the location of the calcium in the cell. However, calcium is present throughout the cell in its role as a cell signalling mechanism (Steinhorst and Kudla 2013), therefore, the route calcium takes was to be investigated using Strontium as an analogue for the calcium and freeze substitution (FS) as an alternative method of TEM specimen preparation, a method that minimises the dislocation of the Ca/Sr ions and allowed their route to be mapped using x-ray micro analysis and uses a Reichert AFS processor (Leica, Wetzla, Germany) (Edelmann, 1990).

The initial ‘cryofixation’ (rapid freezing of the samples to avoid ice crystal damage) was achieved using ‘slam freezing’ using a Reichert MM80 E (Leica, Wetzla, Germany). The images produced using this method (figure 5.1, below) show that slam freezing was not the appropriate method of

cryofixation as it wasn't rapid enough and failed to produce images that look like those produced with conventional techniques (figure 5.2). These rely on chemical fixatives and alcohol dehydration that would remove the dissolvable ions (see chapter 2)-i.e. the strontium, from their initial location meaning that mapping the position of the strontium would be impossible.

A comparison of these two images show the obvious limitations of Slam freezing: if the calcium (strontium) is being transported to the CV via the endoplasmic reticulum (ER) and golgi as Berry *et al.*, (2002) suggested then I would need to visualise the ER in order to see if it was full of strontium. In 5.1 there is no ER, therefore this is not an adequate method. However, if an alternative to slam freezing for the cryo-fixation was found (for example plunge freezing in liquid propane/butane mix maintained in a liquid state in a surrounding bath of liquid nitrogen (Thirion *et al., 1997*) then the FS after the strontium spiking could be used to ascertain the route for calcium sequestration using a combination of SEM and xray microanalysis.

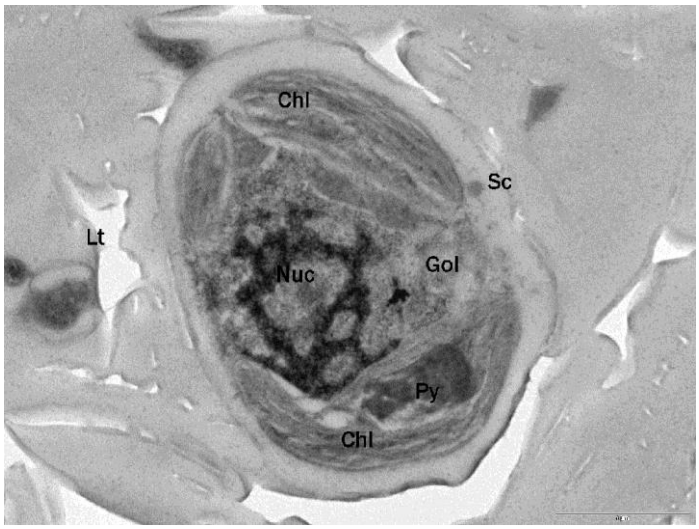

Figure 5.1 *Coccolithus pelagicus* imaged after processing with 'slam freezing' and freeze substitution. (Lt, coccolith; Nuc, nucleus;Chl, chloroplast, Gol, golgi; Py, pyrenoid: Sc organic scale).

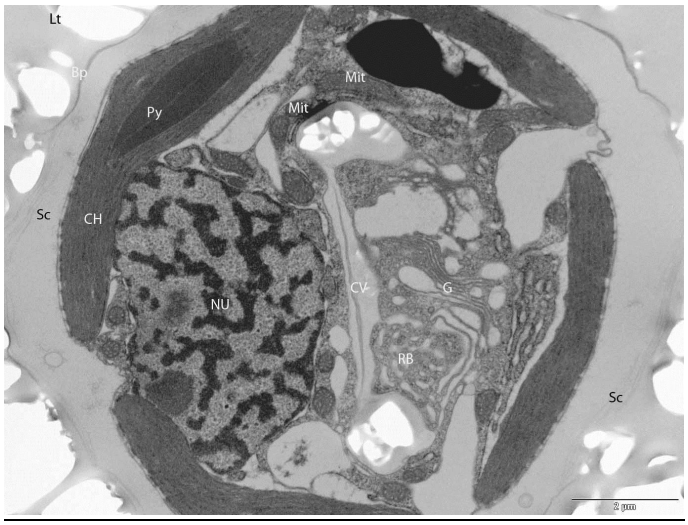

Figure 5.2 Transmission electron micrograph *Coccolithus pelagicus* Coccoliths after conventional specimen preparation. (Lt). Also (NU) Nucleus, (Mit) Mitochondria, (Gg) Golgi apparatus, (RB) Reticular Body, (CV) Coccolith Vesicle, (CH) Chloroplast, (Py) Pyrenoid, (Bp) Base plate of coccolith and (SC) organic scales. Scale bar = 2um.

There can be no denying the global significance of coccolithophores (Monteiro *et al.* 2016) and much work has been done to increase our understanding of these organisms. However, there is still a great deal more to do.

References.

Anning T., Nimer N.A., Merrett M.J., Brownlee C., (1996)

Costs and benefits of calcification in coccolithophores.

Journal of Marine Systems, **9**: 45-56.

Ackerly C.A., Nielsen C. and Hawkins C.E. (2006)

Experiences with wet capsule imaging exploring the possibility for live cell imaging.

Microscopical Microanalysis, **Supplement 2.**

Bach L T., Bauke C., Meier K J S., Riebesell U. And hulz K G. (2012)

Influence of Changing Carbonate Chemistry on Morphology and Weight of Coccoliths Formed by *Emiliania huxleyi.*

Biogeosciences, **9**, 3449-3463.

Balch W.M., Holligan P.M., Kilpatrick K.A., (1992)

Calcification, photosynthesis and growth of the bloom-forming coccolithophore, *Emiliania huxleyi.*

Continental Shelf research. **12**: 1353-1374.

Barcelos e Ramos J. Muller M.N. and Riebesell U. (2010)

Short-term Response of the Coccolithophore *Emiliania huxleyi* to an Abrupt Change in Seawater Carbon Dioxide Concentrations.

Biogeosciences, **7**, 177-186.

BarShack I., Kopolovic J., Chowers Y., Gileadi O., Vainshtein A., Zik O. and Beher V. (2009)

A novel method for "wet" SEM.

Ultrastructural Pathology, **28:** 29-31.

Beaufort L., Probert I., de Garidel-Thoron T., Bendif E.M., Ruiz-pino D., Metzl N., Goyet C., Buchet N., Coupel P., Grelaud M., Rost B., Rickaby R.E.M. and de Vargas C. (2011)

Sensitivity of Coccolithophores to Carbonate Chemistry and Ocean Acidification.

Nature. **476**, 4 August 2011.

Bedi S. (1991)

Plasticity of Phenotypic Expression in Cultured Shoot Explantd of *Pinus caribaea* Morelet.

Environmental and Experimental Botany. **31**, 405-412.

Bendif E. M. and Young J. (2014)

On the Ultrastructure of *Gephyrocapsa oceanica* (Haptophyta) Life Stages.

Cryptogamie Algologie, **35 (4)**:379-388.

Bendif E.M., Probert I., Young J.R. and von Dassow P. (2015)

Morphological and Phylogenetic Characterisation of New *Gephyrocapsa* Isolates Suggests Introgressive Hybridization in the *Eiliania/Gephyrocapsa* Complex (Haptophyta).

Protist, **166**: 323-336.

Berge G., (1962)

Discolouration of the sea due to *Emiliania huxleyi* "bloom".

Sarsia, **6**: 27-40.

Berridge M.J., Bootman M.D. and Roderick H.L. (2002)

Calcium Signalling: Dynamics, homeostasis and Remodelling

Nature reviews Molecular Cell Biology, **4**, 517-529

Berry L. Taylor A.R., Lucken U., Ryan K.P., Brownlee C., (2002)

Calcification and inorganic carbon acquisition in coccolithophores.

Functional Plant Biology, **29**: 289-299.

Billard C. And Inouye., (2004)

What is new in coccolithophore biology?

'In' Theirstein H.R. And Young J.R., '*Eds' Coccolithophores-From Molecular Process to Global Impact,* Springer-Verlang Berlin, 31-49.

Brenner S. and Horne R.W. (1959)

A Negative Staining method for high resolution electron microscopy of Viruses.

Biochimica et Biophysica Acta **34:** 103-107

Brownlee C., Davies M., Nimer N., Dong L.F., Merrett M.J., (1995)

Calcification, photosynthesis and intracellular regulation in *Emiliania huxleyi*.

Bulletin of the Institute for Oceanography, Monaco. **14**: 19-36.

Brownlee C. and Taylor A.T., (2002)

Algal Calcification and Silification

'In' *Encyclopaedia of Life Sciences*, *www.els.net*, London: Nature publishing group.

Brownlee C. And Taylor A.R., (2004)

Calcification in Coccolithophores: a Cellular Perspective,

'In' Theirstein H.R. And Young J.R., '*Eds' Coccolithophores-From Molecular Process to Global Impact,* Springer-Verlang Berlin, 31-49.

Brownlee C., Wheeler G L. and Taylor A R. (2015)

Coccolithophore Biomineralisation: New Questions, New Answers.

Seminars in Cell and developmental Biology. (2015)

Brand L.E., (1981)

Genetic Variability in Reproduction Rates in Marine Phytoplankton Populations

Evolution. **35** (6): 1117-1127.

Cook S S., Whittock L., Wright S W. and Hellegraef G M. (2011)

Photosynthetic Pigment and Genetic Differences Between two Southern Ocean Morphotypes of *Emiliania huxleyi* (Haptophyta).

Journal Phycology.**47**:615-626.

Cortes M.Y., (2000)

Further Evidence for the Heterococcolith – Holococcolith combination *Calcidiscus leptoporus – Crystallolithus rigidus.*

Marine Micropaleontology, **39:** 35-37.

Corstjens P L A M., van der Kooij A., Linsscooten C., Brouwers G-J. Westbroek P. De Vrind-de Jong E W. (1998)

GPA, Calcium-Binding Protein in the Coccolithophorid E*miliania huxleyi* (Prymnesiophyceae).

Journal Phycology,**34**, 622-639.

Cros L., Kleijne A., Zeltner A., Billard C., Young J.R., (2000)

New Examples of Holoccolith - Hetrococcolith combination coccospheres and their implications for coccolithophirid biology.

Marine Micropaleontology, **39:** 1-34.

Cros L. and Fortuno J-M. (2002)

Atlas of North-western Mediterranean Coccolithophores.

Scientia Marina, **66**: 7-182.

Davey M.S., Sugget D.J., Geider R.J. and Taylor A.R. (2003)

Phytoplankton plasma membrane redox activity: effect of iron limitation and interaction with photosynthesis.
Journal Phycology, **39 (6)**, 1132-1144.

Doney S C., Fabry V J., Feeley R A. and Kleypas J A. (2009)

Ocean Acidification: The Other CO_2 Problem.

Annual Review of Marine Science, **1**:169-192.

Drescher B., Dillaman R.M. and Taylor A.R. (2012)

Coccolithogenesis in *Scyphosphaera apsteinii* (Prymnesiophyceae).

Journal of Phycology, **48**, 1343-1361.

Edelmann L. (1990)

Freeze substitution and the preservation of diffusible ions.

Journal of Microscopy, **161**, 217-228.

Fagerbakke K.M., Heldal M., Norland S., Heimdal B.R., Batvik H., (1994)

Emiliania huxleyi, Chemical compositions and size of coccoliths from enclosure experiments in a Norwegian fjord.

Sarsia, **79**:349-355.

Falini G., Fermani S. and Goffredo S. (2015)

Coral Biomineralisation:A Focus on intra-skeletal Organic Matrix and Calcification.

Seminars in ell and Developmental Biology. (2015)

Feng Y., Warner ME. And Zhang Y. (2008)

Interactive effects of increased pCO_2, temperature and irradiance in the marine coccolithophore *Emiliania huxleyi* (*Prymnesiophyceae)*

European journal of Phycology, **43**:87-98

Fiorini S., Middelburg J J. and Gattuso J-P. (2011)

Testing the Effects of Elevated pCO_2 on Coccolithophores (Prymnesiophyceae): Comparison Between Haploid and Diploid Life Stages.

Journal of Phycology, **47**:1281-1291.

Frada M., Not F., Probert I. and de Vargas C. (2006)

$CaCO_3$ Optical Detection with Fluorescent *in situ* Hybridisation: a New Method to Identify and Quantify Calcifying Microorganisms from the Oceans.

Journal of Phycology **42**, 1162-1169 (2006).

Gartner S. And Bukry D., (1969)

Tertiary hollococcoliths.

Journal Palaeontology, **43:** 1231-1221.

Geisen M., Billard C., Broerse A., Cros L., Probert I and Young J.**Life-cycle associations involving pairs of holococcolithophorid species: intraspecific variation or cryptic speciation?**

European Journal of Phycology, **37 (4):** 531 – 550.

Giulard R. R. L. And Ryther J. H. (1962)

Studies of Marine Planktonic Diatoms *I. Cyclotella nana Husdedt* and *Detonula confervacea* Cleve.

Journal Microbiology, **8**, 229-239.

Glauert A. M. and Glauert R.H. (1957)

Araldite as an embedding medium for Electron Microscopy.

The journal of Biophysical and Biochemical Cytology

Griffiths G. (1993)

Introduction to Immunocytochemistry and Historical background.

Chapter 1 Page 1-2

Hagino K., Bendif E.M. Young J.R., Kogame K., Probert I., Takano Y., Horiguchi T., de Vargas C. and Okada H. (2011)

New Evidence for Morphological and Genetic Variation in the Cosmopolitan Coccolithophore *Emiliania Huxleyi* (Prymnesiophyceae) from the *Cox1b-ATP4* Genes.

Journal of Phycology, **47**:1164-1176 (2011).

Hannisdal B., Henderiks J. and Liow L H. (2012)

Long-term Evolutionary and Ecological Responses of Calcifying Plankton to Changes in Atmospheric CO_2.

Global Change Biology, **18**:3504-3516.

Harris R.P. (1994)

Zooplankton grazing on the coccolithophore *Emiliania huxleyi* and its role in inorganic carbon flux.

*Marine Biology***, 119**: 431-436.

Henriksen K., Young J R., Bown P R. and Stipp S L S. (2004)

Coccolith Biomineralisation Studied with Atomic Force Microscopy.

Palaeontology, **47,** 725-743

Hildebrand M. (2008)

Diatoms, Biomineralisation Processes, and Genomics.

*Chemical review,***108**,4855-4874.

Hildebrand M and Lerch S J L. (2015)

Diatom Silica Biomineralisation: Parallel Development of Approaches and Understanding.

Seminars in Cell and developmental Biology. (2015)

Holligan P.M., Viollier M., Harbour D.S., Campus P., Champagne-Phillipe M., (1983)

Satellite and ship studies of coccolithophore production along a continental shelf edge.

Nature, **304**: 339-342.

Holligan P.M., Fernandez E., Aiken J., Balch W.M., Boyd P., Burkhill P.H., Finch M., Groom S.B., Malin G., Muller K., Purdic D.A., Robinson C., Trees C.C., Turner S.M., van der Wal P., (1993)

A biochemical study on the coccolithophore *Emiliania huxleyi* in the North Atlantic.

Global Biochemical Cycles, 7**:** 879-900.

Houdan A., Billard C., Not D.M.F., Saez A.G., Young J.R., Probert I. (2004)

Holococcolithophore-heterococcolithophore (Haptophyta life cycles: flow cytometric analysis of ploidy levels.

Systematics and Biodiversity, **1:** (453-465).

Kuo J (ed.) (2007)

Electron Microscopy-Methods and protocols.

Humana press Inc.

Nott J. A. (1995)

Application of X-ray Microanalysis to Metals in Marine Food Chains.

Microbeam Analysis, **4:** (277-285)

Nyska A., Cummins C.A., Vaishtein A., Nadler J., Ezov N., Grunfeld Y., Gileadi O. and Behar V. (2004)

Electron microscopy of Wet Tissues: A Case Study in Renal Pathology.

Toxic Pathology, **32:** 357-363

Krueger-Hadfield S.A., Belestreri C., Schroeder J., Highfield A., Helaouet P., Allum J., Moate R., Lohbeck K.T., Miller P.I., Riebesell U., Reusch T.B.H., Rickaby R.E.M., Young J., Hallegraeff G., Brownlee and Schroeder D.C. (2014)

Genotyping an *Emiliania huxleyi* (prymnesiophyceae) Bloom Event in the North Sea Reveals Evidence of Asexual Reproduction.

Biogeosciences, **11**: 5215-5234

Laguna R., Romo J., Reda B.A. And Wahlund T.M. (2001)

Induction of phase variation events in the life cycle of the marine coccolithophorid *Emiliania huxleyi.*

Applied and Environmental Microbiology, **9:** 3834-3831.

Langer G., Jan de Nooijer L.and Oetjen K. (2010)

On the Role of the Cytoskeleton in Coccolith Morphogenesis:the Effect of Cytoskeletal Inhibitors.

Journal of Phycology, **46**, 1252-1256.

Langer G., Probert I., Nehrke G. And Ziveri P. (2011)

The Morphological Response of *Emiliania huxleyi* to Seawater Carbonate Chemistry Changes: An Inter-Strain Comparison.

Journal of Nannoplankton, **32 (1)**, 29-34.

Marlowe, I.T., Green, J.C., Neal, A.C., Brassell, S.C.and Course, P.A. (1984) "Long-chain (*n*-C_{37}-C_{39}) alkenones in the Prymnesiophyceae. Distribution of alkenones and other lipids and their taxonomic significance." *British Phycological Journal* **19**, 203-216

Marsh M.E., Ridall A.L., Azadi P. And Duke P.J. (2002)

Galacturonomannan and Golgi-derived membrane linked to growth and shaping of Biogenic Calcite.

Journal of Structural Biology, **139(1)**, 39-45.

Marsh M.E. (2003)

Regulation of $CaCO_3$ formation in coccolithophores.

Comparative Biochemistry and Physiology Part B, **136:** 743-754.

Martinez Martinez J., Schroeder D C. and Wilson W H. (2012)

Dynamics and Genetic Composition of *Emiliania huxleyi* and their co-occuring Viruses during a Coccolithophores Bloom in the North Sea.

Federation of European Microbiological Societies, **81**:315-323.

Mackinder L., Wheeler G., Schroeder D., Riebesell U. And Brownlee C. (2010)

Molecular Mechanisms Underlying Calcification in Coccolithophores,

Geomircobiology journal, **27**: 585-595

Mlandineo I., Segvic-Bubuc T., Stanic R. and Desdevises Y. (2013)

Morphological Plasticity and Phylogeny in a Monogenean Parasite Transferring between Wild and Reared Fish Populations.

*Plosone.***8**: issue 4.

Monteiro F.M., Bach L.T., Brownlee C., Brown P., Rickaby R.E.M., Poulton A.J., Tyrell T., Beaufort L., Dutkiewicz S., Gibbs S., Gutowska M.A., Lee R., Riebesell U., Young J. and Ridgwell A. (2016)

Why do marine phytoplankton calcify.

Science Advances **2**: 7.

Muller W E G., Rothenburger M., Boreiko A., Tremel W., Reiber A. and Schroder H C.(2005)

Formation of Siliceous Spicules in the Marine Demosponge *Suberites domuncula.*

Cell tissue res. **231**: 114-1145.

Nanninga H.J. And Tyrell T. (1996)

Importance of light for the formation of algal blooms by *Emiliania huxleyi.*

Mar Ecol Progr Ser. **136:** 195-203

Nielsen M.V., (1997)

Growth, dark respiration and photosynthetic parameters of the coccolithophorid *Emiliania huxleyi* (Prymnesiophycaea) acclimated to different day-length irradiance combinations

Journal of Phycology. **33:** 818-822

Noel M., Kawachi M., Inouye., (2003)

Induced dimorphic life cycle of a coccolithophorid, *Calyptrosphera sphaeroidea* (Prymnesiophycaea, Haptophyta).

Journal of Phycology, **40:** 112-129.

Outka D.E And Williams D.C., (1971)

Sequential coccolith morphogenesis in *Hymenomonas caterae*

Journal of Protozoology. **18:** 285-297.

Paasche E., Brubank S., Skattebol S., Young J.R. Green J.C., (1996)

Growth and calcification in the coccolithophirid *Emiliania huxleyi* (Haptophyceae) at low salinities.

Phycologia, **35:**394-403.

Paasche E. (2002)

A review of the coccolithophorid *Emiliania huxleyi* (Prymnesiophyceae), with particular reference to growth, coccolith formation and calcification-photosynthesis interactions.

Phycologia, **38:** 503-529.

Palade G. E. (1952)

The fine structure of mitochondria.

The Anatomical record, **114:** (v3)427-521.

Palade G.E. 1955

A small particulate component of the cytoplasm.

Journal Biophysics, Biochemistry and Cytology. **1:** (1) 59-68.

Probert I., Fresnel J., Billard C., Geisen M. and Young J R. (2007)

Light and Electron Microscope Observations of *Algrosphaera robusta* (Prymnesiophyceae).

Journal of Phycology, **43**: 319-332.

Rahn-Lee L and Komeili A. (2013)

The Magnetosome model: Insights into the Mechanisms of Bacterial Biomineralisation.

Frontiers in Microbiology, **4**:352.

Read B. *et al.*(2013)

Pan Genome of the Phytoplankton *Emiliania huxleyi* underpins its Global Distribution.

Nature, **499**:209.

Reibesell U., Zondervan I., Rost B., Tortell P.D., Zeebe R.E., Morel F.M.M., (2000)

Reduced calcification of marine plankton in response to increased atmospheric CO_2.

Nature, **407:** 364-367.

Relyea R.A. (2002)

Costs of phenotypic plasticity,

The American Naturalist, **159**:272-282.

Rost B., And Riebesell U. (2004)

Coccolithophores and the biological pump: responses to environmental changes.

'In' Theirstein H.R. And Young J.R., '*Eds' Coccolithophores-From Molecular Process to Global Impact,* Springer-Verlang Berlin, 1-29.

Saez A G., Probert I., Geisen M., Quinn P., Young J R. and Medlin L K. (2003)

Pseudo-Cryptic Speciation in Coccolithophores.

Proceedings of the Nationl Academy of Science, **12**:7163-7168.

Sanders D., Pelloux J., Brownlee C., Harper J.F. (2002)

Calcium at the crossroads of signalling.

The Plant cell, **14:** S401-S417.

Saruwatari K., Satoh M., Harada N., Suzuki I. And Shiraiwa Y.

(2015)

Change in coccolith morphology by responding to temperature and salinity in coccolithophore *Emiliania huxleyi* (Haptophyta) isolated from the Bering and Chukchi Seas.

Biogeosciences, **12**:17751-17780.

Schroeder D C., Oke J., Malin G. And Wilson W H. (2002)

Coccolithovirus (*Phycodnavividae*):Characterisation of a New Large ds DNA Algal Virus that Infects *Emiliania huxleyi.*

Archives of Virology, **147**, 1685-1698.

Schroeder D.C., Biggi G. F., Hall M., Davy J., Martinez J.M., Richardson A.J., Malin G. and Wilson W.H. (2005)

A Genetic Marker to Separate *Emiliania huxleyi* (Prymnesiophyceae) Morphotypes.

Journal of Phycology, **41**: 874-879.

Siesser W.G. (1994)

Historical background of coccolithophores

'In' Winter A., And Siesser W.G., (Eds) *Coccolithophores* (Cambridge University press) 1-11.

Simon N., Campbell L., Ornolfsdotter E., Groben R., Guillou L., Lange M and Medlin L.K. (2000).

Oligonucleotide probes for the identification of three algal groups by dot blot and fluorescent whole-cell Hybridisation.

Journal of Eukaryotic Microbiology, 47 (1): 76-84

Steere R.L. (1957)

Electron microscopy of Structural Detail in Frozen Biological Specimens.

Journal of Cell Biology **3** (1) :45

Steinhorst L and Kudla J. (2013)

Calcium and Reactive Oxygen Species Rule the Waves of Signalling.

Plant Physiology, **163**, 471-485.

Swillen I., Vanoverbeke J. and De Meeser L. (2015)

Inbreeding and Adaptive Plasticity:an Experimental Analysis on Predator-Induced Responses in the Water Flea *Daphnia.*

Ecology and Evolution (2015)

Sym S and Kawachi M. (2010)

'Ultrastructure of *Calyptroshaera radiate*, sp. Nov. (Prymnesiophyceae, Haptophyta).'

European journal of Phycology,**35:**, 283-293.

Taylor A.R. And Brownlee C. (2003).

A novel Cl^- inward rectifying current in the plasma membrane of the calcifying marine phytoplankton *Coccolithus pelagicus.*

Plant Physiology, **131:** 1391-1400.

Taylor A.R., Russell M.A., Harper G.M., Collins T., Brownlee C. (2007)

Dynamics of formation and secretion of herterococcoliths by *Coccolithus pelagicus (spp Braarudii).*

European Journal of Phycology, **42(2)**: 125-136.

Thirion S., Troadec J D., Pagnotta S., Andrews S B., Leapman R D> and Nicaise G. (1997)

Calcium in Secretory Vesicles of Neurohypophysial Nerve Endings: Quantitative Comparison by x-ray microanalysis of Cryosectioned and Freeze-Substituted Specimens.

*Journal of Microscopy***, 186**, 28-34.

Uriz M J., Turon X., Bacerro M A. and Agell G. (2003)

Siliceous Spicules and Skeleton Frameworks in Sponges:Origin, Diversity, Ultastructural patterns, and Biological Functions.

Microscopy Research Techniques, **4**, 279-299.

Van Der Wal P., de Jong E.W., Westbroek P., de Bruijn W.C., Mulder-Staple A.A., (1983)

Ultrastructural polysaccharide localisation in calcifying and naked cells of the coccolithophorid *Emiliania huxleyi.*

Protoplasma, **118:** 157-168.

Westbroek P., de Jong E.W., Van Der Wal P., Borman A.H., de Vrind J.P.M., Kok D., de Bruijn W.C., Parker S.B., (1984)

Mechanisms of calcification in the marine algae *Emiliania huxleyi*

Phycological Transaction of the Royal Society London B, **304:** 435-444.

Westbroek P., Young J.R., Linschooten K., (1989)

Coccolith production (biomineralisation) in the marine alga *Emiliania huxleyi*

Journal of Protozoology, **36:** 368-373.

Ribosome

https://en.wikipedia.org/wiki/Ribosome#Discovery

Wikipedia-5 November 2016.

Wilson W.H., Tarran G., Zubkov M.V., (2002)

Virus dynamics in a coccolithophore dominated bloom in the North Sea.

Deep Sea Res, **49:** 2951-2963.

Winter A., Jordan R.W. and Roth P.H. (1994)

Biogeography of living coccolithophores in ocean waters.

‘In’ Winter A., And Siesser W.G., (Eds) *Coccolithophores* (Cambridge University press) 161-177.

Young J.R., Didymus J.M. Brown P.R., Prins B., Mann S., (1992)

Crystal assembly and phylogenetic evolution in heterococcoliths.

Nature (London), **356:**516-518.

Young J.R. (1994)

Functions of coccoliths.

‘In’ Winter A., And Siesser W.G., (Eds) *Coccolithophores* (Cambridge University press) 63-82.

Young J R., Geisen M., Cros L., Kleijne A., Sprengel C., Probert I. And Ostergaard J. (2003) A Guide to Extant Coccolithophore Taxonomy.

Journal of Nannoplankton Research, Special issue, **1**: 1-125.

Young J R., Geisen M. and Probert I. (2005)

A Review of Selected Aspects of Coccolithophore Biology with Implications for Paleobiodiversity Estimation.

Micropaleontology, **51**:1-22.

Young J R., Andrulait H. and Probert I. (2009)

Coccolith Function and Morphogenesis:Insights from Appendage-Bearing Coccolithophores of the Family *Syracosphaeraceae* (Haptophyta).

Journal Phycology, **45**, 213-226.

Young J.R., Liu H., Probert I., Aris-Brosou S. and de Vargas C. (2014)

Morphospecies *versus* Phylospecies Concepts for Evaluating Phytoplankton Diversity: the Case for Coccolithophores.

Cryptogamie Algologie, **35**: 353-377.

Young J.R., Poulton A.J. and Tyrell T. (2014)

Morphology of *Emiliania huxleyi* coccoliths on the northwestern European shelf-is there an influence of carbonate chemistry?

Biogeosciences. **11**: 4771-4782.

Zhu P., Chaertova E., Bess J., Lifson J.D., Arthur L.O., Taylor K.A. and Roux K.H. (2003)

Electron Tomography analysis of envelope Glycoprotein Trimers on HIV and Simian Immunodeficiency virus virions.

Proceedings of the National academy of sciences of the USA. **100**: 15812-15817.

Zondervan I. (2007)

The effects of light, macronutrients, trace metals and CO_2 on the production of Calcium Carbonate and organic carbon in coccolithophores-A review.

*Deep sea research II,***54**, 521-537.

Appendix 1-publications

A1.1 Introduction: -

During the course of undertaking work for my thesis, I also became involved in research with several other groups. These groups fall into three categories. The first investigated the mechanisms, morphology and ultrastructure of the inner ear of certain fish and domestic pigs. The second investigated aspects of coccolithophore life cycles and the third looked at the effect of certain dietary variations had on the effect of certain species of farmed fish.

My involvement in all of these papers was that I was responsible for the use of both scanning Electron Microscope (SEM) and Transmission Electron Microscope (TEM) and how it contributed to the overall understanding of the work.

This work resulted in the production of published papers all of which have been included here.

I will briefly discuss each paper in turn and expand on the contribution Electron Microscopy made to the published article.

A1.2 Inner ear papers.

The polarisation of hair cells from the ear of the European bass (*Dicentrarchus labrax*). Lovell, J.M, Findlay, M.M, Harper, G, Moate, R.M & Pilgrim, D.A (2005).

This paper investigated the ultrastructure of ciliary hair cells within the ear of the European Bass (*Dicentrarchus labrax).* It used SEM to show that the hair cells are arranged in bundles that are specifically orientated within a structure known as the saccule. The saccule is a

structure with the inner ear that contains sensory cells and it is these cells that send signals from the hair cells to the brain.

The SEM also was used to investigate the differences in the quantity of these cells as fish aged and it showed that there was an addition of sensory cells within the saccule as fish got older (with an estimated 80,000 cells in a fish measuring 170mm as opposed to 40,000 cells in a younger fish measuring 70mm).

This paper also used the TEM to examine the saccular hair cell in more detail. These examinations revealed the actin filaments contained within the hair cells responsible for 'rooting' of the hair cell to the hair cell.

My contribution to this paper involved working with Dr. J.M. Lovell in the production of the SEM images and processing the samples for TEM. I also worked with Dr Lovell to produce the TEM images.

Below (figures A1.1 and A1.2) show an SEM image of the hair cells and a TEM image of the actin filaments used in the paper.

Figure A1.1 SEM image showing ciliary bundles in the saccular of the inner ear of The European Bass.

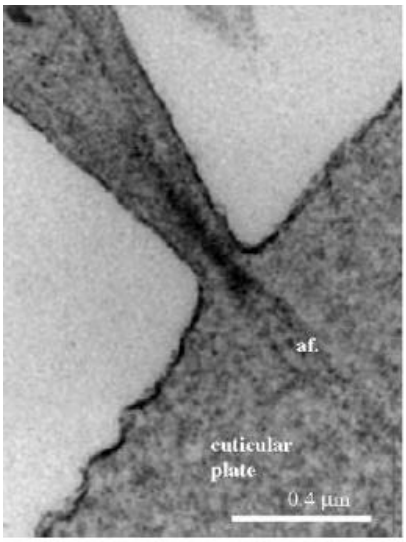

Figure A1.2 TEM image showing the base of the cilia and the actin filaments (af) that connect it to the cuticular plate.

The information produced in the paper was used to gain an understating of the inner ear of the European Bass and as part of larger study looking at the morphology and physiology of the hearing systems of both vertebrate and invertebrate animals.

The inner ear ultrastructure from the paddlefish (*Polydon spathula*) using transmission electron microscopy. Lovell, J.M., Findlay, M.M., Harper, G.M., Moate, R.M. (2006).

Again I worked with Dr Lovell on this paper in the production of the EM images.

This paper used TEM and SEM to examine the ultrastructure of the inner ear of the Paddlefish. It showed that the structure was similar to that found in other bony fish. However, it was the

first to show that the afferent cell body (the afferent nerve cell to which the hair is attached) was almost twice the size of those observed in other bony fish.

The work in this paper was used to study the inner ear in order to establish the effects of anthropogenic noise and the likely damage it would cause to the hair cells of the inner ear.

Figure A1.3 (below) shows detail of the hair cells in the nerve fibres in a TEM image of a cross section through the nerve bed.

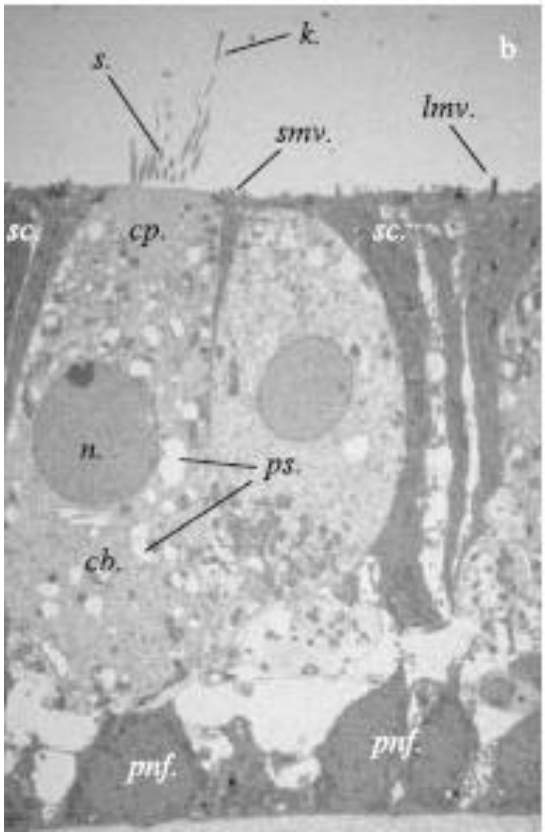

Figure A1.3 A TEM cross section through the hair cell and nerve fibres of the inner ear of the Paddlefish. *cb*, cell body; *cm*, cell membrane; *cp*, cuticular plate; *ga*, golgi apparatus; *jc*, junctional complex; *k*, kinocilia; *lm*, long microvilli; *m*,mitochondrion; *n*, nucleus; *ps*, phagosomes; *pnf*, peripheral nerve fibres; *sc*, support cells; *s*, stereocilia;*smv*, short microvilli.

The polarisation of hair cells from the inner ear of the lesser spotted dogfish (*Scyliorhinus canicula*). Lovell, J.M, Findlay, M.M, Harper, G.M, & Moate, R.M. (2007).

Again I worked with Dr Lovell on the SEM to investigate how the sensory hair cells from the inner ear of the lesser spotted were arranged.

The inner ear is divided into two main areas, the *pars superior* and the *pars inferior*. Within the *pars inferior* are two fluid filled pouches, the saccule and the lagena and it is within the saccule that the *macula neglecta* is located. The *macula neglecta* is made of two areas of sensory epithelial tissue and it is on these areas that, using the SEM, the polarisation of the hair cells was noted for the first time. On the utrilcular epithelium (see Figure A1.4 below), a structure closely located to the *pars superior*, the hairs were orientated horizontally as opposed to the hairs on the *macula neglecta* where the hairs were orientated vertically. This was only observable in the SEM and resulted in a finding not previously observed.

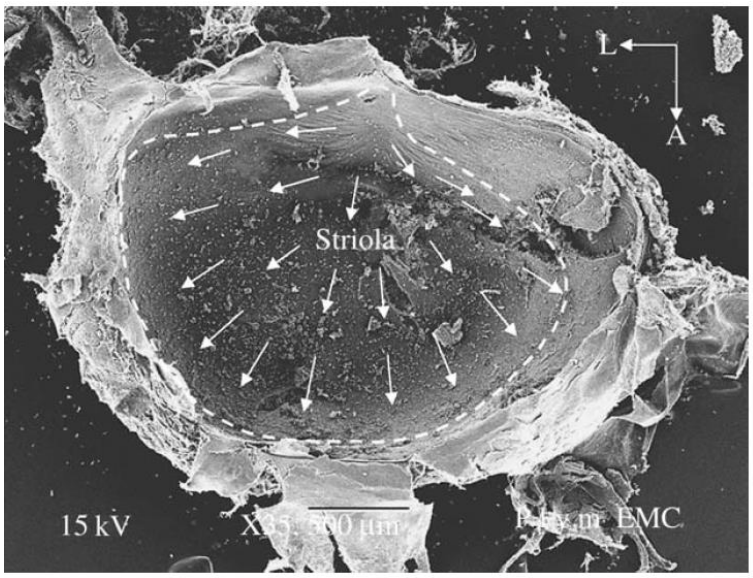

Figure A1.4 The utricle. The arrows indicate the orientation of the hair cells across the macula surface. (scale bae = 500 mm.) The annotations anterior (A) and left (L) represent the orientation of the utricle if it were in the fish.

The morphology of the inner ear from the domestic pig (Sus scrofa). Lovell, J.M., and Harper, G.M. (2007)

Until the publication of this paper, the inner ear of the domestic pig had never been studied with the SEM and TEM. Working with Dr Lovell again and his novel approach to the removal of the inner ear it was possible to study the hair cells present on the cochlea, saccule and utricle. The information acquired about the anatomy of the inner could provide important information in pathological diagnosis following ear trauma and the development of of biotechnical systems (such as cochlea implants) associated with the enhancement of hearing.

The information revealed in this work could also be used as an analogue in the study of cetacean hearing. Particularly useful as using cetaceans for scientific research is illegal in many countries.

The images below (figures A1.5 and A1.6) are and SEM and TEM image of the hair cells found in the basal region of the cochlea.

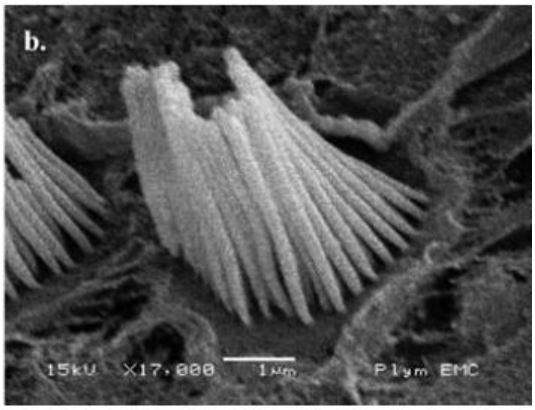

Figure A1.5 SEM Image of the outer hair cells found in the basal region of the cochlea of the domestic pig.

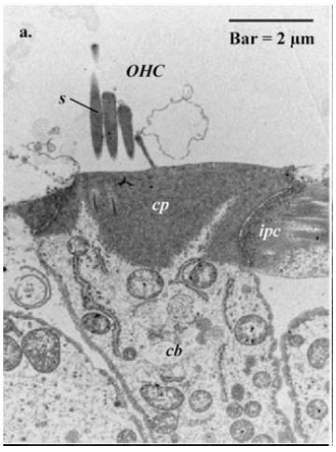

Figure A1.6 TEM image of the Outer Hair Cells (OHC) of the basal region of the cochlea of the domestic pig. Stereo cilia (S) can be seen associated with the cuticular plate (cp) which itself is associated with the cell body (cb) and the inner pillar cells (ipc).

A1.3 Coccolithophore papers.

Dynamics of formation and secretion of heterococcoliths by *Coccolithus pelagicus* ssp. Braarudii. Taylor, A.R, Russell, M.A, Harper. G.M, Collins, T. and Brownlee C. (2007).

This paper dealt with coccolithogenesis in *Coccolithus pelagicus.* The contribution the TEM made to this paper is fully discussed in chapter 3. It dealt with not only the general morphology (see figure A1.7, below) of *C. pelagicus* but also the formation and secretion of the organic scales.

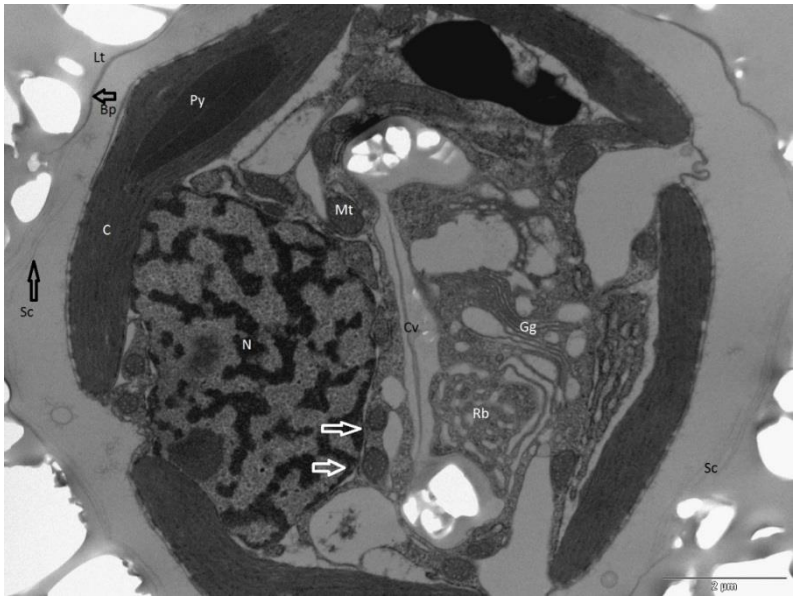

Figure A1.7 *C. pelagicus* ultrastructure as observed with a TEM. Clearly visible are the voids in the resin left by the external coccoliths (Lt) and their close association with the baseplate of the coccolith (Bp) and the layer of organic scales (Sc). Above the Nucleus (N) is one of the Chloroplasts (C) with a single thylakoid traversing Pyrenoid (Py).

A unicellular algal virus, *Emiliania huxleyi* virus 86, exploits an animal-like infection strategy. Luke C. M. Mackinder, Charlotte A. Worthy, Gaia Biggi, Matthew Hall, Keith P. Ryan, Arvind Varsani, Glenn M. Harper, William H. Wilson, Colin Brownlee and Declan C. Schroeder (2009).

This study looked at the way *Emiliania huxleyi* virus 86 (EhV-86) infected the cells. It demonstrated for the first time, that EhV-86 capsids were enveloped by a lipid membrane and that the lipid membrane remained intact after the virus endocytotically entered the cells. This differs from how similar viruses infect other algae. It also differs in the way the EhV-86 exits; budding from the host cell using the hosts plasma membrane to cover the virion as it leaves (see figure A1.8 below). This is much more like virus infection in animals.

My contribution to this paper was principally involved in the preparation and production of material for examination in the TEM. I was also involved in assisting with the imaging.

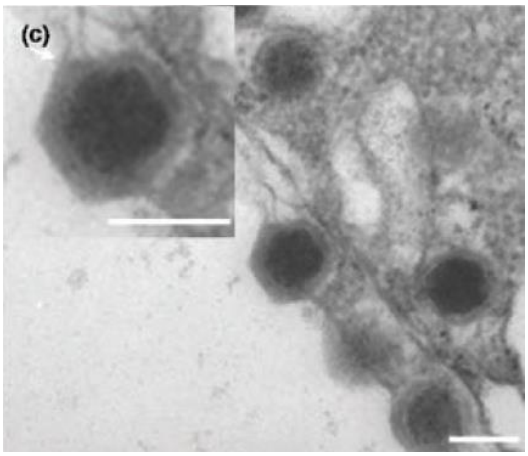

Figure A1.8 The EhV-86 virus being released extracellularly via a 'budding' mechanism. In the inset image the viral particle can be seen surrounded by a host derived lipid coating.

A1.4 Aquaculture and fish nutrition papers.

All of the papers (with the exception of the Merrifield *et al., 2013)* involving aquaculture investigated the effects of various probiotic/prebiotic or dietary supplements had on various farmed fish. My involvement was assisting with the SEM sample preparation and imaging and all of the TEM work (including Sample preparation, ultramicrotomy and imaging). The subsequent data interpretation was undertaken by the other collaborative authors. The common collaborator in all of these paper is Dr D. L. Merrifield. He was either the lead author on the paper or the head of the research group carrying out the work.

Here I discuss the papers that used EM images that I produced.

Possible influence of probiotic adhesion to intestinal mucosa on the activity and morphology of rainbow trout (*Oncorhynchus mykiss*) enterocytes. Merrifield, D. L., Harper, G. M., Dimitroglou, A., Ringø, E. & Davies, S. J. (2010).

An improved gut microbiota in fish leads to healthier fish and fish that have an improved growth performance. As such, the feeding of supplemental probiotics to commercially farmed fish is significant to aquaculturalists.

Up until this paper had been published, the effects of feeding farmed fish prebiotics in order to improve the intestinal microbiota had never been imaged with an electron microscope.

The rainbow trout were fed a diet that was supplemented with four probionts – *Bacilus subtilis, Bacilus licheniforms, Pediococcus acidilactili* and *Enterococcus faecium.* Once the feeding trials were finished, the samples of the gut were processed and imaged.

In figure A1.9 below *P. acidilactici* like particles can be seen in the trout intestinal mucosa. Inset to this picture are *P. acidilactici* on a Nucleopore filter. This was done in order to help positively identify the particles in the SEM image as being the dietary supplemental bacteria. Figure A1.10 (below) is a TEM image again showing a bacteria-like particle closely associated with the gut mucosa.

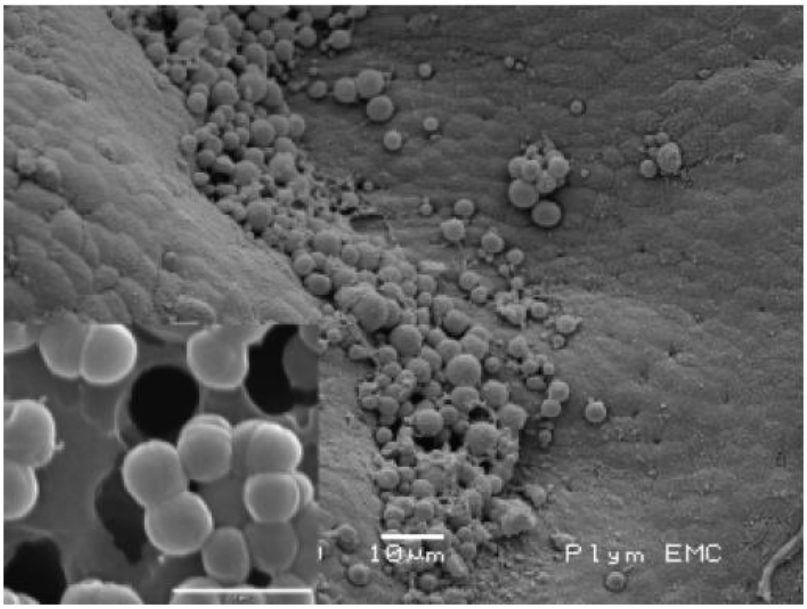

Figure A1.9 SEM micrograph of the distal region of rainbow trout intestinal mucosa showing a localized colonization of *Pediococcus acidilactici*-like cells; scale bar510 mm. Inset: *P. acidilactici* on 1 mm Nucleopore filter; scale bar52 mm.

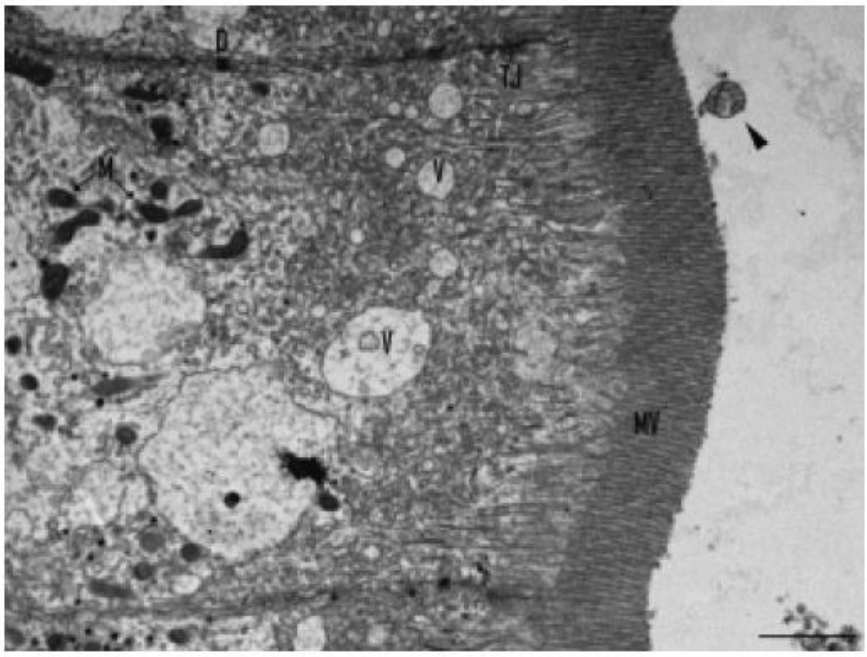

Figure A1.10 TEM image of the proximal region of rainbow trout intestinal mucosa showing associated-*Pediococcus acidilactici*-like cell (arrowhead). D, desmosome; M, mitochondria; MV, microvilli; TJ, tight junction; V, vacuole. Scale bar 2 um.

Effect of dietary alginic acid on juvenile tilapia (*Oreochromis niloticus*) intestinal microbial balance, intestinal histology and growth performance. Merrifield, D. L., Harper, G., Mustafa, S., Carnevali, O., Picchietti, S., Davies, S. J. (2011).

Tilapia (*Oreochromis niloticus*) are commercially farmed fish and as a consequence, improvements to the breeding of these fish is always going to be of interest to the aqua culturists.

In this study, Ergosan which is a commercial source of alginic acid was assessed to see if it made any difference to the microbial balance, growth and intestinal.

Alginic acid has been shown to improve the immune response in fish (Fujiki *et al.* 1994) and as such adding it in the form of a dietary supplement it was hoped that an improved immune response in the tilapia would occur and as a consequence the fish would be healthier and show improved growth

The results of the study showed that the addition of the Ergosan to the diet of the tilapia showed no adverse effects on the fish either on the gastrointestinal microbial balance (this was shown with PCR analysis) or the epithelial brush border (see figure A1.11 below). This study showed that the maintenance of gut morphology and gastric microbial communities is fundamental for proper gut functionality and the successful breeding of farmed fish.

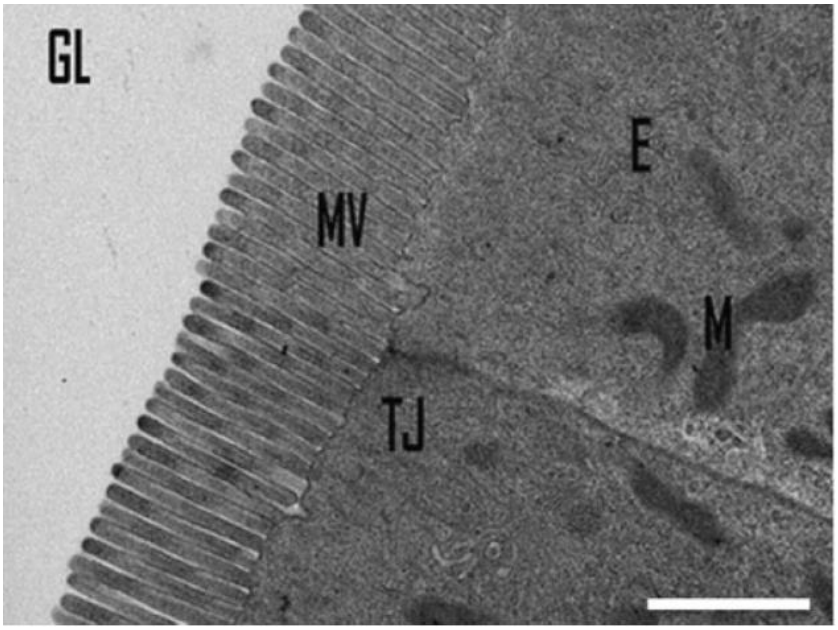

Figure A1.11 TEM of tilapia proximal intestine showing (E) enterocyte, (GL) gut lumen, (M) mitochondria, (MV) microvilli, (TJ) tight junction. Scale bar 1μm

An *ex vivo* approach to studying the interactions of probiotic *Pediococcus acidilactici* and *Vibrio (Listonella) anguillarum* in the anterior intestine of rainbow trout *Oncorhynchus mykiss.* Harper, G.M., Monfort, M., Saoud, I.P., Emery, M., Mustafa, S., Rawling, M., Eynon, B., Davies, S.J., & Merrifield, D.L.* (2011)*corresponding author.

The aim of this study was to investigate the antagonistic relationship between the probiotic *Pediococcus acidilactici* and the pathogen *Vibrio (Listonella) anguillarum* in the gut of rainbow trout (*Oncorhyncus mykiss*). In order to undertake the study, the fish were fed a diet supplemented with *P. acidilactici* for two weeks and then a portion of the gut was removed. The gut was then secured at one end producing sacs. Into these sacs was either the probiotic, the pathogen or a mixture of both. After one hour, the gut was assessed either with PCR, culturing to assess the microbial colonisation or TEM to assess the gut ultrastructure and if there was any damage to the gut mucosa.

Figure A1.12 (below) are TEM images of the gut and the probiotic and pathogen like cells. The TEM work showed that sacs that were filled with the pathogen were damaged as opposed to the sacs filled with just the probiotic, which were undamaged. The TEM of the sacs filled with both the probiotic and the pathogen revealed that the gut ultrastructure showed increased levels of goblet and leucocyte cells. The results suggest the probiotic; *P. acidilactici*, can be used to control fish infected by the pathogen, *V. anguillarum* and as such further work looking at this relationship in *in vivo* studies is warranted.

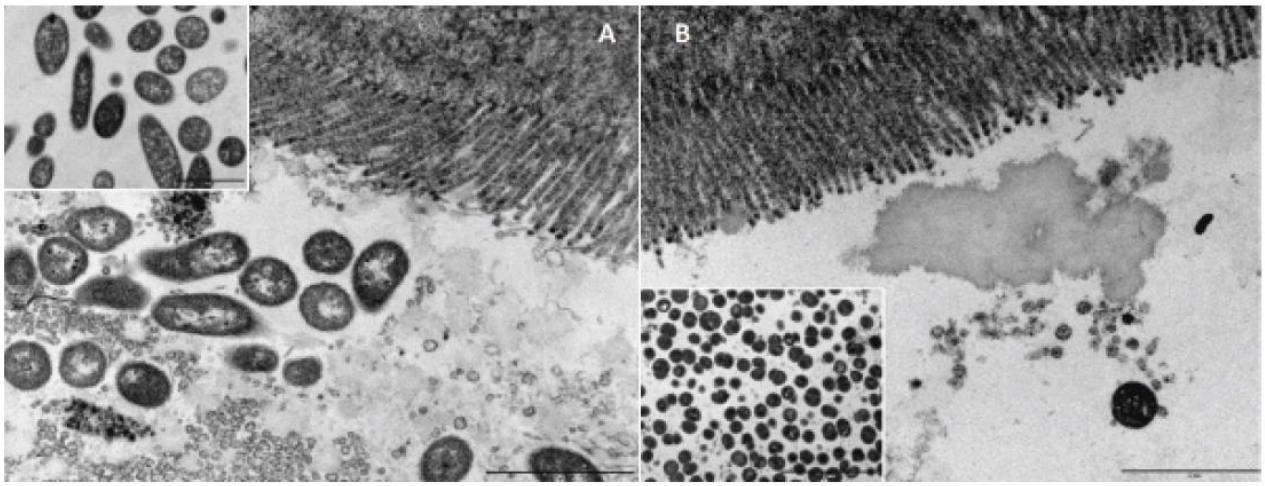

Figure A1.12 TEM micrographs demonstrating localised bacterial populations in close proximity and association with the epithelial brush border in the anterior intestine of rainbow trout. A) *V. anguillarum*-like cells (probiotic fed fish exposed to *V. anguillarum*) and B) *P. acidilactici*-like cells (probiotic fed fish exposed to *P. acidilactici*) in the lumen and in close association with microvilli. Inset figures show respective cell morphologies of known samples of the bacterial strains used within the assays. Scale bars 2 μm (except B inset: 5μm).

Ingestion of metal-nanoparticle contaminated food disrupts endogenous microbiota in zebrafish (*Danio rerio*). Merrifield DL, Shaw BJ, Harper GM, Saoud IP, Davies SJ, Handy RD, Henry TB. (2013).

Nanoparticles (NP) are particles that measure between 1 and 100nm (MacNaught and Wilkinson, 1997). They can be made from any material, ranging from plastics to metals. The aim of this study was to investigate the effect certain metal NP have on the gut of fish, specifically zebrafish. The metal NP used were silver-NP and copper-NP. Both of these

metal NP have shown to have antimicrobial properties and as such, ingestion could potential have harmful effects on gut microbiota and then ultimately to the gut.

The TEM (figure A1.13, below), showed that there was no difference in the gut ultrastructure in the control, the fish fed the silver or the copper NP. However, when the microbial community of the gut were examined with PCR it revealed that the fish exposed to copper NP had a reduction in the levels of some beneficial bacteria thus indicating that metal NP could have a detrimental effect on gut microbial communities. This warrants further investigation.

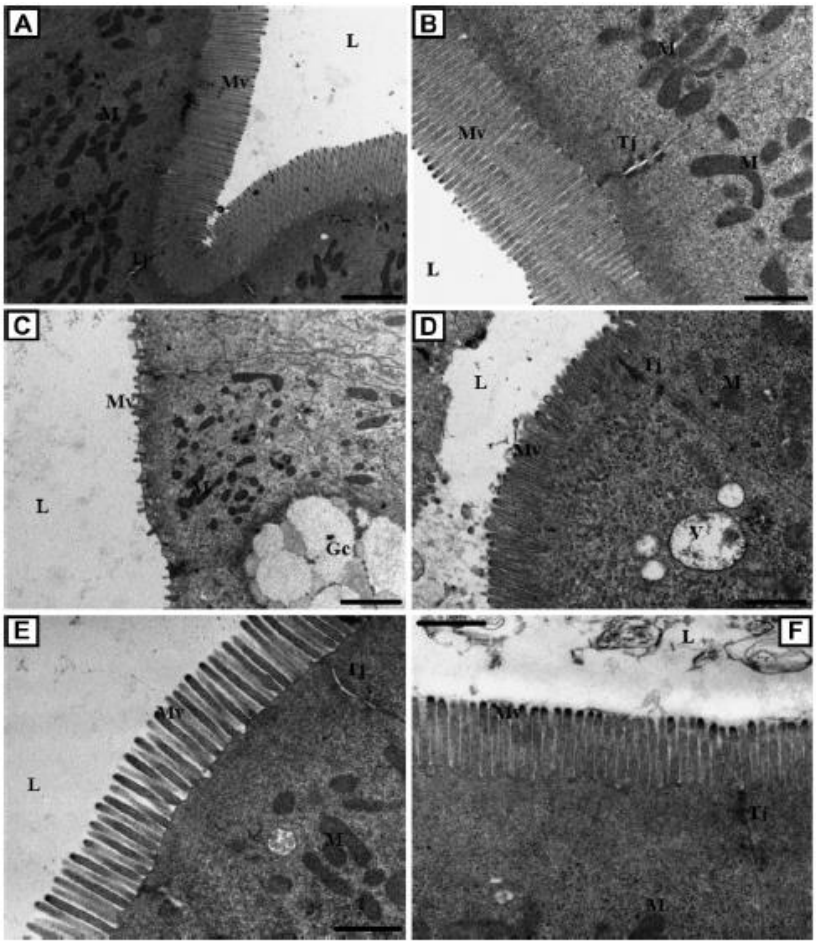

Figure A1.13 TEM images of the intestine of fish fed the control (A-D), Ag-NP (E) and Cu-NP (F) diets. Micrographs show variation between the anterior (A and B) and posterior (C

and D) regions of the intestine. No observations of epithelial damage, loss of integrity or microvilli disruption were observed in the Ag-NP (E) or Cu-NP (F) fed fish.
Key: Gc - goblet cell, L - lumen, M- mitochondria, Mv - microvilli, Tj - tight junction, V - vacuole. Scale bars: A - 2 um, B -1 um, C -2 um and D - F - 1 um.

Effects of a dietary β-(1,3) (1,6)-D-glucan supplementation on intestinal microbial communities and intestinal ultrastructure of mirror carp (*Cyprinus carpio L.*). Kühlwein H. Emery M., Rawling M., Harper G., Merrifield D. & Davies S.. (2013)

As with the previous work undertaken in the field of aquaculture, the aim of the work undertaken in this paper was to assess the role a dietary supplement, in the case of this paper *Saccharomyces cerevisiae* (Macrogard) had on the microbiota in the intestine and the brush border within the gut of the fish.

In the experiment, fish were either fed a 'normal' diet, or one supplemented with different concentrations of the Macrogard®.

The results were then assessed with culture dependent microbiology. This revealed that the gut microbiota was affected and that certain types of gut microbes became reduced in number. PCR was used to identify that the variety of the microbes in the gut of the fish became increased as a result of the supplementation of the diet with the Macrogard®.

Using TEM (figure A1.14 below) it was observed that the intestinal microvilli's overall length and density was significantly increased and it was concluded that supplementation of the diet of the fish with Macrogard® had an effect on the gut microbiota and brush border. The paper then suggests, that this is likely to lead to better feed utilization and as a result have a positive effect on the fish and their farming.

The paper didn't publish any of the TEM images taken, however, figure A1.14 is an image of the gut that was used in the analysis.

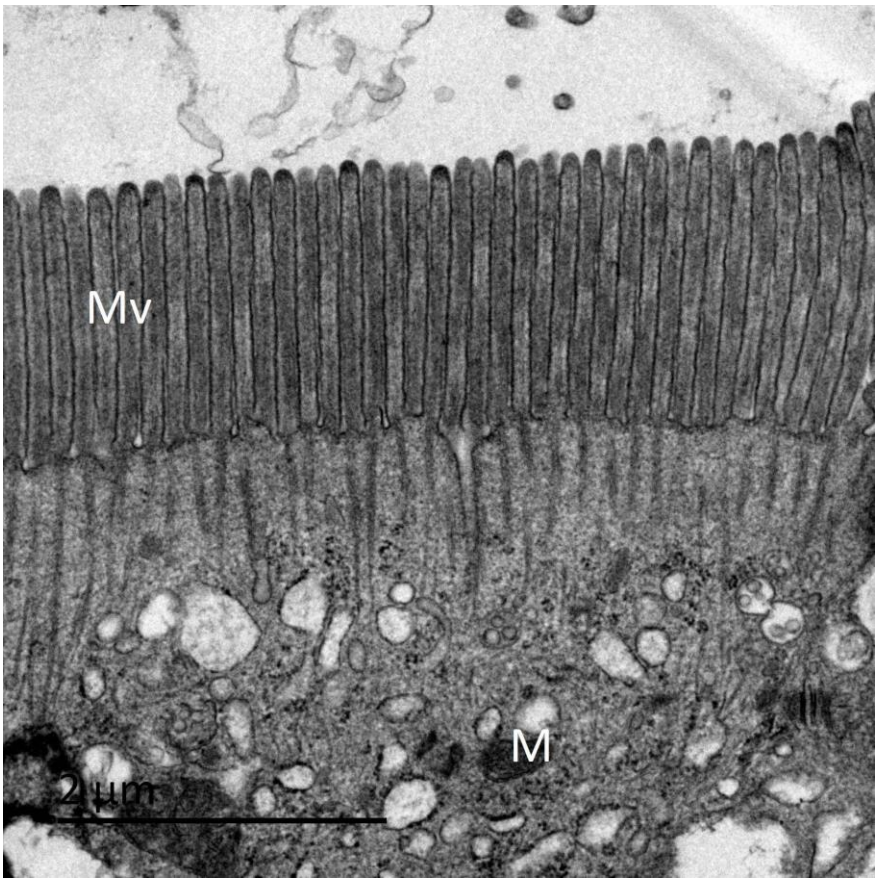

Figure A1.14 TEM image of the anterior intestine of the mirror carp. It was images such as this that were used to establish that Macrogard® had an effect on the brush border of the gut

Appendix A2

The role of Electron microscopy in modern Biological research.

The Electron Microscope was used extensively during this project and warrants some discussion.

A2.1 Introduction- the history of the electron microscope.

The idea of using a beam of electrons was pioneered by Hans Busch in 1928 after Busch developed the first electromagnetic lens (critical in Electron microscope operation). However, it was three years later the German physicist Ernst Ruska and electrical engineer, Max Knoll built the first operational Transmission Electron Microscope (TEM). It demonstrated the possibility of using electrons as the illuminating source in a microscope, however the magnification was limited to 400 x. Within three years, further work resulted in magnification that exceeded what was attainable with a light microscope.

The company, Siemens and Halske patented the Microscope and they financed work to develop applications for the microscope, in particular work with biological specimens. (source for this information is Bozzola J.J. Principles and techniques for Biologists, 1998).

The Scanning Electron Microscope was first developed in 1937 by Manfred von Ardenne and along with the TEM was limited in its use for biological specimens until the 1950s when specimen preparation techniques were developed to produce images that were useful to biologists (source for this information is Bozzola J.J. Principles and techniques for Biologists, 1998).

A2.2 The use of the Electron Microscope in biological research.

It is easy to forget that all of the major subcellular organelles were first visualised (or at least imaged at higher resolution with finer detail) with, principally the TEM in the 1950s and 60s. The imaging of these cell components allowed researchers to describe initially and then understand the function of various cell components. For example, in 1952, the ultrastructure of mitochondria was first described by G E Palade in his paper 'The fine structure of Mitochondria'. He was also the first person to describe ribosomes in 1955 in his paper 'A small particulate component of the cytoplasm'. This work would ultimately lead to him wining the Nobel prize in 1974. (https://en.wikipedia.org/wiki/Ribosome#Discovery)

During the 50s and 60s, much of the work undertaken on the Electron Microscope was about describing the structures visualised what then followed was a period of ascertaining the functions of these structures (as with Palade and the Ribosome). The work that then followed this was attempting to ascertain how the various structures imaged actually worked.

The use of the EM for biology was pioneered by people such as Albert Claude who won the Nobel alongside Palade in 1974 for his work investigating the ultrastructure of biological cells. Scientists such as Audrey Glauert who pioneered specimen preparation techniques such as the use of Araldite as an embedding media to allow better sectioning for TEM (Glauert, A. and Glauert R., 1957). All of the people who worked on the development of the EM in Biological research have allowed it to become the powerful tool it is today.

The EM has crossed many disciplines within the area of Biological research. These include Anatomy, Botany, Biochemical research, Forensics, Medicine and Pathology all of which utilise the EM to image, understand and explain biological systems.

EM has contributed greatly to the field of Biology and many journals reproduce EM images, However, it is often the case as with Taylor *et al.* (2007) that EM (both TEM and SEM) as well as light microscopy can be used in conjunction with one another to investigate different features of the same subject.

Alternatively, as with Ferguson *et al.* (2010) and Merrifield *et al.* (2013) the EM can be used in addition to other wholly non-microscopical techniques to investigate the different effects of a material on an organism.

A2.3 Specialist techniques used in biological research.

The basics of EM have remained fairly constant since the 50s and 60s. Samples for the SEM need to be dehydrated and samples to be imaged in the TEM need to be resin embedded, sectioned and stained before the can be imaged.

However, refinement to these techniques has allowed the EM to 'see' more and more.

For examples, the freeze fracturing; the rapid freezing of samples and subsequent fracturing to reveal internal features helped overcome one of the limiting factors of the SEM. The SEM images the surface of the sample, with freeze fracturing, the inside surface is exposed and this become the 'surface' of the sample and this can be subsequently images. Techniques such as this were used by Steere in his 1957 paper: 'Electron microscopy of Structural detail in biological specimens' where he successfully imaged various viruses using freeze fracturing.

Other techniques available include Immunocytochemistry. This is a technique where an antibody is raised to identify a particular and specific protein or antigen in a sample. This is the Primary antibody. Once it has been used to stain the sample, a secondary antibody which

attached to the primary antibody is used. Attached to the secondary antibody is a small gold particle which is visible in the TEM, this therefore allows the localisation of the original protein or antigen. This was a technique developed in the early 1970's by Farrent, McClean and Singer when they used it to image blue-green algae and chloroplasts (Griffiths, 1993).

Elemental analysis is also possible in the EM. As a result of specimen/beam interaction, x-rays are generated. These x-rays have a characteristic energy and wavelength. With appropriate equipment it is then possible to detect the x-rays and use them to identify the element that is producing them.

This technique is used predominantly by mechanical engineers, however, work by researchers such as J. Knott in 1995 used x-ray analysis to great effect to identify the bioavailability of metals to marine organisms living near ore refineries in the Mediterranean Sea.

In 1959, RW Horne and S. Brenner developed a technique known as negative staining. This is a method where a sample of (in the case of Horne, a tobacco mosaic virus) is placed on a TEM grid which is coated with a supporting film. The grid is the subsequently stained with either phosphotungstic acid or Uranyl acetate, this stains the background of the viruses and allows them to be imaged. This is a technique that is still used today and it allows rapid virus characterisation in the TEM.

A2.4 Recent advances in Biological Electron Microscopy.

Biological processes are dynamic by nature and one if the limiting factors with the EM is the processing of the samples for imaging; drying for SEM, resin embedding and sectioning for

TEM, results in the cessation of the dynamic processes, i.e. The EM typically images things when they are dead!

There are techniques available which allow the imaging of living things in the EM. One of these is the Quantomix capsule (WETSEM^{TM}). This a sealed, vacuum resistant capsule with an electron-transparent window through which the fully hydrated, potentially still living, sample is imaged.

In Ackerley *et al.* (2006) bacteria were grown on the 'window of the capsule and it was possible to image the whole cell 'live'. Thus meaning that using these capsules it is possible to overcome the inability to image live cells.

The capsules also allow the imaging of samples with minimal specimen preparation and therefore minimal chances for artefact formation.

The capsules have been used by a wide variety of researchers including Barshack *et al*. (2009) who investigated gut tissue and Nyshka *et al.* (2004) used WETSEM to investigate renal pathology. Both papers describe the ability of the Quantomix capsules to allow imaging of 'wet' samples with as 'life like' appearance as possible and the value of doing so.

One of the limitations of the use of Wet SEM is that the samples are imaged using backscattered electrons with a relatively large beam of electrons (needed to get the beam through the window) and as such the resolution is restricted.

One of the drawbacks of The TEM is that it produces 2 dimensional images (as opposed to the SEM which typically produces images with a three dimensional-3D quality). However, recent advances have resulted in the production of 3D images being produced with a TEM, TEM-Tomography.

This involves the reconstruction of a 3D image from a series of images of the section in the TEM whilst rotating it on a single axis. It is then possible to reconstruct a variety of 3D models using this information. (Kuo 2007).

This technique has been used to image sub-cellular macro molecular objects as the glycoproteins on the surface of the HIV virus as Zhu *et al.* did in his 2003 paper. In the paper, they describe how TEM-tomography was used to identify and count the number of trimers (surface proteins on the virus) and understand the virus interactions with the host cell and ultimately the production of a vaccine for the HIV virus.

A2.5 Conclusions

Electron microscopes have been in existence for less than 100 years and the advances that have been made in that time have allowed biologists to initially image sub-cellular organelles and the gain an understanding of their function. Continued development of techniques has allowed to EM to become an analytical tool as well as a tool that produces images.

EM has developed into a powerful tool in many aspects of Biological research especially when used in conjunction with other techniques (e.g. light microscopy and Confocal microscopy and has allowed a greater understanding of the world around us.